Technische Universität München

Lehrstuhl für Nanoelektronik

Organic Field-Effect Transistors for Biosensing Applications

Alexandra M. Münzer

Vollständiger Abdruck der von der Fakultät für Physik der Technischen Universität München zur Erlangung des akademischen Grades eines

Doktors der Naturwissenschaften

genehmigten Dissertation.

Vorsitzende(r):

Univ.- Prof. Dr. Alessio Zaccone

Prüfer der Dissertation:

1. Univ.- Prof. Paolo Lugli, Ph.D.
2. Prof. José Antonio Garrido Ariza, Ph.D. Barcelona Institute of Science and Technology / Spanien

Die Dissertation wurde am 15.04.2015 bei der Technischen Universität München eingereicht und durch die Fakultät für Physik am 28.09.2015 angenommen.

Zusammenfassung der Doktorarbeit

Im Rahmen dieser Arbeit wurden Kohlenstoff-Nanoröhren-Feldeffekttransistoren sowie Feldeffekttransistoren basierend auf Poly(3-Hexylthiophen) hergestellt und als Proteinsensoren in wässrigen Lösungen verwendet. Beide Halbleiter sind aus der Flüssigphase verarbeitbar und bergen das Potenzial in intelligente, flexible und kostengünstige medizinische Bauteile integriert zu werden. Für dieses Projekt wurden beide Transistortypen hinsichtlich ihrer Stabilität in biologischen Puffern getestet sowie hinsichtlich ihrer Sensitivität bezüglich der elektrolytischen Eigenschaften dieser Puffer. Es wurde festgestellt, dass P3HT Transistoren im Allgemeinen eine niedrigere Stabilität aufweisen, letztlich konnten jedoch mit beiden Bauteilen reproduzierbare Ergebnisse erzielt werden. Weiters wurden in dieser Arbeit Protein-Liganden Interaktionen in verschiedenen pH-Werten und Ionenstärken mit verschiedenen Proteinen gemessen, wozu die Liganden auf der Oberfläche der Nanoröhren immobilisiert wurden. Unter Verwendung von SWNT Transistoren als Biosensoren wurde außerdem die Dissoziationskonstante eines Proteins bestimmt und es konnte zwischen zwei verschiedenen Proteinen anhand der unterschiedlichen pH-Abhängigkeit unterschieden werden. Die experimentellen Ergebnisse dieser Doktorarbeit wurden in mehreren von Experten begutachteten Fachartikeln veröffentlich.

Abstract

For the present work single-walled carbon nanotube (SWNT) field-effect transistors and field-effect transistors based on poly(3-hexylthiophene) (P3HT) were fabricated and used as protein sensors in aqueous environment. Both semiconductors are solution-processable and feature the potential to be integrated in smart, flexible and cost-effective personalized medical devices. Within this thesis the stability of both transistor types in biological buffers was tested along with their sensitivity upon alterations of the electrolytic conditions. It was found that P3HT transistors reveal a generally lower stability than SWNT transistors, yet reproducible results could be obtained from both devices. In the frame of this thesis also the interactions of various proteins with ligands, which were attached onto the sidewalls of the carbon nanotubes, were analyzed under different pH conditions and different ionic strengths. Using biofunctionalized SWNT transistors as biological sensors the dissociation constants of a protein was probed and it was possible to distinguish between two different other proteins by their pH-dependent sensor response. The experimental results of this work were published in several peer-reviewed articles.

Contents

1 Introduction

Today about 4500 papers on biosensors are published each year. The interest in this technology is enormous and it is still increasing.[1] Academic and industrial researchers envision wearable, flexible, implantable, biocompatible and biodegradable sensing devices that can fulfill the extremely high requirements of personalized medicine. Yet, this interest is not only driven due to its nature as a profitable 13 billion US$ per year business but also due to a fundamental question: “how does life work?”. In the following several requirements of biosensors for medical and research purposes are discussed:

First, biosensors have to be highly sensitive. For example, for the purpose of fundamental research and certain fields of medical diagnosis, sensitivities down to a single molecule level can be required. In addition to that also the ability of gaining large sets of data for stochastic analysis is desirable.[2,3,4] Gaining large sets of data requires however that a biosensor should be stable at least several hours or even several days.

Second, it is desirable that biomolecules can be detected via so-called “label-free” methods. These methods are less susceptible to unwanted interactions such as interactions that are caused by steric hindrance (whereat steric hindrance means that a relatively large label that is attached to a relatively small biomolecule obstructs “natural” interactions of that biomolecule due to the size or volume of the label)

However, labeling costs time and demands qualified personnel, which is significant drawback.[5,6]

Third, a biosensor should function in liquid environment including even crude blood samples[7], saliva[8] and other body fluids. This seemingly insignificant feature provides the scientists with a difficult task as such a device would require an extremely specific biosensor.

Biosensors based on field-effect transistors (FETs) are expected to be excellent candidates when it comes to meeting the above mentioned points. This is because FETs are fundamental building blocks of electronic circuitry that can be used as electronic switches and that are as well able to amplify electronic signals. Yet, the FET-biosensor technology faces several issues that need to be overcome before a commercialization is conceivable:

The surface functionalization, for example, presents an issue. In this context, reliable and straight-forward protocols to functionalize the active surface of FET sensors with bio-receptors have to be developed. As a consequence collaborations of interdisciplinary research groups have to be established and tightened (chemistry, engineering, physics, biology, mathematics). Furthermore hurdles and constraints (e.g. Debye screening) of this technology have to be addressed.

It is the task of this thesis to assess the suitability of two different types of FETs as biosensors, namely organic thin-film transistors based on poly(3-hexylthiophene) (P3HT-FETs) and FETs based on a network of single-walled carbon nanotubes

(SWNT-FETs). Both semiconductors have in common that they can be processed from solution and thus they are candidates for the next-generation printing technology.

This thesis begins in Chapter 2 with an introduction to biosensors, followed by an overview of the state of the art. In Chapter 3 the underlying theoretical aspects of this work will be explained. The fabrication methods of polymeric and carbon nanotube based devices are briefly explained in Chapter 4. Additionally experimental methods and fabrication methods were adapted to the needs of the particular experiments. This is why experimental sections can also be found in each of the subsequent chapters. Chapter 5 and Chapter 6 are assessments of the suitability of organic field-effect transistors as biosensor. In Chapter 5 also the performance of polymeric field-effect transistors and carbon nanotube field-effect transistors under electrolytic conditions are compared, whereat in Chapter 6 the performance of back-gated carbon nanotube devices in electrolytes is probed. Finally, Chapter 7 and Chapter 8 show the results from experiments with proteins. The thesis concludes in Chapter 9 with a general conclusion and an outlook.

2 Biosensors: a state of the art

A biosensor is an analytical device that converts a biological response into an electrical signal. A biosensor comprises a sensitive element (II) which is sensitive to the analyte (I) under study. The sensitive element is immobilized onto a transducer (III). The transducer detects the signal caused by the interaction of the sensitive element with the analyte and converts it into an electrical signal. A biosensor further comprises an electronic system that amplifies processes and displays the electrical signal. (see e.g. [9]) The working principle of a biosensor is illustrated in Figure 2.1.

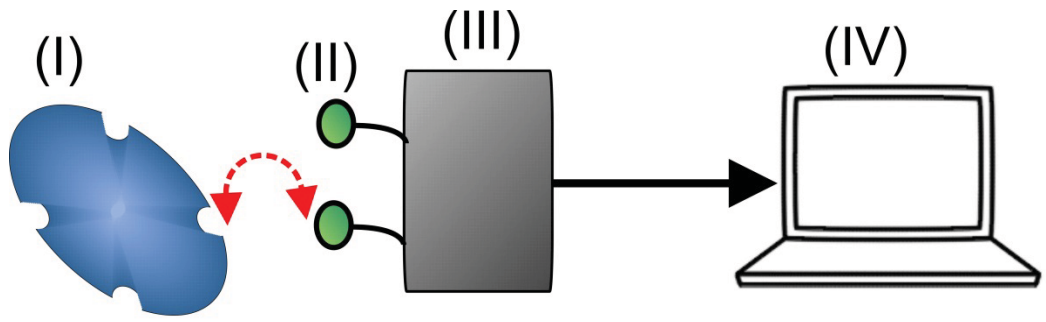

Figure 2.1: A sketch that illustrates the working principle of a biosensor: the analyte (I) interacts (illustrated with red arrow) with the sensitive element (II). The sensitive element is immobilized onto the transducer (III). The transducer is connected to the electronic system (IV).

The analyte can be any biological molecule or another component of interest (e.g., DNA, proteins, enzymes, cells, and organelles). The sensitive element needs to be an element (e.g. a biological molecule) that interacts specifically with the analyte. For

example, a DNA-strand (analyte) may interact with its complementary DNA-strand (sensitive element) by forming a double helix structure. There is a variety of transducers, for example, optical transducers, electronic transducers and piezoelectric transducers. Different transducer types are usually based on different physical principles. It is important to note, that the field of biosensors is a huge field when it comes to the variety of physical, chemical and biological principles that are involved when creating and employing biosensors.

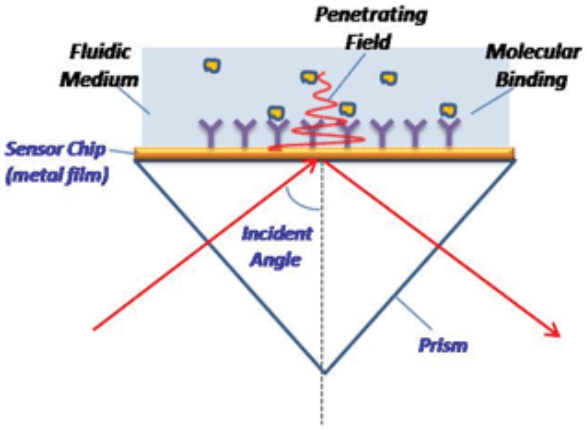

Figure 2.2.: A schematic representation of the working principle of a SPR biosensor. The gold surface is functionalized with ligands and SPR is used to detect the adsorption of analytes to the ligands. For this light, which is reflected on the gold surface, is detected and the reflection is measured. The adsorbing analyte causes a change in the local refractive index which in return causes a change in the resonance conditions of the surface plasmon polariton. (Image taken from [10])

Therefore only the principle of surface plasmon resonance (SPR) biosensors is briefly discussed due to their importance. This is because the development of the SPR protein sensor is a prominent scientific success story. In the 1980s the first SPR

immunoassay was introduced by Liedberg et al. and by now the so-called Biacore sensor became an integral part in a lot of research labs and pharmaceutical labs all around the globe.[11] A schematic representation of the working principle of an SPR sensor is shown in Figure 2.2. SPR relies on the concept of surface plasmon polaritons, which are electromagnetic waves that propagate along a metal/dielectric or a metal/air interface. Surface plasmon polaritons are very sensitive to changes that occur at the metal/dielectric interface. Figure 2.2 shows that the SPR device comprises a gold surface. The gold surface is functionalized with ligands and SPR is used to detect the adsorption of analytes to the ligands. For this light, which is reflected on the gold surface is detected and the reflection is measured. The adsorbing analyte causes a change in the local refractive index which in return causes a change in the resonance conditions of the surface plasmon polariton.[12] The analyte molecules are allowed to bind and unbind under a constant flow of buffer solution, which can be monitored. Information like binding constants can be gained without the need of labeling by using SPR technology. However, a drawback of this technology is the optical system that is used. A laser or an equivalent light source is often very expensive. That is why it is interesting to evaluate, if it is possible to develop alternative biosensing systems that can give reliable information but at low cost.

In this context an overview of the achievements in the field of biosensing with carbon nanotube based devices and OTFTs is given with a focus on protein sensing with SWNT-FETs. [5]

Clinical diagnosis as well as fundamental research stands to benefit from the development of cost-effective and reliable protein detection methods. Detection of protein-protein or protein-ligand interactions deepens the understanding of diseases as they are indispensable in vital processes of living organisms. Hence, much effort was put in assessing the suitability of field-effect transistors based on one-dimensional nanomaterials such as nanowires and carbon nanotubes as versatile and label-free electronic biosensors. This is not only due to the potential ease of integration in next-generation electronic circuits but also due to their one dimensional structure, which is comparable to the size of individual molecules.[13,14,15] Next-generation medical diagnostics demands novel biosensors and biological assays that can fulfill the requirements of a high-throughput, cost-effective, and ultrasensitive alternative to conventional methods.

Equivalently and with no less enthusiasm polymeric thin-film transistors were tested regarding their feasibility as biosensors, as well. This is also because polymeric thin-film transistors offer the advantage to be integrable in flexible electronics, which makes it imaginable that polymeric biosensors can be electronic components in every-day life such as smart clothing or as disposable and biodegradable one-way sensors.[16,17]

When testing the feasibility of a biosensor, well-known biosystems such as the hybridization of single-stranded nucleic acids or the binding of streptavidin or avidin to biotin play an important role. Usually one of the components of the biosensor-system is immobilized onto the sensitive area of the sensor and the other one is

detected. The fact that both of those testing systems reveal properties that are exceptional in nature, meaning that there is no natural biomolecule that is more highly charged than DNA (q = 2e/0.34 nm)[18,19] and there is no binding affinity between a protein and a ligand that excels the one of streptavidin or avidin to biotin (K_D is in the order of 10^{-14} M) [20], makes these two systems so interesting for using them to characterize the properties of novel biosensors. Those features helped immensely in understanding the underlying sensing mechanisms and restrictions of FET sensors in detail. It became commonly accepted that the dominant sensing mechanism for functionalized SWNT FETs is electrostatic gating due to the presence of charged moieties in the proximity of the nanotube's surface, leading to a shift of the threshold voltage of the transistor.[21,6] While this effect is the major cause for the ability of label-free sensing, it also limits those devices in terms of the electric double layer present at every solid-liquid interface.[22,23,24] The formation of the so-called Debye screening length (see 3.2.2) renders sensing in physiologic conditions challenging.

Next-generation medical diagnostics demands novel types of biosensors and biological assays that can fulfill the requirements of that vastly flourishing field. In this context and as a consequence of the discovery of nanomaterials and the feasibility of nano- and microfabrication, tremendous efforts have been made to develop carbon nanotube-based platforms for a highly-efficient screening of biomarkers. These efforts have been focused on two approaches: substituting or complementing existing biomedical assays with new, high-throughput, cost-effective and ultra-sensitive

alternatives and engineering tools that can give additional insight into biological and biophysical phenomena that are hard to address with conventional methods.

2.1 SWNT-based biosensors

The most prominent biosensing approach based on carbon nanotubes is integration into chemiresistors and field-effect transistors (FETs). These devices can be comprised of either a single semiconducting SWNT or a random network of SWNTs connecting the metallic source and drain electrodes. While the former has potential applications in single molecule detection and monitoring subtle biological interactions, the fabrication process is time consuming and requires demanding fabrication steps such as growing the SWNTs on the chip using chemical vapor deposition and subsequent lithography.[25] The latter, however, offers the benefit of a cost-effective and simple production. In figure 1a, a common architecture for liquid gated SWNT FET biosensors is depicted. This particular device is gated by a Ag/AgCl reference electrode directly immersed in the liquid dielectric. The biosensing merit of SWNTs lies in their one-dimensional shape combined with the fact that charge transport through a device can only take place at the nanotube surface. Therefore, even slight alterations in the environment surrounding the SWNT surface will lead to an electrical signal. Such alterations can be caused by charged moieties on the surface of proteins, or by a number of other mechanisms.[21] As a consequence, functionalization of nanotubes is a fundamental prerequisite for sensing applications. Ten years ago, research groups introduced SWNT FETs as

highly specific and sensitive instruments to detect the presence of proteins.[26,27] Starting from this point, functionalized SWNT FETs have been established as robust biosensors for medical diagnostics and constant effort was put in understanding the physical concepts behind different sensing mechanisms occurring in those devices.

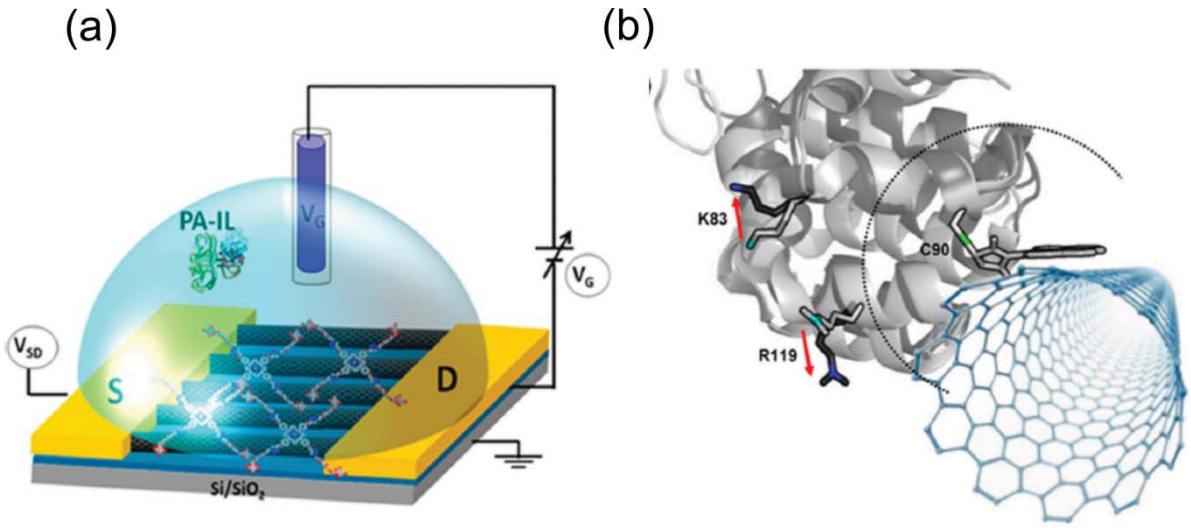

Figure 2.3.: (a) a sketch of a single-walled carbon nanotube field effect transistor that is gated via a Ag/AgCl reference electrode and functionalized with glycosylated porphyrins for selective detection of bacterial lectins. (b) Image of a single lysozyme attached to a single carbon nanotube via a pyrene-maleimide linker. The catalytic activity of the enzyme lysozyme was monitored online via the motion of the charges at residues 83 and 119 relative to the SWNT. (Image taken from [5])

Recently, the Star research group reported a sensor specific to certain bacterial lectins.[28] An AC dielectrophoresis (DEP) approach, which could also be applied on wafer-scale, was used to fabricate the SWNT devices. The devices showed excellent behavior in terms of sensitivity, selectivity and robustness. Specific detection of bacterial lectins was enabled by porphyrin-based glycoconjugates, synthesized using azide-alkyne “click” chemistry, immobilized on the CNTs. A detection limit of about

2 nM lectin concentration was observed and interactions between lectins and glycoconjugates could be probed by extracting the dissociation constant (K_D). This method can compete with standard techniques such as electrochemical surface plasmon resonance (E-SPR) and electrochemical impedance spectroscopy (EIS).

Nanotube devices not only have the potential to be integrated amongst standard biomedical assays, but also open the way to gaining additional scientific insight into biological processes. Hence, scientific frontiers are recently pushed forward with the help of SWNT-FETs. Understanding enzymatic activities, for example, is of fundamental importance as they are involved in numerous physiological tasks and thus are connected to many genetic diseases. Enzyme catalysis is accompanied by conformational changes of specific domains of the protein. Such motions, occurring at different rates, are commonly observed by fluorescent techniques such as Förster Resonance Energy Transfer (FRET).[29] One of the major draw-backs of this technique, however, is bleaching and quenching of the fluorophore labels attached to certain parts of the enzyme. The fluorophore itself also must be conjugated to the target enzyme, which can cause unwanted effects such as steric hindrance and conformational changes. The Collins research group overcame these restrictions of FRET by using a label-free electrical method, namely a field-effect transistor with a single semiconducting SWNT bridging source and drain electrodes.[25] A noncovalent functionalization scheme using a pyrene-maleimide linker was used to immobilize a single lysozyme on the surface of the carbon nanotube (Fig 1b). Consequently, the

dynamics of this lysozyme can be monitored for several minutes, which has not been achieved by any other method so far. They observed that upon introduction of this substrate, 100 glycosidic bonds are progressively hydrolyzed by the lysozyme at a hinge-binding rate of 15 Hz, followed by a nonproductive slow rate of 330 Hz. Considering that most of the surface charges of this molecule are screened by the electrical double layer (EDL), these rates are solely probed due to the 1 to 2 Å motion of two positively charged residues taking place at a distance of about 1-1.2 nm from the nanotube surface. Furthermore, they were able to probe the catalytic activity of lysozymes at different pH conditions leading to a set of independent parameters characterizing that system, such as the mean time the enzyme resides in each of its physical states and the separation energy between those states. In another recent publication, the Collins group used engineered variants of the S90C lysozyme with differently charged residues, such as negatively charged glutamates and neutral alanines to track down the net charge of the dominant (closest to the SWNT surface) sites of the lysozyme. This was accomplished by analyzing the effective change in gate voltage from the dynamic signals during catalytic activity of the lysozyme variants.[30] In other words, depending on the net charge of a residue that is moving relatively close to the SWNT surface, either a positive or a negative shift in the effective gate voltage is observed, which leads to quantitative conclusions about the electric landscape on the surface of the enzyme. In general, their findings represent an innovative way to monitor enzyme activity and dynamics. Due to the simplicity of the underlying physical mechanisms, this process can be applied to a vast number of proteins and enzymes without restricting their catalytic activity.

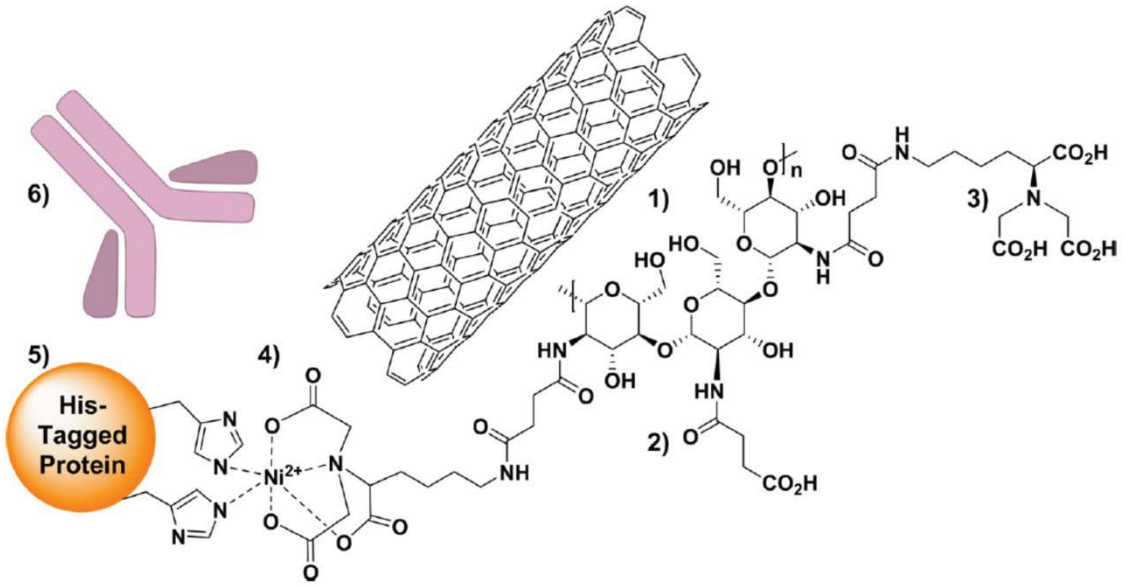

Figure 2.4.: Functionalization scheme for creating a single-walled carbon nanotube-based sensor array according to [31]: (1) SWNTs are wrapped with chitosan. (2) chitosan is reacted with succinic anhydride. (3) NTA groups are attached to the SWNTs via EDC-NHS coupling. (4) $Ni2^+$ is chelated to NTA group. (5) His-tagged proteins are attached to $Ni2^+$. (6) Protein-protein interactions lead to a displacement of $Ni2^+$ relative to the SWNT, which causes a change in NIR fluorescence. (Image taken from [5])

As can be seen in connection with the above-mentioned publications significant advancements have been made recently, yet medical diagnostics requires high throughput methods in realistic applications. In this context, Heath and co-workers have successfully exploited the Zweifach-Fung effect to separate blood cells from whole blood and direct small volumes of protein rich plasma to an array of sensors.[7] Future techniques involving SWNT electronic devices may rely on microarray chips integrated with microfluidics to allow for specific detection of bacteria, proteins, or other biomarkers in crude samples including soil, water or human specimens. Such

systems would allow for detection with minimum required sample volume in rapid point-of-care (POC) diagnostics.

2.2 Biosensors based on polymeric semiconductors

Besides the great achievements that were made towards SWNT-FET-based biosensors much effort was also put into OFET-based biosensors. As discussed above, the tremendous potential of SWNT-based sensors is essentially based on two features: (1) bio-functionalization of SWNTs has emerged as very reliable and stable since well-known chemistry can be applied here. (2) It is possible to fabricate SWNT-FETs with just one single-walled carbon nanotube bridging the source and drain electrode, which leads to extremely low detection limits, meaning not only single protein ligand interactions but much more also the detection of the motions of single domains of a protein. Of course, these benefits are not featured by OFET-sensors, at least not at this point. Yet, meaningful research in this context is also possible, when looking at the possibilities of this type of biosensor from a different perspective: indeed fundamental research demands ultra-sensitive single SWNT sensors, yet the requirements on a biosensor from an industrial, medical or every-day life perspective can be much lower. For example, when intending to detect signals from living cells, without doubt a polymeric sensor can be the biosensor of choice as it is more simple to produce and the size of cells is in the order of a few to a few tens of micrometers. In this context the applicability of P3HT-FETs for monitoring cell signaling was tested with the results that a P3HT-FET is able to easily detect changes in the electrolytic

environment that are in a relevant concentration regime, whether by simple electrostatic gating effects[32] or by a more sophisticated method, namely functionalizing the liquid-gate electrode with an ion-selective membrane.[33] Furthermore, by using methods such as surface functionalization with fibronectin, cells (mouse fibroblasts) are growing vividly onto the P3HT surface, meaning that the surface of the polymer can be made biocompatible.[34] And also equivalently to DNA sensing with SWNT-FETs, this type of sensing was also conducted with OTFTs by the group of Zhenan Bao.[35] Referring to the detection of DNA hybridization with OTFTs the work of the group of Ana Bonfiglio is also worth mentioning: they developed a OTFT biosensor (here TIPS pentacene was used, a solution processable variant of pentacene[36]) that cannot be harmed by the contact with water as only the gate electrode, inert gold, is getting in contact with the analyte.[37] Figure 2.5 shows the sensing device which enabled sensing of DNA hybridization without letting the semiconductor itself get in contact with the harmful electrolyte.

Contributions by the group of Luisa Torsi concerned the detection of biotin[38] and of streptavidin. The latter employed the formation of a supported lipid bilayer functionalized with biotins on the surface of P3HT-FETs.[39]

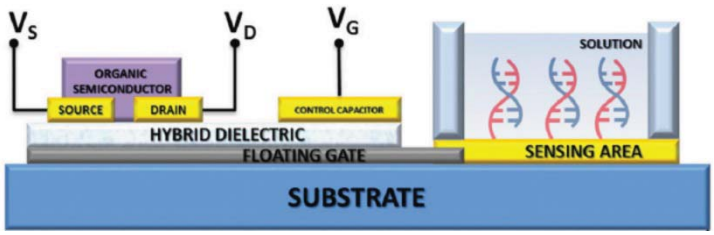

Figure 2.5.: DNA sensing device developed by the group of Bonfiglio. The gold electrode allows for simple functionalization schemes using thiols. Further the organic semiconductor is not in contact with the harmful electrolyte, preventing the device from degrading. (Image taken from [37])

2.3 Conclusion

Carbon nanotubes are on their way to being established as a versatile component in next-generation biomedical assays[5]. They offer the ability to be utilized as high-end biophysical tools to reveal subtle dynamics of single biomolecules as well as the potential to compete with common biological assays. For glycoprofiling, liquid chromatographic techniques (LC - for compound separation) are typically used in combination with mass spectrometry (MS - for detailed structural analysis). However, LC/MS requires relatively large sample volumes, is time-consuming, and glycan liberation from the protein is needed.[40] Other traditional techniques rely on labeling with fluorescently active molecules (ELISA, resazurin-reduction assay), complex and expensive equipment and are severely limited by photobleaching. In contrast, as the Strano group demonstrates, SWNTs which fluoresce in the NIR, are not susceptible to photobleaching and samples can be analyzed in a matter of minutes. SWNT array-based platforms could outperform conventional methods in terms of label-free and

rapid online monitoring of biological interactions without suffering from a loss in simplicity and sensitivity.

While recent progress towards advancing biomedical techniques with SWNTs has been significant, attention still must be paid to several areas. Electrical sensors built on nanotube structures are highly susceptible to Debye screening, and therefore the surrounding media and size of functionalization molecules is vitally important. Further work must be done to adapt these sensors for applications in complex media while still retaining selectivity and sensitivity.

In summary it is to say that also the field of biosensing with organic thin-film transistors made big advances in the last years. This is remarkable as, in contrast to SWNT-FETs, the biofunctionalization of OTFTs turned out to be very challenging. Yet it is believed that when combining several features that are supported by these devices such as processing biodegradable[16] electronic biosensors and using standard functionalization schemes[41] it is possible that OTFT-biosensors can be employed as sensors for medical diagnosis as well[42].

3 Basic principles

In this section a general overview of the theoretical aspects and underlying principles of this thesis is be provided.

First, carbon nanotubes and polymeric semiconductors will be introduced. Subsequently it will be discussed briefly what a field-effect transistor is and how it works. Next the properties of electrolytic solutions will be discussed and finally the protein, which serves as a model system for this work, will be presented.

3.1 Semiconductors

3.1.1 Carbon nanotubes

In this chapter carbon nanotubes are discussed as semiconducting components for field-effect transistor based biosensors. The fact that carbon nanotubes consists exclusively of surface atoms clearly poses significant consequences for biosensing, namely that all yet so slight changes of the electrostatic environment of the SWNT lead to conductance changes of the SWNT-FET. Therefore one expects that SWNT-FETs are very sensitive biosensors.

A carbon nanotube is a sheet of graphene that is rolled up in a way that the resulting structure reveals a cylindrical shape. Further the resulting cylinder has a diameter in the range of roughly 1 nm and a length ranging up to ca 500 mm.[43] Yet not only are their physical properties interesting but also their electrical properties.

Carbon nanotubes may be metallic or semiconducting depending on how the graphene sheets are wrapped up. The electrical nature of carbon nanotubes results from different possibilities to fold a sheet of graphene as depicted in Figure 3.1, wherein this is given by the so called chiral vector $\overrightarrow{C_h}$, which is defined according to the equation below:

$$\overrightarrow{C_h} = n\overrightarrow{a_1} + m\overrightarrow{a_2} \equiv (n, m) \qquad 3.1$$

And wherein n and m are integers with $0 \leq |m| \leq n$. Further the diameter of a single walled carbon nanotube is defined by the absolute value of the chiral vector and thus:

$$d = \frac{|\overrightarrow{C_h}|}{\pi} = a/\pi\sqrt{n^2 + nm + m^2} \qquad 3.2$$

and also $a = \sqrt{3}a_{CC}$,whereat a is the lattice constant of the hexagonal graphene lattice with $a_{CC} \cong 1.42$ Å is the length of a carbon-carbon (CC) bond.

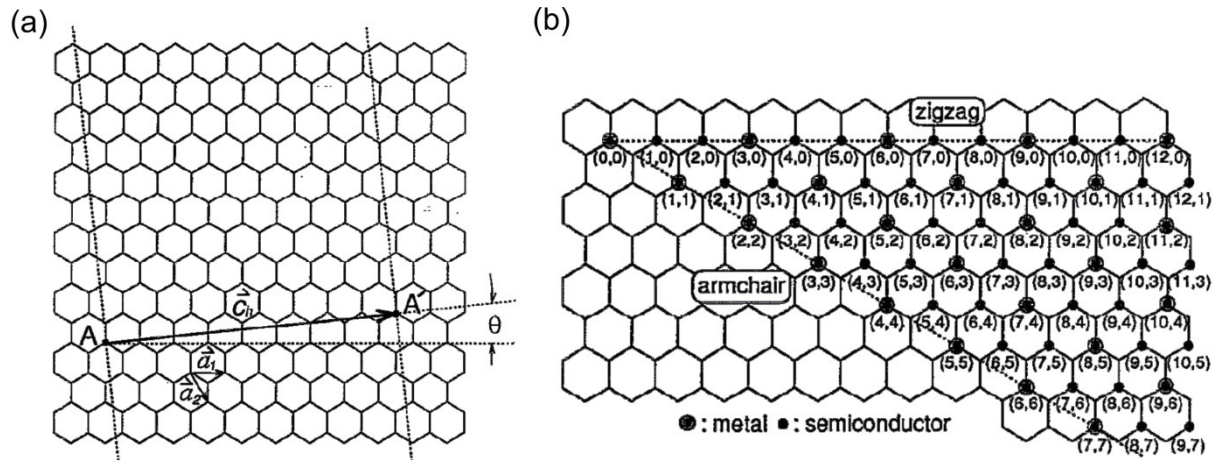

Figure 3.1.: Single walled carbon nanotubes (SWNTs) are formed by wrapping graphene sheets into cylinders. The type of wrapping is determined by their lattice or chiral vector $\overrightarrow{C_h}$. Θ is the chiral angle and $\overrightarrow{a_1}$ and $\overrightarrow{a_2}$ are the unit vectors of graphite. In (b) possible vectors are depicted that lead to either a metallic or semiconducting nature of the nanotubes. (Image taken from [44])

The chiral angle Θ that is the angle between $\overrightarrow{C_h}$ and $\overrightarrow{a_1}$ defines the twist of the hexagons relative the axis of the SWNT and its numeric value is between 0° and 30° due to the hexagonal symmetry. Θ = 0 (or m = 0) results in a zigzag-SWNT, Θ = 30° (n=m) results in the so-called armchair configuration, in all other cases ($n \neq m \neq 0$) the SWNT is called chiral. In Figure 3.2 sketches of all three examples are shown. (a) shows a tube with a chiral vector of (12,0) resulting in the zigzag configuration, (b) a tube revealing an armchair configuration and an (6, 6) and (c) shows a chiral carbon nanotube.

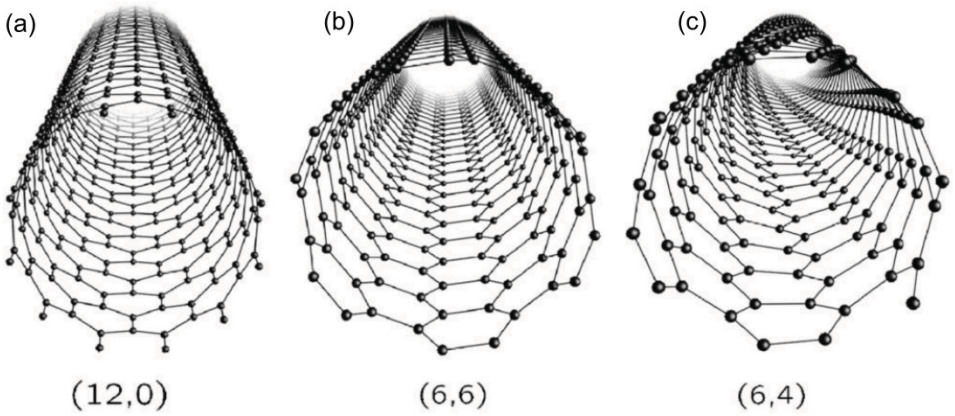

Figure 3.2.: Sketches of the atomic structure of SWNTs with (a) $\overrightarrow{C_h}$.= (12,0) resulting in a zigzag configuration, (b) $\overrightarrow{C_h}$.= (6,6) yielding the so-called armchair configuration and (c) $\overrightarrow{C_h}$.= (6,4), a so-called chiral nanotube. (Image taken from [45])

Amongst other theoretical methods such as the "tight-binding method" [46] also the "zone-folding approximation" [45] give an excellent approximation of the band structure of SWNTs. According to the zone-folding approximation a general rule for the semiconducting behavior of nanotubes is derived, namely carbon nanotubes are metallic if $n - m = 3l$ with an integer l ($n - m = 3l \pm 1$). As a consequence it is to say that most SWNTs are semiconducting in nature and only 1/3 is metallic. The band structure of SWNTs which is derived in this approximation from the band structure of graphene (a zero band gap semiconductor[47]).

The band structure of metallic and semiconducting SWNTs is shown in Figure 3.3. For metallic SWNTs the valence and the conduction band cross each other at the Γ-point. Yet, the semiconducting carbon nanotubes in the zigzag configuration reveal a finite band gap at the Γ-point.

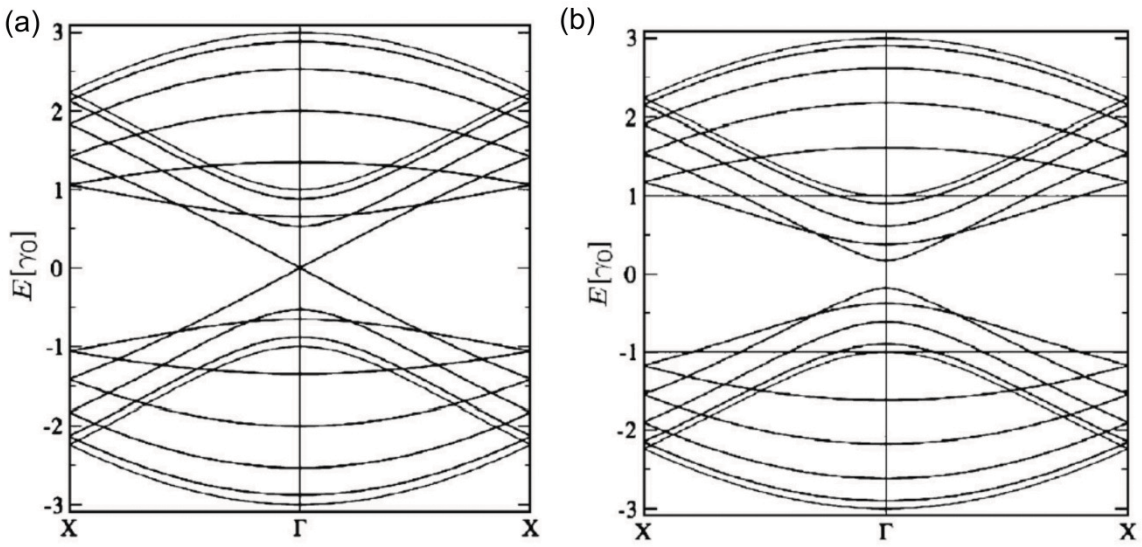

Figure 3.3.: The band structures for metallic SWNTs (in the zigzag configuration with (9.0)) (a) and semiconducting SWNTs (in the zigzag configuration with (10, 0)) (b) according to the zone-folding approximation. (Image taken from [45])

3.1.2 Polymeric semiconductors

Within the work for this thesis besides carbon nanotubes also a polymeric semiconductor was used to build field-effect transistors and to perform biosensing experiments. In the following the fundamental principles of this type of semiconductor shall be discussed:

Foremost it is noteworthy that organic semiconductors comprise two major material groups, namely polymeric organic semiconductors and so called semiconducting small molecules. Probably the most prominent example for low-molecular organic semiconductor is pentacene, which consists of five linearly-fused benzene rings.[48] In contrast to polymeric semiconductors, small molecules are usually deposited from

the gas phase onto the substrate. Depositing a material from the gas phase may hold several disadvantages: a deposition from the gas phase requires a suitable deposition facility (including vacuum pumps, e.g.). Further it requires personnel and money to service such a facility. This is in contrast to a spin-coater (or even simpler, a pipette) which is extremely cost effective and easy to handle. With a spin-coater polymeric semiconductors can be easily spun onto a desired substrate. Throughout this work only polymeric semiconductors were used for experiments thus we will focus on them also in the theory-part of this thesis.

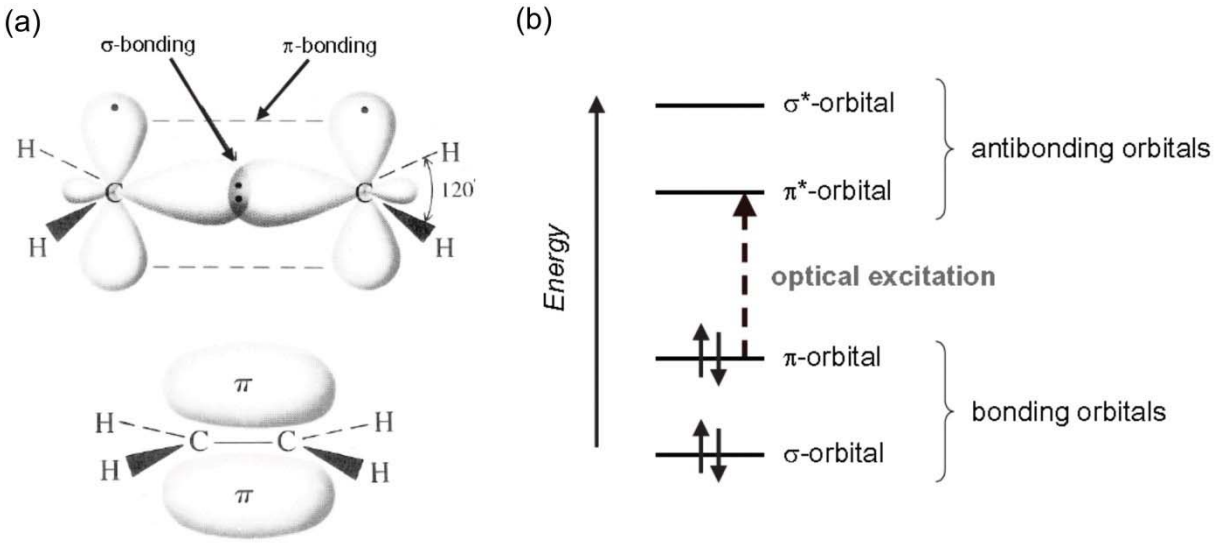

Figure 3.4. (a) is a sketch of a conjugated π electron system showing π and σ bond of ethane ($H_3C–CH_3$). (b) is a sketch of the energy levels of a conjugated π electron system, showing that the lowest electronic excitation state is between the boning π orbital and the antibonding π* orbital. (Image from [49])

The polymeric semiconductor used for experiments within this thesis is a regioregular poly(3-hexylthiophen-2,5-diyl), poly(3-hexylthiophene), abbreviated rr-

P3HT or throughout this work simply as P3HT. P3HT is a p-type semiconductor which has gained attention as component in thin-film transistors and optoelectronic devices due to its excellent electrical properties as it reveals high field-effect mobilities (~ 0.045 $cm^2/(Vs)$) and relatively high on/off ratios (~ higher than 10^3).[50,51]

In the following the reason of the semiconducting behavior of organic semiconductors and especially polymeric semiconductors is be explained briefly:

The semiconducting behavior arises from their nature as so-called conjugated systems. A conjugated system is a molecular or polymeric system of interconnected π-orbitals with delocalized electrons. The sketches in Figure 3.4 illustrate what conjugated π-systems are by means of ethane, which is the simplest conjugated π-system. P3HT however, reveals alternating single and double carbon-carbon bonds and thus the π-system is similarly formed by p_z orbitals of sp^2-hybridized carbon atoms.[49] Organic semiconductors are intrinsically very different from inorganic semiconductors (e.g. Si) as bonding in inorganic semiconductors occurs via covalent interactions whereas bonding in organic semiconductors is due to much weaker van-der-Waals interactions. Generally this leads to many differences in the material properties such as a much weaker delocalization of the electrons in organic semiconductors. However, similarly to their inorganic counterparts, conjugated systems reveal something like “valence” and “conduction” bands that are called highest occupied molecular orbital (HOMO) and lowest unoccupied molecular orbital (LUMO). The bandgap lies usually within 1.5 eV to 3 eV (for P3HT the gap between

HOMO and LUMO is reported to be around 2 eV[52], which also leads to light emission or absorption in the visible part of the electromagnetic spectrum.

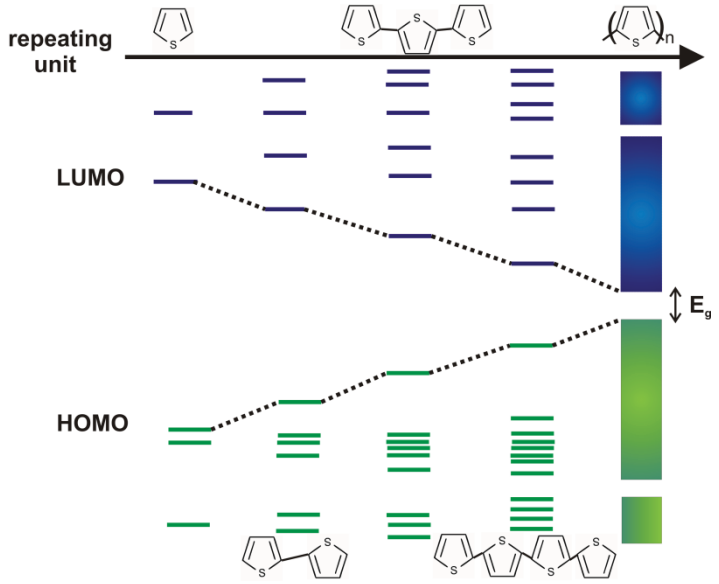

Figure 3.5.: Illustration of the energy level splitting and band formation of a polymer originating from the states of a thiophene molecule. For an infinite long polymer chain the bonding and antibonding orbitals result in continuous HOMO and LUMO bands. (Image taken from [53])

Figure 3.5 shall illustrate the origin of the band formation of a polymer (based on thiophene molecules, respectively). As shown in [49] and [54], the amount of bonding and antibonding orbitals in a system increases directly proportional to the number of carbon atoms. Hence, for an infinite long polymer chain the bonding and antibonding orbitals result in continuous HOMO and LUMO bands. Electrons in the LUMO state are considered to be delocalized and to be able to travel around the backbone of the polymer, which leads to a semiconducting (and also fluorescent) behavior.

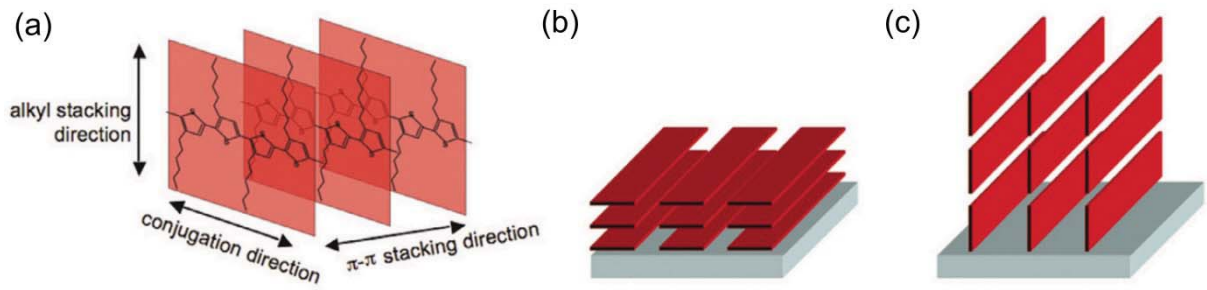

Figure 3.6.: A schematic representation of the crystallite structure of polythiophenes. In (a) the different transport directions are depicted. Depending on the orientation of the crystallites, the transport of the charge carriers can occur slower or faster[55] (Image taken from [55])

The mobility of the charge carriers in P3HT is intrinsically highly anisotropical as sketched in Figure 3.6. This is a result of the supramolecular ordering of the P3HT crystallites. The crystallites are ordered in a way that the π-orbitals that belong to different polymer chains are stacked cofacially. Herein charge transport occurs preferably in the conjugation direction. There is also charge transfer along the π-π-stacking direction due to overlapping π-orbitals. However, in the third direction, the direction of alkyl stacking, barely any charge transfer occurs. P3HT thin films are known to crystalize in fibrillar mesostructures, crystallites with a rod-like shape after spin-coating. It is suggested in literature that the polymer backbones is located perpendicular to the long axis of the rods (π-π-stacking direction) and that the width of the P3HT rods is directly proportional to the average chain length.[55]

3.2 Field-effect transistors as biosensor

3.2.1 Field-effect transistors

Generally speaking, a field-effect transistor is a three-terminal device which shows a current between the source and drain electrode (throughout this thesis this current is denoted as drain current (I_D) or source drain current (I_{SD})). The drain current depends on the modulation of the applied potential between the source and the drain electrode and the drain current is additionally a function of the voltage that is applied between the source and the gate electrode. Sketches of electrolyte-gated and back-gated field-effect transistors are shown in Figure 3.7. In the schematic representation of Figure 3.7 the semiconductor is depicted as a carbon nanotube. However, this is only an example and the following principles are not limited to the type of semiconductor. Yet, also polymeric semiconductors or simply bulky semiconductors such as silicon may be taken into consideration. Naturally different types of semiconductors require different mathematical approaches. Still the very fundamental aspects of field-effect transistors hold true regardless of the type of the semiconductor and can be used as a first approximation, even for more exotic types such as carbon nanotube field-effect transistors.

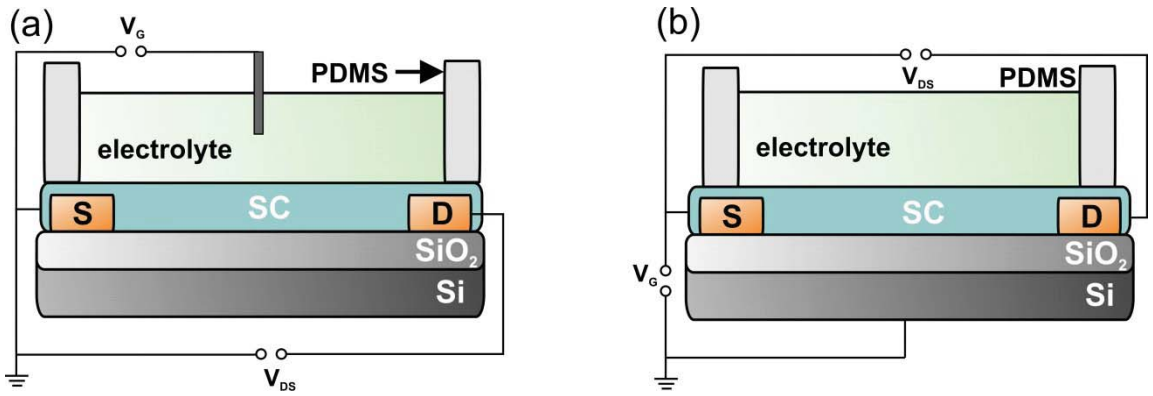

Figure 3.7.:(a) is a schematic representation of a an electrolyte-gated field-effect transistor device. The substrate is a Si-wafer with a SiO_2 layer on top. The letters "S" and "D" denote the metallic source and drain electrodes. Between the source and drain electrodes a semiconductor is deposited. Within the borders that are posed by the PDMS chamber a liquid dielectric is be inserted. For an electrolyte-gated FET the gate voltage is be applied via an electrode that is directly immersed in this dielectric. (b) shows a back-gated field-effect transistor. In this case, the silicon oxide layer acts as the gate dielectric.

Figure 3.8 shows the characteristic electric curves from a field-effect transistor. In Figure 3.8 (a), a so-called output curve is depicted. An output curve shows the drain current as a function of the drain bias while keeping the gate voltage fixed at certain values. It is possible to distinguish between the so-called "linear regime" and the so-called "saturation regime". In the latter the drain current does not depend anymore on the drain voltage. However, the drain current does depend on the drain voltage in the linear regime. Figure 3.8 (b) is a sketch of a so-called transfer curve. A transfer curve gives the dependence of the drain current on the modulation of the gate bias at a fixed drain potential. The threshold voltage is defined as the voltage at which the transistor switches from its "off-" to its "on-" state. Mathematically the charge transport through the channel of a transistor can be described as follows:[56,57]

For a gate potential (V_G) that is higher than the threshold voltage (V_{th}) equation 3.3 holds true for charges along the channel length:

$$Q = C(V_G - V_{th} - V(x)) \tag{3.3}$$

In the equation above C is the gate coupling capacitance of the gate oxide, with

$$C = \epsilon_0 \epsilon_{ox} \frac{1}{d_{ox}} \tag{3.4}$$

Further the current that flows from the source electrode to the drain electrode can be described as:

$$I_D = W \mu Q E(x) \tag{3.5}$$

with μ the charge carrier mobility and $E(x)$ is the electric field along the channel. Using the equations above and integrating it over the channel length L, one yields an expression for the drain current:

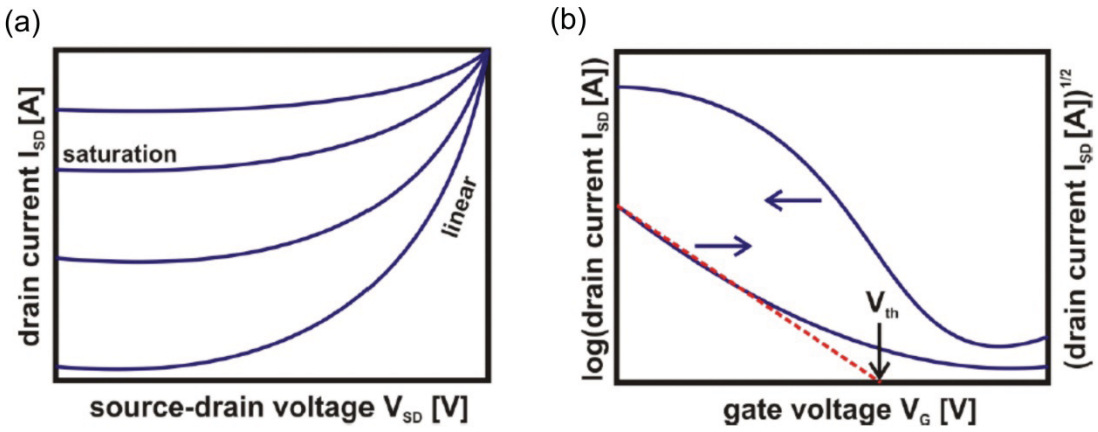

Figure 3.8.: Sketches of the electrical transistor characteristics. (a) shows an output, which is the drain current as a function of the drain voltage at different gate biases (the higher the gate bias, the higher the absolute value of the drain current). An output curve reveals a so-called saturation regime and a linear regime. (b) is a transfer curve, that gives the dependence of the drain current on the gate voltage. The threshold voltage (V_{th}) gives the gate base limit at which the device switches from its on-state to its off-state. (Image taken from [53])

$$I_D = \frac{W}{L}\mu C\left[(V_G - V_{th})V_D - \frac{V_D^2}{2}\right] \qquad 3.6$$

In the linear regime which is characterized by small drain biases (meaning, $|V_D| \ll |V_G - V_{th}|$) the equation can be simplified to:

$$I_D = \frac{W}{L}\mu C(V_G - V_{th})V_D \qquad 3.7$$

The transconductance of a transistor is defined as:

$$g_m = \left.\frac{\partial I_D}{\partial V_D}\right|_{V_G=const.} \qquad 3.8$$

Using the approximation $Q = C(V_G - V_{th})$ and 3.7 yields:

$$g_m = \frac{W}{L}\mu C V_D \qquad 3.9$$

Now that the fundamentals of field–effect transistors were discussed briefly, it will be described how the operation principles of a field-effect transistor can be exploited to detect biomolecules.

3.2.2 Electrolytes

Biosensing with field-effect transistors relies in many cases on alterations of the transfer characteristic of a field-effect device with respect to the presence of a biological species. The natural environment of biological species is a liquid and electrolytic environment, such as a buffer solution or a cell medium. Hence the composition of an electrolyte is of importance to understand a field-effect biosensor. An aqueous electrolytic solution, for example water, contains a certain amount of salt (the amount of salt is not necessarily fully dissociated in water).

A popular example for a salt is sodium chloride (*NaCl*). In water sodium chloride can dissociate into a positive sodium ion (Na^+) and a negative chloride ion (Cl^-). For sodium chloride the suitable dissociation/association reaction writes as follows:

$$NaCl \leftrightarrow Na^+ + Cl^-$$

Hence an electrolyte reveals ionic charge carriers in solution. This results in the fact that an electrode or a charged particle, which is put into an electrolyte, causes the

formation of a so-called electrical double layer at the interface to the electrolyte. There are several models and approximations that describe the potential at the electrode/electrolyte interface; amongst those methods one of the most prominent ones is the Gouy-Chapman-Stern model. According to this model several layers occur at the interface. These layers are illustrated in Figure 3.9.

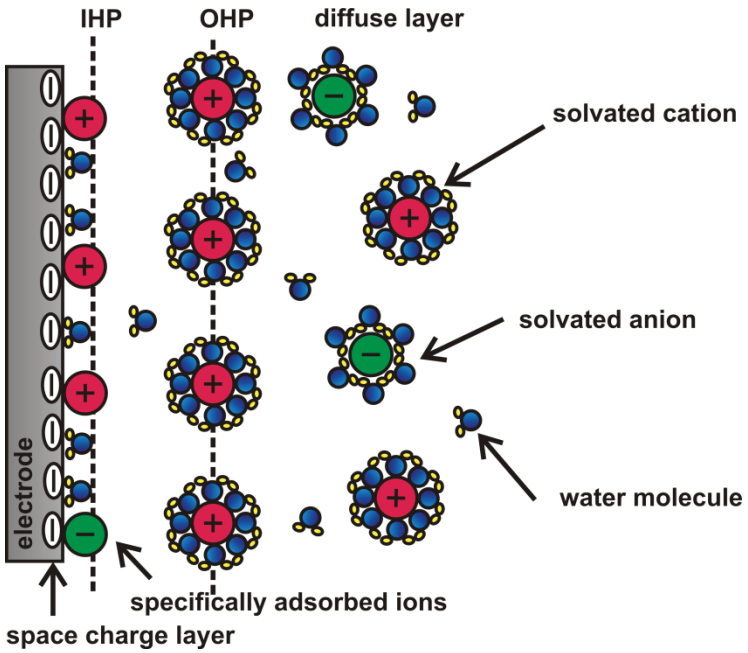

Figure 3.9.: A schematic representation of the electrical double layer at an electrode/electrolyte interface. Ions and water molecules in solution are screening electrical charges in solution. The higher the ionic strength of the electrolyte the more effective is the screening.

The layers will be described in the following: There exists the so-called space charge layer that is a diffusive layer consisting of charge carriers in the electrode. Further there is the so-called inner Helmholtz plane (IHP) that arises due to specifically adsorbed ions and water molecules at the electrode. Next to the IHP

comes the OHP, the outer Helmholtz plane, which is a layer of solvated ions that is closest to the metal. Hence those charged species arrange themselves around a charged surface and are screening the charge of the surface from the outside. Consequently the potential that is caused by a charged particle (a protein or a DNA-strand) at a certain distance from the surface of that particle depends on the ionic strength of the electrolyte. This gives rise to a fundamental feature of species and surfaces in liquid, namely the Debye screening length that can be described mathematically according to equation 3.10.

$$L_D = \frac{1}{\sqrt{4\pi L_B \sum \rho_i z_i^2}} \qquad 3.10$$

L_D gives the distance that is required to screen local surplus charges in an electrolyte. With L_B is the Bjerrum length (0.7 nm) and ρ_i and z_i the density and the valence of ion species *I*. The Bjerrum length is :

$$L_B = \frac{e^2}{4\pi\varepsilon_0\varepsilon_r k_B T} \qquad 3.11$$

with *e* is the elementary charge, ε_r is the relative dielectric constant and ε_0 the vacuum permittivity. Thus, for water at room temperature the Bjerrum length is about $L_B \approx 0.7\,nm$. From the equation above it can be deduced that a high ionic strength leads to a more effective screening.

Looking at Figure 3.9 the resulting structure resembles a capacitor and thus for a flat surface the capacitance can be described according to:

$$C_{DL} = \frac{1}{L_D} \qquad 3.12$$

In summary following features should be considered when conducting electrical sensing experiments in electrolytes:

The higher the buffer and the electrolyte concentrations, the smaller the Debye screening length and thus the more effective biomolecules are screened from the sensitive surface of FETs. That means a low ionic strength is advantageous for biosensing. Further it is noted that also solely water molecules without the presence of buffer or salt cause electrical screening. This is as water is a polarized molecule and it also auto-dissociates into hydronium and hydroxide.[58] Additionally it has to be considered that in the natural environment of a protein relatively high salt concentrations occur. That is, in standard experiment buffer concentration of around 100 mM are usually preferred. These concentrations, however, may lead to screening lengths that are smaller than the diameter of the protein that is analyzed.

3.2.3 Biosensing

With the help of the principles that are described above, it is now possible to outline what is expected when sensing biomolecules (e.g. proteins) with FETs. Figure 3.10

below is a schematic representation of an FET (a), including different effects and phenomena that occur at the interface between semiconductor and electrolyte (b-e):

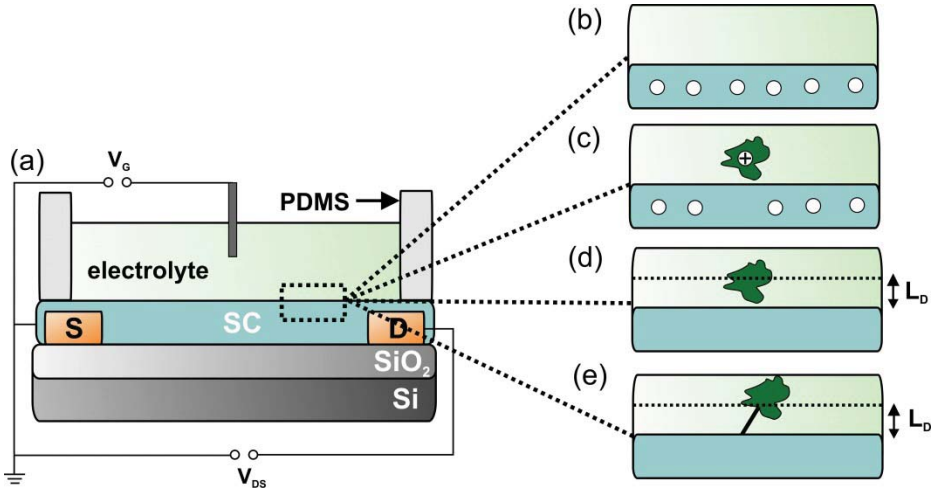

Figure 3.10.: (a) is a schematic representation of an electrolyte gated FET. (b) to (e) depict the interface between the semiconductor and the electrolyte. The white circles in (b) depict charge carriers that are present in the channel of the semiconductor. (c) is a sketch of the charged protein. (d) shows that the Debye screening length (L_D) screens a fraction of the protein form the semiconductor channel. (e) shows a ligand that is tethered to the semiconductor surface and binds specifically to the protein.

Figure 3.10 (b) is a sketch of a part of the interface between semiconductor (SC) and electrolyte. Charge carriers (in our case, holes) are present in the semiconductor and causing an electric current between the source and the drain electrode. A protein is electrically charged (for a detailed discussion of this concept see Chapter 8. The presence of the charge of the protein can cause alterations of the current between the source and the drain electrode (c). These alterations should be detectable via the transistor characteristics (e.g. depending of the potential of the biomolecule a left shift

or a right shift of the transfer curve is expected)[21]. However, additional effects make sensing more complicated. That is, for example, Debye screening (d). Only a fraction of the protein is not screened by ions that are present in the electrolyte. Additionally unspecific adsorption makes biosensing difficult (see Chapter 7). Usually the semiconductor surface is functionalized with ligand molecules (represented as a black rod in (e)) that bind specifically to a protein. However, the actual size of the ligand molecule causes even a larger fraction of the protein to be screened from the sensitive semiconductor surface (e).

In order to experimentally test the above described concepts not just an arbitrary protein/ligand system was chosen, but a system that is expected to provide more benefits compared to standard systems. This protein/ligand system is introduced in the following:

3.2.4 The CaptAvidin-biotin system

Throughout this thesis the properties of SWNT-FET and P3HT-FET biosensors were tested based on a particular protein-ligand system, namely CaptAvidin (the protein) and biotin (the ligand). In the following the features and benefits of this system shall be summarized.

It is of importance to pick a biological system that is well known when assessing the feasibility, advantages and disadvantages of a new biosensor. Additionally it can be beneficial if the biosystem would allow for repeating an experiment. That is because protein sensors are usually developed in a way that a protein ligand is immobilized

onto a sensitive surface of the device. Sensing is then probed by “binding” proteins that bind to that specific ligand onto the surface. The usual biosystem for this bench test experiment is biotin in combination with avidin or streptavidin. However, the binding affinity of biotin to avidin to streptavidin is so strong (almost covalent), that harsh conditions have to be applied in order to unbind avidin or streptavidin from the surface again. Hence, the respective sensor can only be used one single time. In this regard a system was chosen that has the following advantages:

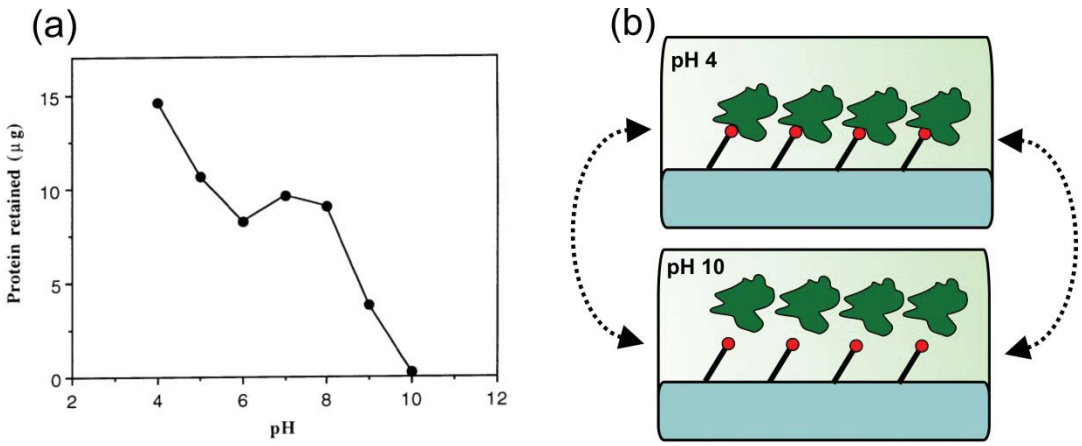

Figure 3.11.: (a) The interaction of a biotinylated BSA with an avidin-Sepharose column. Best binding was found by Morag et al. at pH 4 and complete dissociation occurs at pH 10 (image taken from [59]). (b) is a schematic representation of the sensing principle with CaptAvidin and biotin.

CaptAvidin binds reversible to biotin, the binding affinity of CaptAvidin to biotin depends on the pH value of the buffer solution and is consequently adjustable, CaptAvidin has the highest affinity to biotin at pH 4 and at pH 10 the bond should be completely dissociated, which was evaluated from experiments with Sepharose

columns (Figure 3.11 (a)) and by surface plasmon resonance.[59,60] The features of CaptAvidin are expected to be beneficial when it comes to sensing with FETs. One obvious advantage is that a lot more data can be obtained from one single transistor device. This is because the transistor can be recovered by washing it with a pH 10 buffer solution. After that the transistor should be regenerated and CaptAvidin can be incubated on the device once more (depicted in Figure 3.11 (b)). That means that the error that occurs by comparing two unequal transistor devices is eliminated.

3.3 Conclusion

In conclusion it is to say that organic field-effect transistors are promising candidates for next-generation biosensing applications. This is, amongst other reasons, due to the fact that organic materials could be integrated in small and flexible sensing platforms and thus many portable applications are thinkable.

However, biosensing means, the sensor needs to endure operation in electrolytic environment. This alone poses a lot of challenges. An electrolyte contains positive and negative ions that might cause shielding effects. Meaning, an analyte might get screened from the sensitive surface of the biosensor instead of being detected by it. This thesis will assess the suitability of organic FETs as biosensors and address the challenges mentioned above.

4 Methods and fabrication

This chapter is intended to give the experimental methods that were used to fabricate SWNT- and P3HT-based biosensors as well as the methods that were applied to conduct biosensing experiments with those devices. However, methods and parameters throughout this thesis were adapted to the needs of the respective experiments. Hence, much more details and parameters are provided in the experimental sections in the subsequent chapters. For example, in Chapter 5 a comparison of P3HT-FETs and SWNT-FETS is given, whereat the devices of both types were fabricated via spin-coating. Also in the same chapter the majority of electrical data were recorded under a constant flow of electrolytes in order to analyze the dynamic behavior of the FETs. Additionally those data were obtained using the electrolyte gate architecture. In contrast to that, the experimental methods of Chapter 6 differ in parts to that of Chapter 5. This is, for example, the deposition method. In Chapter 6 the SWNTs were disposed via spray coating, instead of spin coating. However, the deposition methods used in Chapter 5 and Chapter 6 rely both on CMC-based carbon nanotube inks (see section below), the method that was used to fabricate SWNT-FETs in Chapter 8 is based on dielectrophoresis, which does not require a dispersant such as CMC.

This section will provide a first insight how the field-effect transistors were fabricated from solution, by a description how measurements in liquid could be realized.

4.1 Solution processing

As mentioned in the previous sections, carbon nanotubes as well as P3HT feature the possibility of being deposited from solution onto a pre-patterned substrate. The pre-patterned substrate is shown in Figure 4.1. The substrate comprises a highly doped silicon wafer with a thin silicon dioxide layer on top (the dioxide layer is not shown for simplicity). Gold electrodes were patterned onto the substrate using photolithography (details about this subject are provided in the Chapters 5, 6 and 8).

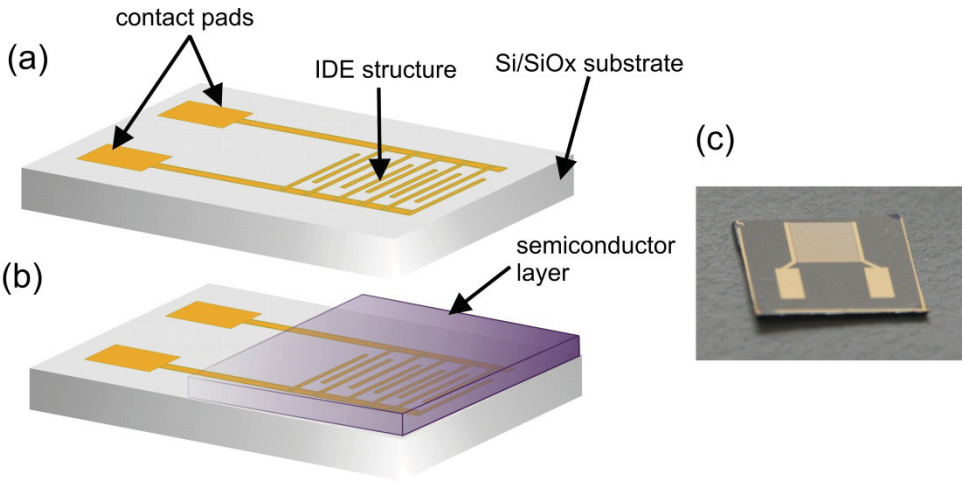

Figure 4.1.: (a) shows a schematic representation of a Si/SiO2 substrate with a interdigitated electrode structure and contact pads. (b) shows a schematic representation of a pre-patterned substrate after the deposition of a semiconductor layer. (c) is a photograph of a pre-patterned substrate prior to the deposition of a semiconductor.

The gold layer had a thickness of 40 nm by default and the adhesion between silicon dioxide and gold was promoted using a 5 nm thick chromium layer. The gold electrodes were formed as an interdigitated electrode structure (IDES). In Figure 4.1 a pre-patterned substrate before (a) and after (b) the deposition of a semiconductor is shown. Figure 4.1 (c) is a photograph of a pre-patterned substrate.

After the preparation of the pre-patterned substrate the semiconductor can be deposited onto the substrate. In Figure 4.2 a spin coating process of a semiconductor is depicted exemplarily. The black rods in Figure 4.2 represent semiconducting particles or molecules and may stand for carbon nanotubes or P3HT molecules. As a part of a spin coating process, the pre-patterned substrate has to be mounted on a rotating disc. While the disc is spinning at a fixed velocity, a semiconductor solution is deposited onto the substrate.

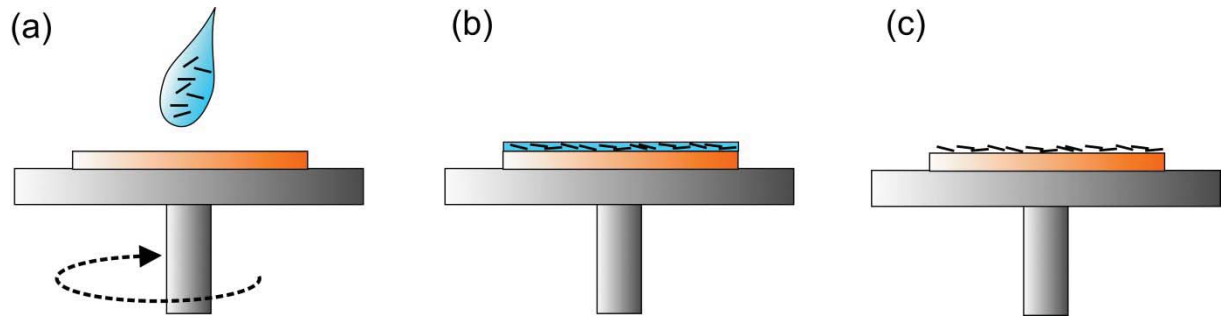

Figure 4.2.: (a): P3HT or carbon nanotubes (black rods) can be dissolved or dispersed in a solvent (blue). A substrate (orange) is placed on a spin-coater (grey) whilst spinning. (b): a uniform layer forms on the substrate. (c): the solvent is removed and the semiconductor remains on the substrate.

The spinning causes the solution to form a uniform film on the substrate (see Figure 4.2 (b)). After spin-coating the solvent needs to be removed, for example by heating the substrate up to a certain temperature (see Figure 4.2 (c)). However, the process of removing the solvent depends on other parameter and is discussed later on in this thesis in more detail.

4.1.1 SWNT-ink

Carbon nanotubes are hydrophobic in nature[61] and as a consequence they form clusters and bundles in an aqueous solution. Naturally, devices that would be fabricated from such a solution would have completely random electrical properties. Thus it is desirable to disperse the tubes in a way that the bundles comprise just a very small number of tubes or if possible to create SWNT-inks that do not feature bundles at all. Other research groups[62] but also researchers at the Institute for Nanoelectronics have developed a way to disperse carbon nanotubes in water with the help of a cellulose gum, namely sodium carboxymethyl cellulose (CMC) – a dispersing agent that wraps itself around the SWNTs during ultrasonication.[63,64] Yet, another aspect of this method is that the CMC has to be removed after the deposition of the SWNTs using a nitric acid treatment. Dispersing approaches comprising CMC feature the advantage that the CMC-SWNT-dispersion is very stable over time in contrast to dispersing SWNT in organic solvents (some organic solvents disperse SWNTs very well, see Chapter 8).[65,66] Organic solvents offer the advantage that no surfactants or the like get in contact with the surface of the carbon nanotubes.[65,66]

This can be advantageous, at least when considering the surface functionalization of the tubes, that requires surfaces of carbon nanotubes that are as “clean” as possible.

4.1.2 P3HT solution

P3HT is also hydrophobic and not soluble in water. Yet, it is soluble in various types of organic solvents and the degree of solubility is very high.[67] The solvent that was used throughout this thesis was 1,2 dichlorobenzene (DCB, $C_6H_4Cl_2$). The resulting features of spin-coated P3HT films were analyzed already in preliminary studies and theses.[67,53] Briefly, dissolving 1 w.t.% of P3HT in DCB and spin-coating the resulting solution onto a silicon wafer with a rate of 1000 rpm for a duration of 90 seconds results in a film thickness of roughly 50 nm. P3HT-wafers have to be put on a hotplate after spin-coating for the remaining solvent to be evaporated. A feature of P3HT devices that was developed within this thesis was that after use of a P3HT-FET, the polymer was removed from the chip by using ultrasonication, q-tips and DCB-baths. This enabled re-using pre-patterned chips after cleaning them.

4.2 Measurements in aqueous conditions

Biosensor measurements need to be performed in aqueous conditions. Hence biosensor setups require a special type of equipment. Perhaps the simplest form of such equipment is a ring made from PDMS (depicted in Figure 3.7, respectively) that is directly mounted on the sensor chip. The volume of the inserted liquid is then controllable via a pipette. A similar type of such simple liquid compartments is

described in Chapter 8.1. There the liquid compartment is formed by a truncated Eppendorf tube. However, the simplicity of such an approach also holds the disadvantage that no measurements can be conducted, that would require a constant flow of an electrolyte. For such measurements a flow chamber is beneficial.

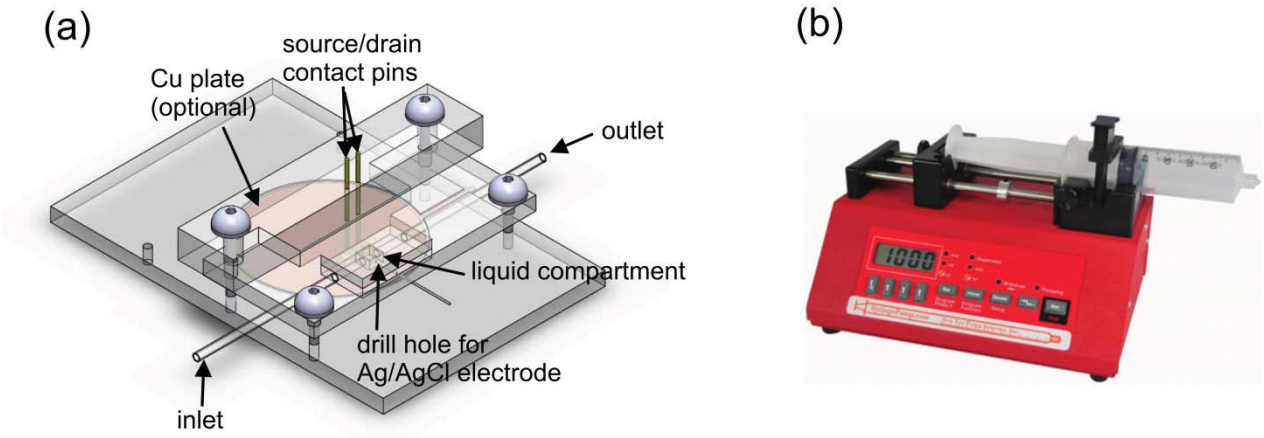

Figure 4.3: In (a) a drawing of a custom made flow chamber as used in Chapter 5 is depicted. Using this flow chamber it is possible to direct an electrolyte from an inlet via a liquid compartment, where the IDE structure of the transistor is located, to an outlet. The flow chamber comprises a drill hole that is needed to insert a Ag/AgCl electrode and to contact pins for the source and the drain electrode. Furthermore the flow chamber comprises a notch where a copper plate can be inserted in order to optionally apply a gate voltage to the back gate. (b) shows a photograph (image taken from [68]) of a NE-1000 programmable syringe pump. Syringe pumps were connected via flexible tubing to the inlet of the flow chamber.

For such purposes a flow chamber as depicted in Figure 4.3 was developed. The flow chamber comprises a drill hole that is needed to insert a Ag/AgCl electrode and to contact pins for the source and the drain electrode. Furthermore the flow chamber

comprises a notch where a copper plate can be inserted in order to optionally apply a gate voltage to the back gate. (b) shows a photograph of a NE-1000 programmable syringe pump (New Era Pump Systems Inc.). Syringe pumps were connected via flexible tubing to the inlet of the flow chamber.

4.2.1 Ag/AgCl electrodes

Silver chloride electrodes were home-made. This has the advantage that very small electrodes (about 1 mm diameter) could be used. Furthermore the electrodes could be replaced after experiments (because of this contamination with proteins could be avoided). For this purpose two clean silver wires were immersed in a 3 M KCl solution. Then a constant current (250 µA) was applied via a current source for about one hour. The chlorinated electrode was rinsed with DI water and ready to use as an electrolyte gate electrode. A sketch of the Ag/AgCl production process is shown in Figure 4.4.

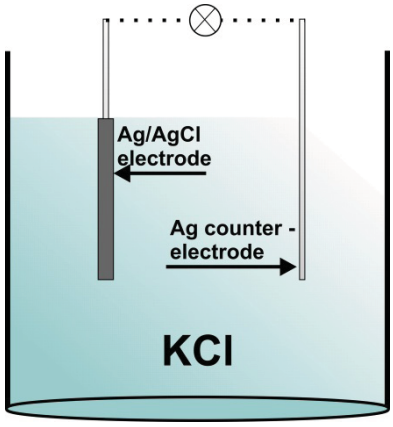

Figure 4.4.: A schematic representation of how silver chloride (Ag/AgCl) were made from silver wires. Two silver wires were immersed in a 3 M KCl solution and a constant current (250 µA) was impinged.Home-made Ag/AgCl electrodes reveal the advantage that the diameter of the Ag/AgCl electrode can be chosen freely.

5 Polymeric and Carbon nanotube based FETs– a comparison

In this chapter electrolyte-gated SWNT-FETs and electrolyte-gated P3HT-FETs are compared regarding their stability in an aqueous environment and their response when exposed to buffers with different pH values.[69] As discussed in Chapter 3.2.4, the biosystem (CaptAvidin/biotin) that was chosen in order to test the performance of SWNT-FETs and P3HT-FETs is strongly pH-dependent. This is one of the reasons why the pH-response of these two devices was tested prior to performing protein experiments.

SWNT-FETs and P3HT-FETs offer different advantages and drawbacks concerning their stability in solution and their ease of fabrication. A discussion of those differences and the underlying sensing mechanisms is shown here.

The instability of P3HT-based devices and of other organic semiconductors is often discussed in literature and partially attributed to extrinsic factors. Extrinsic factors may be trapping effects when exposed to moisture, oxygen and UV light.[70,71] However, the well-known issue of baseline drifts in organic thin film transistors (OTFTs) has also some intrinsic reasons. Those are mainly electrical instability due to shallow and deep trap states at the interfaces or in the bulk.[72,73] There are already different attempts to overcome these problems as for example Yang et al. proposed a pulsed gate sensing operation mode with a minimized duty cycle to overcome that issue.[74] However, the work presented in this section will stick to conventional gating

methods and show that these problems can be circumvented by more differentiated data analysis methods, which leads to a reliable P3HT-FET operation for pH sensing applications and renders device production as time- and cost-effective as possible.

5.1 Device fabrication

In the following the fabrication methods of P3HT- and SWNT-FETs is discussed. The active layer of the P3HT-FETs consisted of a spin-coated regioregular P3HT layer, which serves on one hand as the active sensing element and on the other hand as passivation layer for the source-drain metal contacts of the transistor. The active layer of the nanotube transistors consists of a randomly distributed SWNT-network (> 90% semiconducting tubes) deposited from a SWNT-ink solution by spin-coating.

5.1.1 P3HT FETs

P3HT field-effect transistors were fabricated starting from p-doped silicon substrates with thermally grown SiO_2 (65 nm). Source and drain electrodes (5 nm Cr, 40 nm Au) have been evaporated on Si/SiO_2 substrates using standard optical lithography techniques. 1 wt% regioregular P3HT (Rieke Metals) was dissolved in dichlorbenzene (DCB) (anhydrous, VWR) in a glove box (N_2) and spin-coated (1000 rpm, 90 s) onto the interdigitated (W/L = 900 with a channel length of 50 µm) electrodede structures using a 200 nm polytetrafluoroethylene (PTFE) filter (VWR).

5.1.2 SWNT-FETs

SWNT-FETs were equivalently fabricated also using a spin-coater for thin film deposition. Prior to that a commercially available SWNT powder, purchased from SWeNT, (SG65, chirality 6,5 (>50%) and > 90% semiconducting tubes) was dispersed (0.05 wt %) in deionized water with 1 wt% CMC.[62] The dispersion of the nanotubes was enhanced by sonication for 20 minutes with a horn sonicator (Branson Digital Sonifier 450). The dispersion was then centrifuged to separate the sediment from the well dispersed SWNTs, which were finally spin-coated (3000 rpm for 50 seconds) on the IDE structured substrate. Directly prior deposition of the nanotube film the substrates were exposed to oxygen plasma (30 s) to guarantee a homogenous film formation on the hydrophobic silicon oxide substrate. After the SWNT deposition the wafers were immersed overnight (> 12 h) in a diluted nitric acid (68% HNO_3:H_2O = 1:4) solution to remove the CMC followed by rinsing with water and drying on a hotplate. Subsequently the carbon nanotube network was etched away by another oxygen plasma treatment everywhere on the chip except for the active area on the IDE structure to prevent the occurrence of parasitic currents. To avoid direct contact of the source and drain electrodes with aqueous solutions, the electrodes were covered with a photo resist (AZ 4562, Clariant GmbH) with an additional optical lithography step.

Sketches of the measurement system and the SWNTs and P3HT devices are shown in Figure 5.1.

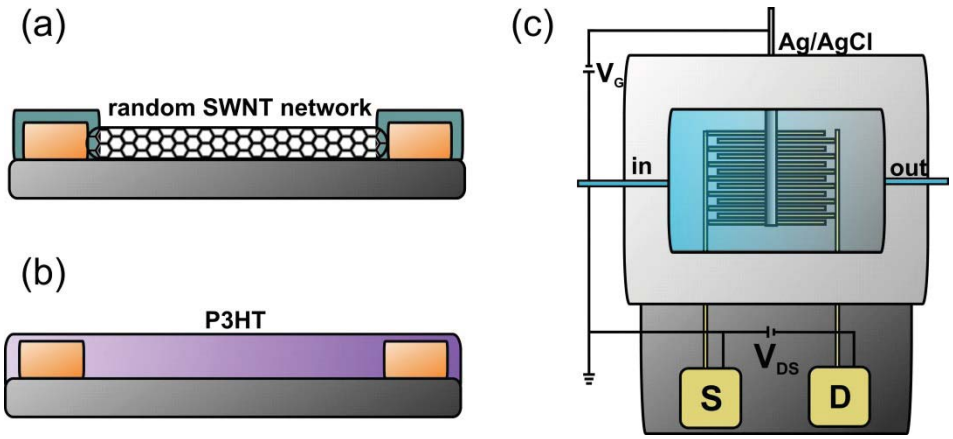

Figure 5.1. (a) Schematic layout of a SWNT-FET: the source and drain electrodes are passivated with photoresist to prevent direct contact of the metal with the electrolytic solution. (b) Schematic layout of a P3HT-FET: source and drain electrodes are not passivated as P3HT covers the source and drain electrodes. (c) Flow chamber setup: transistor devices are mounted in a liquid compartment. The electrolyte can be changed by using syringe pumps. The volume of the flow chamber is 100 µl.

5.2 Methods

To characterize the performance of the transistors in a liquid environment the devices were mounted in a flow chamber made from poly(methyl methacrylate) and sealed with PDMS (polydimethylsiloxane) (Figure 5.1 (c) shows a cartoon of the setup). The liquid compartment having a volume of 100 µl, was filled with deionized (DI) water (the deionized water used in this work and throughout this thesis is classified with a resistivity of about 18 MΩcm) and the drain voltage was kept constant at -0.1 V while the voltage applied at the Ag/AgCl gate electrode was switched between 0 V and -0.6 V. The gate voltage was applied via a home-made Ag/AgCl electrode (see Chapter 4.2.1). The electrolyte gate mode allows for low operation voltages in terms of gate biases, due to the high coupling capacitance at

the interface between the active material and the electrolytic solutions. Hence this mode is very effective.

For online pH measurements, i.e. measurements for which the drain current is monitored over time, the gate and drain voltages were fixed at -0.4 V. The inlet of the chamber was connected to two syringe pumps (NE-1000, New Era Pump Systems, Inc.). Those pumps were programmed in a way that solutions were injected alternatingly, starting from injection of buffer 1 (pH 3.4) for 90 seconds, followed from a five minutes pump break before flushing the chamber with buffer 2 (pH 7.8) for again 90 seconds, and so on. The volume to flush the flow chamber was chosen to be 3 ml to ensure a complete buffer exchange. For all transient measurements a Keithley (2636 SYSTEM) source meter was used.

Transfer curves were recorded using a Keithley 4200-SCS. For the ease of measurements a PDMS compartment was used instead of a flow chamber to serve as a volume for 100 µl buffer. In this case solutions were exchanged manually using a pipette. Transfer curves were recorded at a fixed drain voltage (-0.1 V) while sweeping the gate voltage from 0.6 V to -0.6 V. All buffers were adjusted to an ionic strength of 10 mM using potassium chloride (KCl), while the pH of the buffer was alternated with a 1 mM citric acid / Na_2HPO_4 buffer (Sigma Aldrich). In this way, changes of the ionic strength due to the adjustment of the pH value of the buffer plays an inferior role in the overall ionic strength of the electrolyte and thus the salt concentration of the buffers can be neglected when analyzing the obtained data.

Additionally, due to the high and constant amount of KCl present in the electrolyte a stable potential of the homemade Ag/AgCl electrode can be assured.

5.3 Results and Discussion

5.3.1 Response upon gate voltage variations

Prior to pH sensing experiments transient measurements of P3HT-FETs and SWNT-FETs in deionized water are shown in order to investigate the stability of the transistors under bias stress. The experimental protocol was as follows: After fabrication both devices were exposed to DI-water and the system was allowed to equilibrate for one minute before voltages were applied. A constant drain bias of -0.1 V was applied while the gate voltage was switched between 0 V to -0.6 V keeping each voltage fixed for a period of 4 minutes. The results of the experiments are presented in Figure 5.2. The black lines in (a) and (b) depict the drain currents (I_D) and the dashed blue lines are the gate voltages (V_G) applied via Ag/AgCl. We may refer to the drain current at V_G = 0 V as “off-current” and to the drain current at V_G = 0 V as “on-current”. The SWNT-FET as well as the P3HT-FET shows a decrease of the drain current over time. The current decrease follows an exponential decay during periods at which the gate voltage is set to -0.6 V. Comparing the data of the SWNT device with those of a typical P3HT device, it is apparent that the on-current of SWNTs is much higher (while having similar off-currents of a few hundred nAs) than that of the P3HT transistor, indicating a better performance as a transistor for the SWNT-FET and that P3HT shows a much higher exponential decrease in

drain current. It is worth noting that the geometrical dimensions of the transistor layouts were kept the same for both devices. Obviously a current decrease in transient curves does not only occur for P3HT-FETs but also for the SWNT-FETs. For devices made from polymeric semiconductors this is an often discussed and well-known issue. For devices based on carbon nanotubes this phenomenon was studied, among others, from Lin et al.; they attributed this phenomenon to adsorption of molecules from the ambient on the device as this effect seems not to occur in vacuum.[75] This correlates with our observation that devices that are characterized electrically directly after their fabrication, require relatively longer equilibration times compared to devices that were allowed to sit for days in the laboratory under ambient conditions. A possible explanation for this observation might be that after a certain amount of time under ambient conditions, moisture and oxygen have been adsorbed onto the surface of the carbon nanotubes. Hence, the impact caused by exposing the FETs to a liquid in order to conduct electrical measurements after exposure to room conditions is not as high as when exposing a FET to a liquid for the first time. “Equilibration time” herein is regarded as the time that is required that the transistors show a relatively constant baseline during operation.

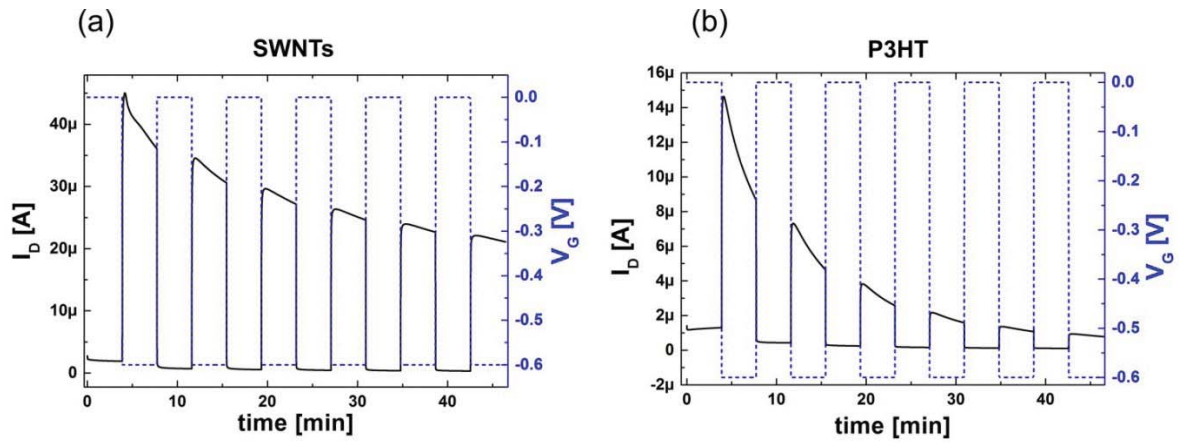

Figure 5.2. Drain current I_D (black lines) of a SWNT-FET (a) and a P3HT-FET (b) in DI-water as a function of the elapsed time. While keeping the drain voltage fixed at -0.1 V, the gate voltage V_G (dashed blue lines) was switched between 0 V and -0.6 V.

Bias stress effects [76] were observed for both types of field-effect transistors. However, the bias stress effects are more pronounced for the P3HT-FETs. This is as in about 40 minutes the P3HT drain current decreases from approximately 15 µA to 800 nA, whereas the drain current of the nanotube device decreases only by about 50% and still shows high drain currents after a long measurement period. Yet, for the nanotubes as well as for P3HT the current at V_G = 0 V stabilizes after 10 minutes of operation.

From both transient curves the rise- and fall-time of the second peak at around t = 14 min were extracted. The results hereof are presented in Figure 5.3. Herein the rise (fall) time is defined as the increase (decrease) in current between 10% and 90% from the lower plateau level (minimum current during off-state) to the maximum of their on-state (plateau level). Figure 5.3 (a) and (b) show the respective graphs for SWNTs and P3HT. Both types of transistors show similar rise and fall times of a few

seconds and several hundred milliseconds. Both devices reveal a similar off-current of a few hundred nAs, but the SWNT-FETs on-current is five times higher. Extrapolating the slope of a linear fit between the 10% and 90% points of the curves gives a relatively faster response of the nanotube transistors. This is in agreement with the higher mobility of holes in the carbon nanotubes compared with polymeric semiconductors.[77,78] It is noted that the response times extracted here do not give the maximum performance of the used semiconductors but serve as a comparison. For instance, the group of Bao found rise- and fall-times for P3HT-devices gated with platinum in water of about 50 ms to 10 ms, and Laiho et al. extracted switching times of 1.9 ms (on) and 0.4 ms (off).[79,80]

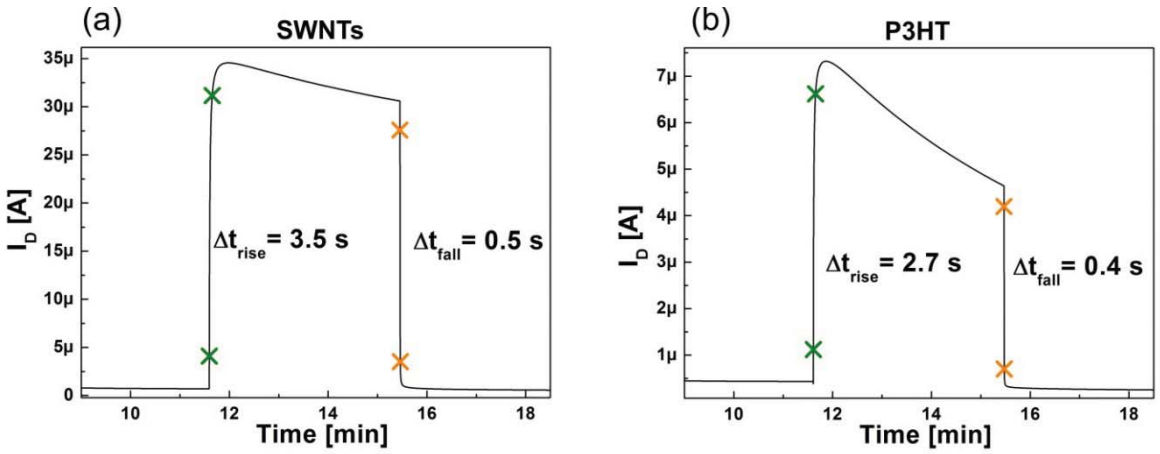

Figure 5.3. Drain current I_D of a SWNT-FET (a) and a P3HT-FET (b) in DI water as a function of the elapsed time. Δt_{rise} and Δt_{fall} give the respective rise- and fall times of the transistors. (a) and (b) are close-ups of the respective curves in Figure 5.2. Δt_{rise} and Δt_{fall} are defined as the increase and decrease of the current between 10% and 90% from the lower plateau level (minimum current during off-state) to the upper plateau level (maximum current during on-state).

5.3.2 Response upon pH switching

In section 5.3.1 an on/off-switching was performed by alternating between a respective “on”-state and “off”-state by switching the gate voltage between 0 V to -0.6 V. In this section it is shown that electrolyte-gated transistor devices can be converted from a low-current-state to a high-current-state by means of changing the acidity of the electrolyte. As described in 5.2, the drain bias and the gate voltage were kept fixed and the buffer solutions were exchanged by using syringe pumps. The results are presented in Figure 5.4. It is obvious that the current does not decrease as significantly as during the previous experiment, which is discussed below:

For polymeric transistors in back-gated configuration Street et al. reported that the current-decay in transient measurements depends on the gate-bias.[81] They showed evidence that this degradation is due to a formation of bipolarons. According to their publication those effects are known to occur in some thiophenes and the authors also suggest that bipolaron formation occurs as well in regioregular thiophenes, although on larger time scales. The formation of bipolarons is dependent on the concentration of holes, which again is proportional to the channel depth and thus to the gate bias.[81,82] Their observations were considered for these pH-switching experiments by fixing the gate and the drain voltage, both at -0.4 V instead of -0.6 V.

Figure 5.4 (a) and (b) show the transient behavior upon alternation of the pH buffer for a SWNT-FET and a P3HT-FET, respectively. The dashed orange lines mark two of the regions where the devices are exposed to buffers with different pH values. At

t = 0 the experiment was started by switching on the voltages with a pH value of pH 3.4. From then onwards the buffers were subsequently exchanged as described in 5.2. According to Figure 5.4 both devices are sensitive to a change of the buffer's pH, in a way that the current increases when the active surface of the transistor, namely the semiconductor, gets in touch with more basic pH values, which is in this case pH 7.8 compared to the acidic pH 3.4. For carbon nanotubes this sensitivity is attributed to charging and discharching of defect states on the tube's surface which is discussed in more detail in another publication.[83]

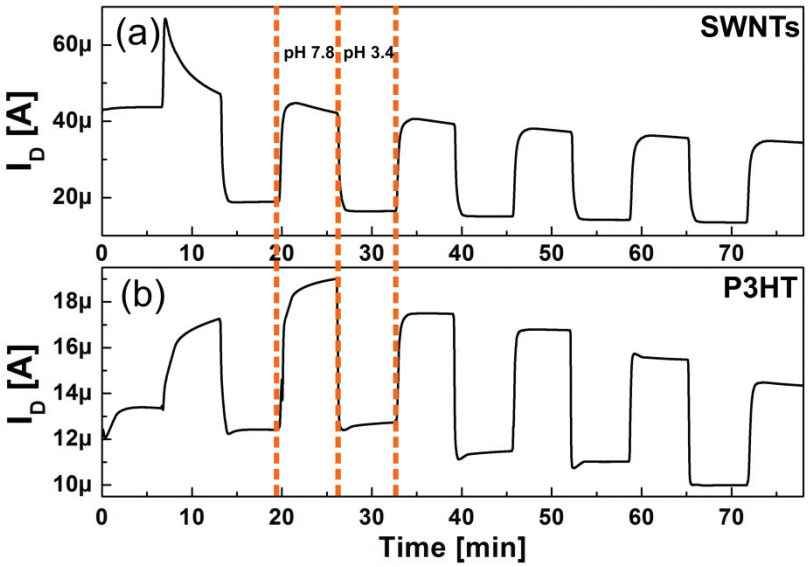

Figure 5.4 Drain current I_D of a SWNT-FET (a) and a P3HT-FET (b) in pH buffers as a function of the elapsed time. The drain bias (V_D = -0.1 V) and the gate voltage (V_G = -0.4 V) were fixed. The buffer pH was altered by using syringe pumps. Subsequently pH 3.4 and pH 7.8 was injected for 90 s time intervals each. The dashed orange lines mark two of the regions where the devices are exposed to buffers with different pH values.

In a recently proposed impedimetric pH sensor based on solution-processable P3HT and carbon nanotubes, it was shown that the impedance for both materials is a suitable parameter for monitoring changes in the pH value of PBS buffer-solutions and that this dependence is different for P3HT and SWNTs.[84] However, it is peculiar that an opposite behavior using back-gated P3HT-devices is observed, meaning that the drain current increases with increasing pH for electrolyte-gated OFETs and decreases with increasing pH for back-gated OFETs.[85] This is consistent with the effect caused by the charges of ions on the respective transistor channels. In fact, with increasing pH value the concentration of negative hydroxide ions in solution increases (OH^-), hence these negative charges are inducing additional positive charges in the semiconductor on the interface to the electrolyte. For electrolyte-gated OTFTs the semiconducting channel finds itself directly at this interface, leading to higher drain currents for an increasing buffer pH. On the contrary, for a back-gated operation the channel is at the oxide-semiconductor interface and as a result a lower pH leads to an increased positive charge in the channel and thus to an increasing drain current. This explanation is accompanied by the sketches of Figure 5.5, which shows an electrolyte-gated OTFT (a) and a back-gated OTFT (b). In our case (a), the P3HT layer is in direct contact with the solution. Thus, a positive charge at the electrolyte-P3HT-interface increases the positive charge in the channel. Roberts et al. also found the drain current to decrease with ascending pH for a back-gated DDFTTF field-effect transistor, while other groups using a dielectric layer on top of the semiconductor such as Bartic et al. found consistently the corresponding same behavior.[86,87] In other words and according to Figure 5.5 the sum of the ions that are

contained in the buffer solution provide a certain electrostatic environment, which is changed if the buffer is exchanged and thus gates the transistor device additionally.

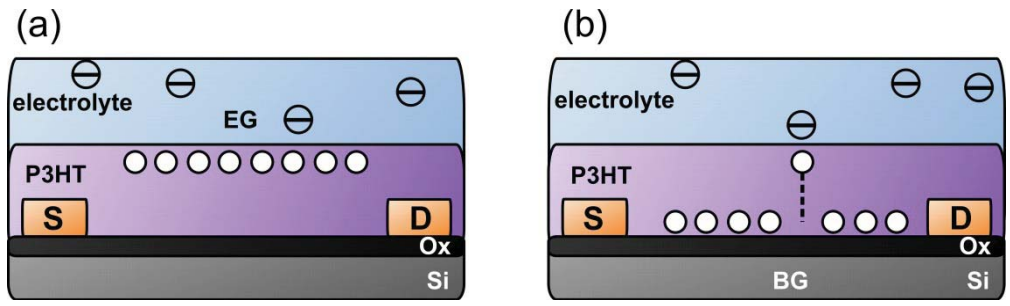

Figure 5.5. (a) is a sketch of the electrolyte-gated (EG) device architecture. In the EG configuration the gate electrode is immersed in the buffer solution causing the channel to form at the P3HT-electrolyte interface. Negative ions from the electrolyte are causing additional holes in the channel, leading to a larger current for high pH values. (b) shows a sketch of the back-gated (EG) device architecture. Here the channel is formed at the P3HT-silocon oxide interface and negative ions from the electrolyte are causing the presence of fewer holes in the channel and thus the current between source and drain is decreasing.

Figure 5.6 shows close-ups of the current traces in Figure 5.4 at around t = 50 min. Similar to 5.3.1 the switching behavior of the FETs was extracted. Figure 5.6 (a) and (b) show the respective results for SWNTs and P3HT. The grey shaded areas mark the time the buffer-exchanges were performed (the buffers were exchanged over a time period of 90 s). Again, the SWNT transistor has longer rise- and fall-times but also reveals a stronger response and generally higher currents. It is eye-catching that after an initial equilibration time the current at the more basic pH value reaches a plateau for P3HT but not for carbon nanotubes. This may indicate that a chemical equilibrium at the more basic pH value cannot be reached during the five minutes

exposure-time for the SWNT device or this may be also attributed to the larger surface area of the carbon nanotube network at the semiconductor/liquid interface. To further investigate the pH sensitivity of our devices in the electrolyte-gated mode, transfer curves were conducted and the results are presented in the next section.

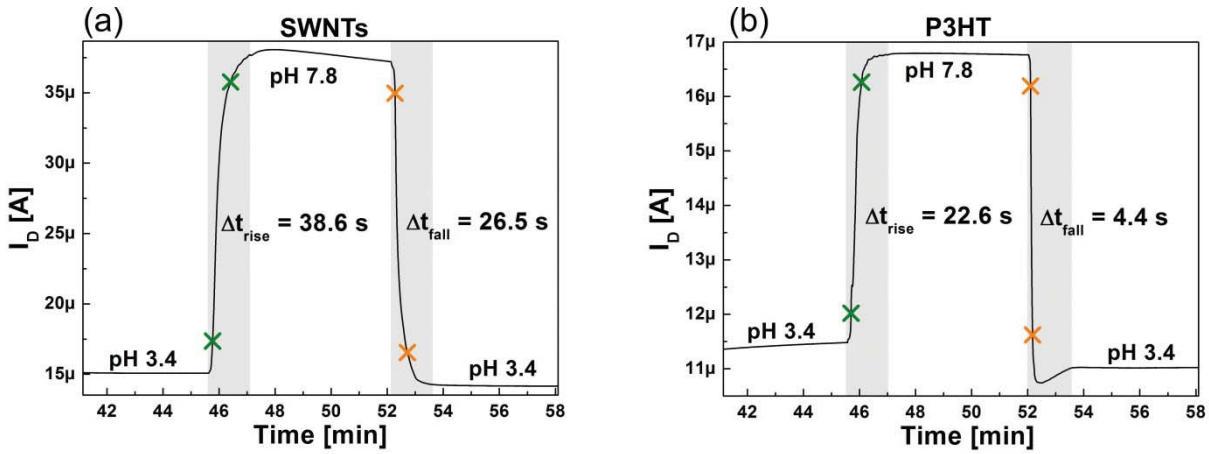

Figure 5.6 Drain current I_D of a SWNT-FET (a) and a P3HT-FET (b) in pH buffers as a function of the elapsed time. . Δt_{rise} and Δt_{fall} give the respective rise- and fall times of the transistors. (a) and (b) are close-ups of the respective curves in Figure 5.4. Buffers were injected during a time period of 90 seconds (grey shaded area) until a plateau was reached. Subsequently, after a 5 minutes hold-time the next buffer was injected.

5.4 Analysis of the transfer curves

To further clarify the pH sensing mechanism, it is helpful to conduct transfer curves under different electrolytic conditions (pH values in this case). Hence, for a transfer curve analysis active areas of the devices were exposed to citric acid buffer solutions with buffer pH values ranging from 3.4 to 7.8. After exposing the semiconductors to the buffers, they were allowed to equilibrate for one minute. Subsequently a drain bias of -0.1 V was applied and the gate voltage was swept between 0.6 V to -0.6 V,

starting from 0.6 V. For each pH value a transfer curve was recorded. Starting from pH 3.4, the pH was increased and after arriving at pH 7.8 it was increased again. This procedure was repeated until seven pH sweeps were recorded. For the sake of clearness the on-currents (I_D at V_G = -0.6 V) were plotted as a function of the order of the measurement (the corresponding graph is shown in Figure 5.7 (a)). The results for the SWNT-FET are presented as blue circles and the one for the P3HT-FET as black circles. The blue and red shaded areas represent measurement cycles for which the pH values of the buffers were changed in an ascending or descending way, meaning from an acidic pH to a more basic pH or vice versa. For this experiment 36 transfer curves were recorded.

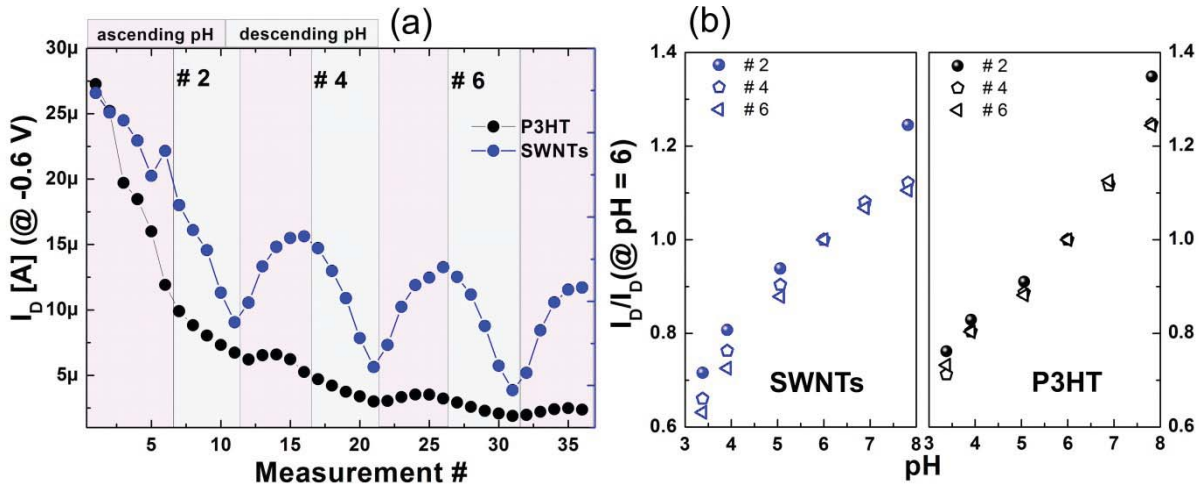

Figure 5.7 (a) Drain current extrated from the transfer curves at V_G = -0.6 V. (b) normalized drain currents from the marked regions #2, #4, #6 for both SWNTs and P3HT devices.

From the on-currents a strong decrease of the drain current for a P3HT device can be observed, which is equivalent to our observations in section 5.3.1. The on-currents show a “zig-zag”- behavior, i.e. the current increases for ascending pH and decreases for descending pH, which holds true for all sweeps except for the first one, which shows decreasing drain current with ascending pH of the solution. In this first regime device degradation or the swinging into equilibrium with the aqueous environment seems to overlap the pH sensitivity of the transistors. After the initial equilibration, the pH sensitivity of the devices dominates over the effects of degradation, even for ascending pH values the current increases clearly. It is worth noting that this and similar experiments were performed multiple times in our laboratories and that those equilibration times do not only depend on the fact that a device is exposed to aqueous conditions for the first time but is also depending on the buffer type, indicating that there occurs also a (electro-)chemical equilibration. That means, if a field-effect transistor was exposed to a PBS buffer and then the buffer was switched to a citric acid buffer, respectively, the device again “needed some time to get used to the new conditions” and that finally a reasonable response upon changes of the electrolytic environment could be observed.

For further analysis only the regions marked #2, #4 and #6 have been considered and the on-current of those regions were plotted as a function of the buffer’s pH as shown in Figure 5.7 (b). The left panel of (b) shows the results for carbon nanotubes (blue symbols) and the right panel the ones of a P3HT (black symbols) device. All data were normalized with respect to the drain current at pH 6 in each plot. A linear

current response could be extracted for the P3HT-FET. Comparing the results for carbon nanotubes and P3HT in (a) and (b), the SWNT-FETs reveal higher currents and higher stability but show a narrower linear pH region and a somehow lower reproducibility, which may occur due to the potential higher sensitivity of SWNTs towards external perturbations. Further it is obvious from plots like this that the reproducibility of the pH sensing response increases with the number of measurements as the results obtained from region #2 and #4 differ more significant from each other than comparing the results from #4 and #6.

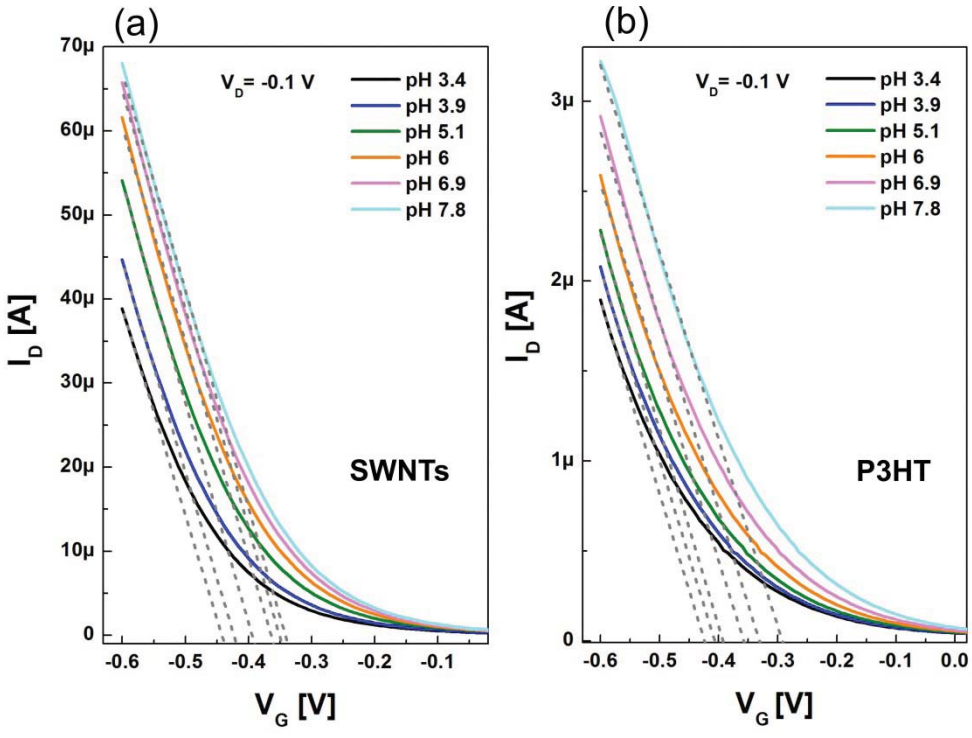

Figure 5.8 Transfer curves measured in buffers with different pH for SWNTs (a) and P3HT (b). Grey dashed lines are linear fits. For increasing buffer pH the threshold voltage V_{th} is shifting towards more positive gate voltages.

In Figure 5.8 the corresponding transfer curves from sweep #6 are shown. The grey dashed lines mark fits in the linear regime of the curves. Thus, pH changes are causing shifts of the threshold voltage of the field-effect transistors, i.e. the threshold voltages are shifting towards more negative gate voltages for increasing acidity of the buffers. For P3HT a threshold shift of roughly 28 mV/pH was observed. Assuming a linear dependence for the nanotube device in the region from pH 3.4 to pH 6.9, a shift of ca. 27 mV/pH was extracted.

The drain current of a field-effect transistor in the linear regime is described by equation 3.7. The equation shows that the drain current is a function of the electrolyte coupling capacitance C, drain voltage V_D, gate voltage V_G, field-effect mobility μ and threshold voltage V_T. We observe a pH dependent behavior of the threshold voltage and neither a variation of the carrier mobility nor of the capacitance of the system, which would result in a pH dependent change of the transconductance of the curves. For α-sexithiophene Buth et al. attributed pH sensing rather to pH dependent surface charges on the polymer than to a change in device mobility.[88] This could also be the case for P3HT, although other effects due to the polymeric interface cannot be excluded and still deserve further investigation. In carbon nanotube devices on the other side, adsorbants induced at the SWNTs-surface due to the acid treatment during the fabrication process (described above) may be the origin of defect states, which get charged and discharged upon varying pH values. To ensure that the observed response is not an artifact of the home-made miniaturized Ag/AgCl electrode, which might be imaginable as the Ag/AgCl wire is in direct contact with the

buffer solution opposed to commercial electrodes for which the electrode is separated from the buffer by a glass tube, experiments with a commercially available Ag/AgCl electrode were conducted as well and no changes in the pH response was observed.

5.5 Conclusion

In this section the performance of electrolyte-gated SWNT-FETs and P3HT-FETs as pH sensors was assessed and the underlying sensing mechanism was discussed. While the P3HT-FETs stand out due to the very fast fabrication process, i.e. no passivation of the gold contacts is required nor purification of the polymer itself and, as we did, also the substrates (in our case silicon) can be cleaned after measurements and be reused, SWNT-FETs show excellent stability and the transistors can be reused even after months and years. Even though the electrical stability of P3HT-devices is lacks behind that of SWNT transistors they perform well as pH sensors and after normalizing the obtained data, the results are comparable to those of carbon nanotube based devices.

6 Feasibility of back-gated SWNT FETs for biosensing

In this chapter the performance of back-gated carbon nanotube thin-film transistors (BG SWNT-FETs) in electrolytic solutions is analyzed in order to assess their feasibility for applications as biosensors. For this purpose thin SWNT networks were spray-deposited on pre-patterned gold electrodes on Si/SiO_2-substrates.[89]

Spray deposition offers the opportunity to integrate the SWNT sensors on flexible sensing platforms at low-cost. The behavior of the transistors was characterized in electrolytes by analyzing the response to different potassium chloride (KCl) solutions and buffers over a wide pH range. A linear response of the drain current on pH changes was observed in diluted buffers (low molarity) and an exponential dependence on the salt concentration of the electrolyte was obtained. These responses can be attributed to electrostatic gating effects that go along with shifts in the threshold voltage. Even though a lot of effort was put into understanding the biosensing mechanism a detailed theory is still missing up to that point. BG SWNTFETs that are operated in electrolytic solutions may present a further tool to investigate and clarify the existing unsolved questions.

In the past years several research groups were working on carbon nanotube-based biosensing devices with the aim to understand the sensing mechanism, optimize existing sensing protocols and generally to functionalize the SWNTs for highly specific detection of biomolecules.[90,91,92,93,94] These sensors are usually operated in

the electrolyte-gated (EG) configuration. A sketch of a typical biosensing setup is shown in Figure 6.1. A gate voltage is applied via an electrode that is immersed in the electrolytic solution. One of the reasons for using an electrolyte-gated configuration is that the electrolyte-gate guarantees a very effective gating due to the high capacitance of the electrolytic dielectric. However, a significant draw-back is posed by the fact that the gate electrode cannot be integrated on the wafer easily, which causes unsatisfying solutions when it comes to designing portable sensors. In fact, the gate electrode is typically a Ag/AgCl reference electrode or it consists of a wire from noble metals like platinum, silver or gold. Thereby a Ag/AgCl reference electrode reveals a very stable potential over time but is hard to integrate in microfluidic systems because of their large size. Further drawbacks of electrolyte-gated devices arise from the fact that additional electrochemical effects can occur at the surface of the gate-electrode (resulting from applying a potential in the electrolyte). Such effects result in a shift of the electrode potential and can overlap the signals originating from the analytes. For example it can happen that the response on protein injection in a fluidic system is rather due to a perturbance of the interfacial potential at the gate electrode or adsorption of proteins on it than a specific adsorption on a functionalized semiconductor surface.[94]

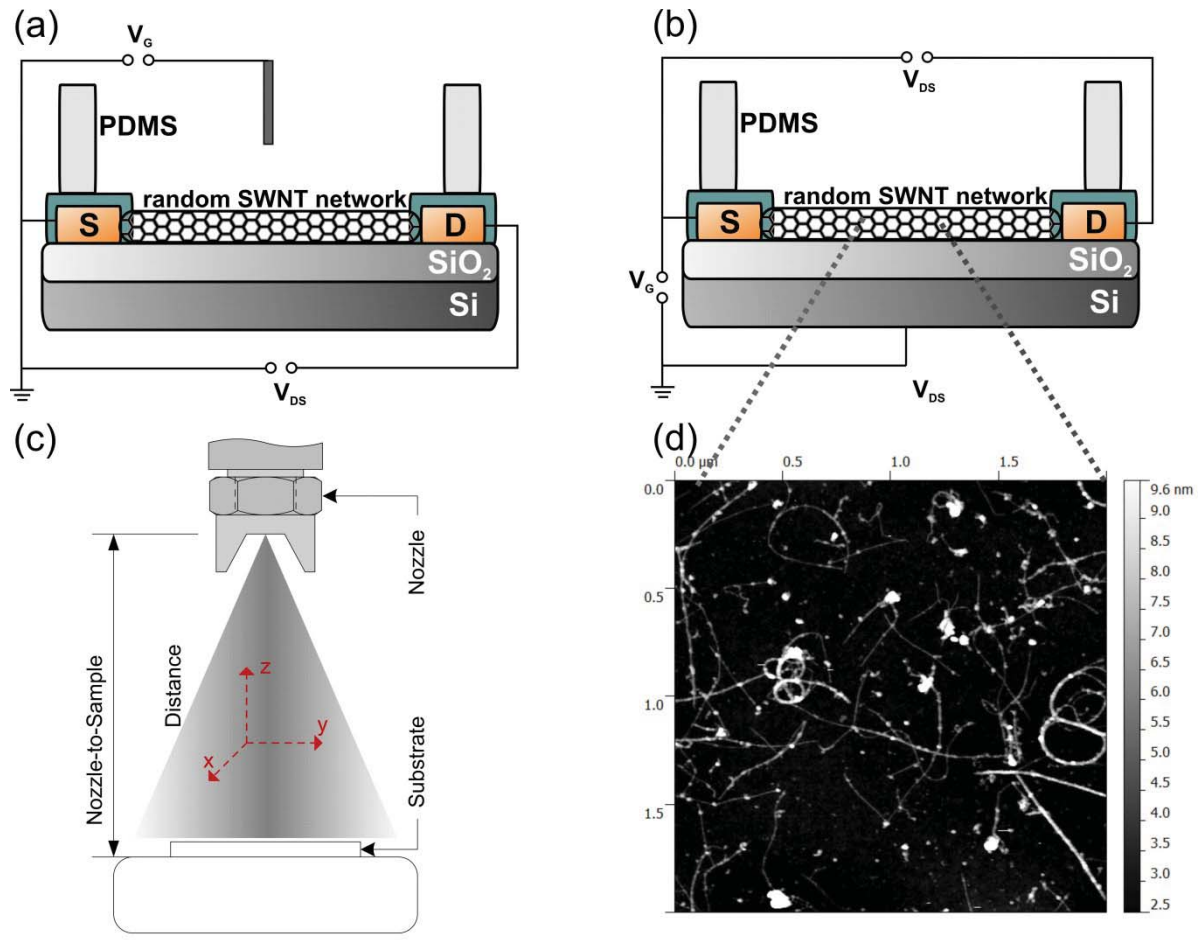

Figure 6.1: (a) is a sketch of a typical electrolyte-gated SWNT-FET with a gate electrode that is directly immersed in the buffer solution. (b) depicts a back-gated SWNT-FET, which is used in for all experiments in this section. For back-gated devices the gate voltage is applied via a p-doped Si-substrate. The SiO_2 dielectric layer has a thickness of 65 nm, allowing for low-operating voltages. (c) is a schematic drawing of the spray-deposition setup. (d) is an AFM-image of the spray-deposited random carbon nanotube layer on top of SiO_2.

A bottom-gate device architecture can be a solution for various problems caused by an electrolyte gate and can pave the way for small and portable SWNT-FET-based biosensors. A promising functionalized back-gated SWNT biosensing device was developed by Star et al., they firstly demonstrated the specific detection of streptavidin binding to a biotinylated SWNTFET device.[26] Those devices were fabricated by growing SWNTs directly on the substrate using chemical vapor

deposition (CVD). Subsequently the protein adsorption was detected. However this was done in the absence of an electrolyte. Here the focus is on simple, fast and reliable solution-based approaches which can be easily applied to large-area printed electronics and investigate the biosensing feasibility of spray-deposited back-gated random-network based SWNTFETs. In contrast to CVD-based methods spray-deposition has the advantage to be applicable directly on flexible substrates without any further processes. “Further processes” would be for example to grow the nanotubes via CVD on a rigid substrate (as high temperatures are required, flexible devices cannot be considered), followed by a transfer of the nanotubes from the rigid substrate to a flexible substrate.[95]

In order to assess the possibility to use randomly distributed SWNT-networks as active layer in biosensing devices that are operated in a liquid environment; an analysis of back-gated transistor devices was performed with respect to different electrolytes under varying parameters. As a necessary biosensor pre-characterization the device response to a range of pH values at low operating voltages is investigated as well as the response on exposure to electrolytes of different ionic strength (see Chapter 3.2.4). On this basis the occurrence of biological processes of interest can be extracted. In this particular case the focus is on pH measurements that were performed in low buffer concentrations to account for suitable conditions for DNA and protein sensing experiments, namely large Debye screening lengths.[22,96,24] An initial characterization is of crucial importance especially when introducing a new device fabrication method as the detection of bio (-chemical)

interactions can be sensitive to the presence of interfacial species that might be introduced unintentionally during the fabrication process. A similar investigation was done by Thu-Hong et al., where spray-coated SWNT resistors were used as pH sensors.[97] In this work their approach and the approach of our previous work is extended to field-effect transistors that are modulated by a back-gate.[83]

6.1 Device fabrication and characterization

Interdigitated electrode structures were (W/L = 900, 5 nm Cr and 40 nm Au) patterned with standard processes of photolithography on Si substrates covered with a 65 nm thick SiO_2 layer (Si-Mat Silicon Materials). Prior to the deposition of the SWNT on the surface of the wafer, the wafer was pre-treated with the aminosilane (3-aminopropyl)triethoxysilane (APTES), that allows for a better adhesion of the SWNTs on the substrate. The carbon nanotube ink solution (>90% semiconducting content) was spray-deposited onto the substrate as described previously.[98,63,99] The SWNT ink is water-based with addition of CMC for a better dispersion of the hydrophobic carbon nanotubes. This dispersant is removed after spray deposition with a mild nitric acid treatment. Before carrying out the measurements the metal contacts were passivated with a standard photoresist to avoid direct exposure of the contacts to the electrolyte. According to our analysis the spray deposition using the parameters from above and including the subsequent fabrication steps results in an average nanotube density on the chip of about 10 nanotubes per μm^2.

For all measurements in this section a PDMS-ring was attached on the active surface of the SWNT-FET to serve as a compartment for 50 µl of electrolyte. During experiments the electrolyte was exchanged per hand using a pipette. A sketch of the setup is shown in Figure 6.1 (b). A drain bias of -0.1 V and a maximum gate voltage of ±5 V was applied with a Keithley 2636 source meter. For measurements of the pH dependency buffers with low ionic strengths were used. As mentioned above the low ionic strength buffers (i.e. highly diluted) were used to account for future biosensing experiments that require a large Debye screening length in order not to screen the charge of biological analytes such as proteins from the channel of the transistor. For a better reproducibility of the results it was necessary to let the system equilibrate for 10 minutes after exchanging the buffer and before taking an electrical measurement, whereas 2 minutes of equilibration time was enough for KCl sweeping experiments. If not stated otherwise pH measurements were conducted using a universal citric acid – Na_2HPO_4 buffer (0.1 mM in 1mM KCl).

6.2 Performance in electrolytic environment

Various groups studied the influence of the Debye screening length on the sensitivity of their biosensors. The outcome of these studies was that the screening of charged species from the ions in solution plays a key role for field-effect based sensing devices with functionalized semiconductor surfaces.[100,24,101,96] The Debye screening length, which is a function of the salt concentration of a buffer or an electrolyte, represents the typical distance that is required for mobile charge carriers

to screen local surplus charges in the electrolyte. It is indirect proportional to the square root of the ionic strength, meaning the higher the concentration of ions in the liquid, the more effective is the screening of surplus charges.

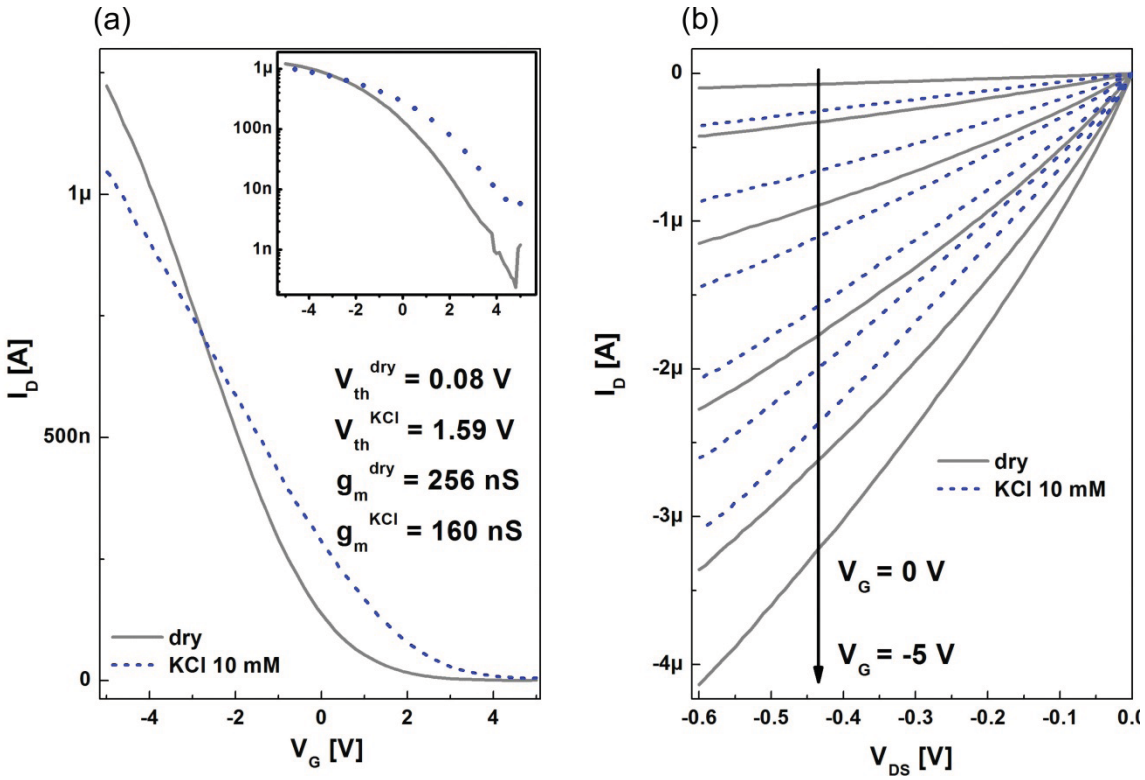

Figure 6.2: (a) Transfer characteristics of the same transistor device before (grey solid line) and after (blue dashed line) addition of a 10 mM KCl solution to the liquid compartment at a constant drain bias of -0.1 V. A shift in the threshold voltage was observed as well as a decrease in transconductance. The inset of (a) shows the results plotted on a logarithmical scale. (b) Output curves for the same device. The gate voltage was swept from 0 V to -5 V.

As far as the sensing mechanisms for field-effect based biosensors are understood yet, a short Debye screening length causes shielding from the charge of the biomolecule in the solution from the semiconductor surface, which in turn avoids

alterations in the source-drain current (I_D). Therefore the electrolyte concentration should be carefully taken into account when designing biosensing experiments and it depends on the particular analyte in terms of the size and the net charge of a biomolecule.

At first the electronic properties of the back-gated SWNT-FETs in dry and wet state are presented. Figure 6.2 shows the transfer (a) and the output characteristics (b) of a typical device. Characteristics of a device in dry state are depicted in grey and the corresponding curves after filling the PDMS compartment with 10 mM KCl solution are plotted in blue dashed lines. Additionally the graphs of (a) were plotted as an inset in a logarithmical scale. It was observed that exposing the transistor to a KCl solution causes a shift of the threshold voltage towards more positive gate voltages and a decrease of the on/off ratio from ca. $5x10^3$ to $2x10^2$ as well as a decrease of the transconductance. According to the equation 3.9 a decrease in the transconductance can be caused by a lower carrier mobility and a change in the effective gate capacitance.

In our measurements, the lower mobility can be explained by taking into consideration that the presence of adsorbants from the electrolytic environment may cause higher scattering rates of the electron holes in the tubes.[102] And the capacitance may change due to the formation of an electrical double layer at the electrolyte/semiconductor interface. It was also suggested the presence of negative charges on the surface of the carbon nanotubes that probably arises from the acid treatment required during the fabrication step. This could also explain the threshold

voltage shift here:[83] As soon as an electrolyte gets in contact with the surface of the nanotubes, a certain amount of negative surface charges gets screened due to the formation of the electrical double layer, thus leading to a threshold voltage shift towards more positive gate voltages. This implicates that a decrease of the amount of KCl in the solution would cause a threshold voltage shift back to more negative gate voltages as the ions that are present in the solution are less capable of screening the negative surface charges. To confirm this theory, a KCl sweep experiment was performed and the results are presented in Figure 6.3.

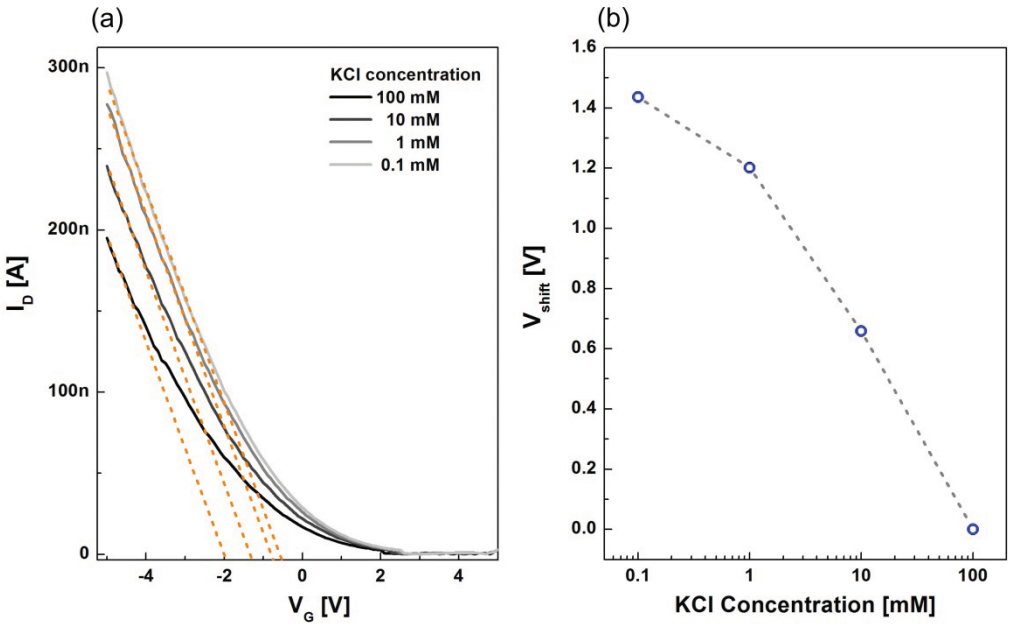

Figure 6.3: Transfer curves obtained from devices exposed to various KCl electrolyte concentrations are shown (different grey shaded lines) along with fits in the linear regime of the drain current (orange dashed lines). The higher the KCl concentration in the electrolytic solution, the more is the threshold voltage shifting towards more negative voltages.

The protocol for this experiment was as follows:

The SWNT-FET was exposed to various KCl concentrations, ranging from 100 mM to 0.1 mM. Panel (a) of Figure 6.3 represents I_D vs. V_G curves for different salt concentrations. The orange, dashed lines mark linear fits to extract the respective threshold voltages. In panel (b) of Figure 6.3 the corresponding threshold voltage shift (V_{shift}) is plotted with respect to the threshold voltage at 100 mM KCl. When the salt concentration is decreased, the threshold voltage shifts about 1.4 V in a range of 4 decades towards more positive gate voltages. Interestingly, it was found that the threshold voltage starts to saturate at about 1 mM. This effect may also be attributed to effects that are arising due to Debye screening. The screening length for monovalent salts may easily be calculated by using equation 3.7.

Monovalent salt [mM]	Debye length [nm]
100	0.96
10	3
1	9.6
0.1	30.4

Table 6-1: The Debye screening length in as a function of the concentration of a monovalent salt.

The Debye lengths for the KCl concentrations used in this experiment are shown in Table 6-1. When considering only the effect of the screening length, it is obvious that at a certain salt concentration all adsorbants and surface species on the nanotubes are located within a distance given by the Debye length and hence, a further decrease of the KCl concentration cannot affect the transistor response anymore.

From atomic force microscope images (one example is shown in Figure 6.1 (d)) it is known that the SWNT networks have a maximum thickness of about 8 nm. When assuming that negative charges are present on this network, it takes a certain KCl concentration to guarantee that all these charges are located within the double layer and participate in the electrostatic field that gates the carbon nanotubes. However, it is worth noting at this point that this is a simplified picture and that in general additionally electrostatic fields that are caused by the applied potentials respectively should be considered. In other words, the saturation of the threshold voltage at low KCl concentrations may be attributed to the extremely high screening lengths. However, for a detailed understanding and analysis also the electrical fields, that are contributing to the effective charge screening from the conductive semiconductor channel need to simulated or mathematically evaluated.

To illustrate the experimental procedure used for the experiments of this section, the “on-currents” (I_D at V_G = -5 V) of the transfer curves are presented in Figure 6.4. The procedure was as follows:

The salt concentration (KCl) was subsequently swept to higher and lower molarities (e.g.: 0.1 mM – 1 mM – 10 mM – 100 mM – 10 mM – 1 mM – 0.1 mM), while recording a transfer-curve at each concentration after a certain equilibration time as described in Chapter 6. This resulted in a zig-zag behavior of the on-current, meaning that the current increases when the KCl concentration decreases and vice versa. The measurement reveals a baseline drift, meaning a slight shift of the on-current to higher values with time (or with each measurement). This might be attributed to a doping of the SWNT-network or to the fact that the potential of the

electrolyte is not controlled (which would be the case for electrolyte-gated SWNT-FETs). But nevertheless the baseline drift seems not to overlap the response of the sensor upon alternations of the salt concentration. In all sweeps the current raises by about 10 to 15 % per decade with decreasing molarity of the electrolyte, proofing that this behavior is reproducible.

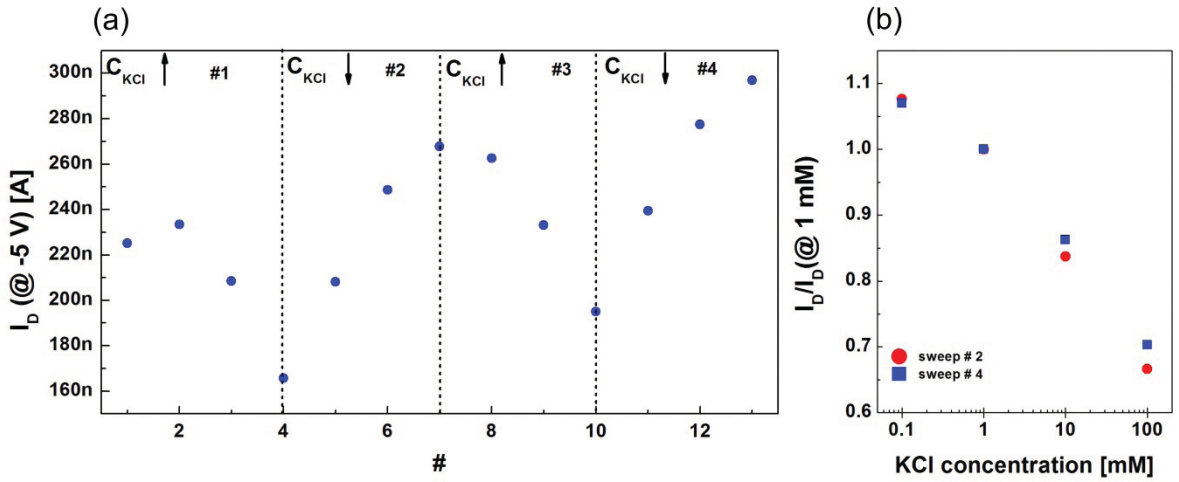

Figure 6.4: (a) shows the on-currents (I_D @ V_G = -5 V) for sequentially recorded transfer curves with increasing and decreasing KCl concentration. The data obtained from sweep #2 and sweep #4 were normalized with respect to the on-current at 1 mM KCl and plotted panel (b). In (b) the red circles depict the data of sweep #2 and the blue squares depict the data of sweep #4, i.e. both sets of data were recorded while the KCl concentration was stepwise decreased for each transfer curve.

Still it is worth noting that additionally another effect may, at least partially, cause the salt concentration dependent behavior of the back-gated SWNT-FETs. Namely, ions in the solution may cause a donation of charge carriers into the carbon nanotubes. That means the current between the source and the drain electrode would increase with increasing ionic strength (which is the case for our experiment).

6.3 pH response

In the foregoing experiments of this chapter, results that show the response of SWNT field-effect transistors for varying salt concentrations of the electrolyte were shown. In this section, however, the response of back-gated SWNT-FET upon a variation of the pH value of the electrolyte is shown while keeping the salt concentration constant.

An analysis of the pH response of biosensors is inevitable as a preliminary characterization of the sensing platform. There are many biological processes that are triggered by a change of acidity of the bio-environment or induce local pH changes. It is therefore necessary to know the pH response of the sensor in order to extract the signals of biological processes of interest. Equivalently to the KCl experiments also all pH measurements were performed in low buffer concentrations to account for ideal biosensing conditions, namely large Debye screening lengths, in which further biosensing with SWNT-FETs needs to be conducted.

For the experiments where the field-effect transistors were exposed to electrolytes with varying pH values the experimental procedure was in general the same as for experiments where electrolytes with different KCl concentrations were used. Namely, after changing the buffer solution (in an increasing or decreasing manner) a transfer curve was taken. The results are presented in Figure 6.5. In Figure 6.5 (a) the drain currents at a back-gate voltage of -2 V are extracted from the respective transfer

curves and plotted as a function of the pH value of the buffer. The results for an increasing pH sweep are presented in blue squares and the ones for a decreasing pH sweep are presented in red circles. In Figure 6.5 (a) a diluted citric acid buffer was used and pH values ranging between pH 3.9 to pH 7.3 were obtained. Those results were also normalized with respect to the data points at pH 3.9, which is shown in Figure 6.5 (b). To assess the influence of the type of the buffer, this experiment was additionally performed using a phosphate buffered saline (PBS) buffer system. The results of the PBS experiment are also presented in (b). Here orange crosses and green triangles depict results that were obtained from sweeps with decreasing and increasing buffer pH, respectively.

A general observation from the results of Figure 6.5 is that the drain current increases from decreasing pH. However, it is again of importance that the transfer curves are analyzed regarding to a shift of the threshold voltage or a change of the transconductance. In order to do so the exemplary curves are presented in Figure 6.6 (a). The orange dashed lines are linear fits. From those fits the shift of the threshold voltages can be extracted, which is depicted in Figure 6.6 (b). From those experiments it was observed that the threshold voltage is shifting towards more negative gate voltages for increasing pH values. The threshold voltage shift that is shown in Figure 6.6 (b) is normalized with respect to the threshold voltage value at pH 7.3. By setting the threshold voltage of the transfer curve, recorded at pH 7.3, to zero, the threshold voltage at pH 3.9 shifted about 0.25 V towards more positive gate voltages. In the following these observations are discussed:

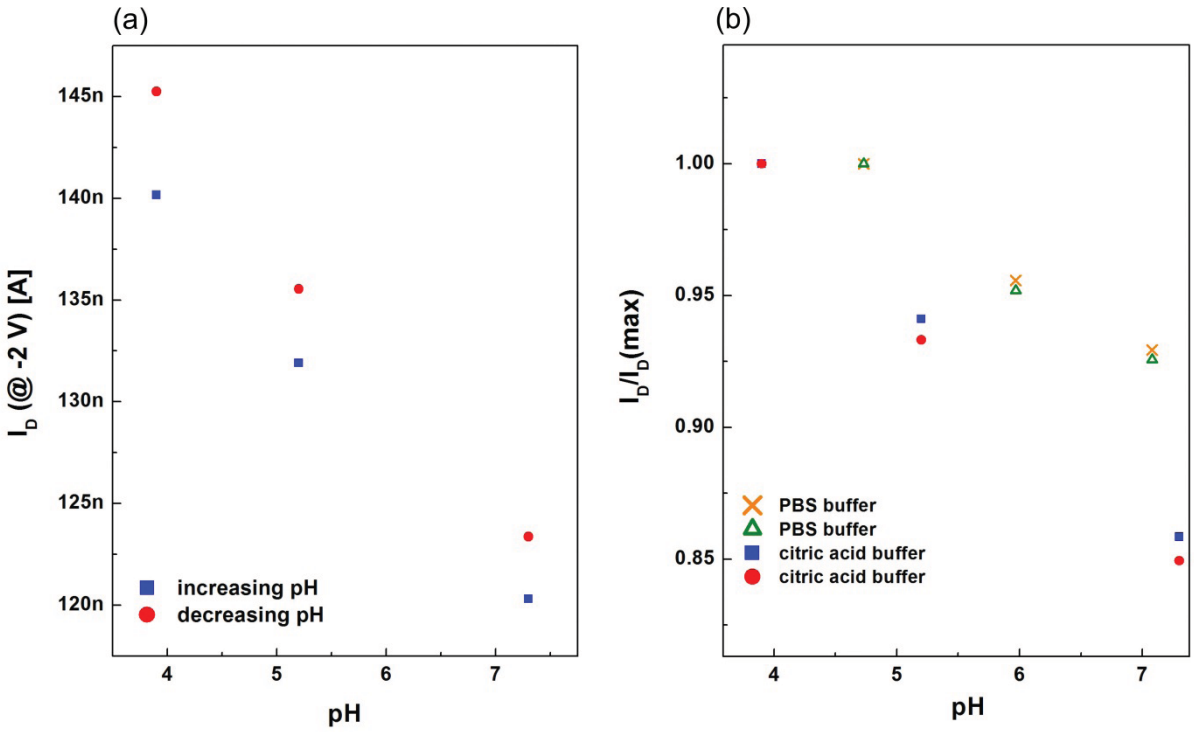

Figure 6.5: (a) On-currents (I_D @ V_G = -2 V) were extracted from two successive pH sweeps. The data of the increasing pH sweep are plotted as blue squares and the results from the decreasing pH sweep are plotted as red circles. In (b) a comparison of the results of two different kinds of buffers are shown. The results of (a) were obtained using a citric acid buffer. In (b) the same results (also depicted with the same symbols and colors) are shown but normalized with respect to the data point at pH 3.9

Several groups, including the Institute of Nanoelectronics, that are working with field-effect transistors in electrolyte-gated configuration that are based on (organic) p-type semiconductors, report that the drain current increases for a decreasing acidity of the electrolyte.[88,83,103,104,69] In a very simple model this is explained by surplus positive (or negative) charges at low pH (or high pH) values that contribute to electrostatic gating of the semiconductor. For back-gated polymeric field-effect transistors the opposite dependence is reported.[86,85] This leads to the suggestion that this behavior can be explained with “mirror charges” or in other words, that negative

charges on the semiconductor surface (or next to it) can induce additional electron holes in the electrolyte-gate-channel (located at the liquid interface). Whereas negative charges on the surface could reduce the electron hole concentration in the bottom-gate-channel (located at the oxide interface) and thus would lead to inverse pH-responses for these two configuration types. For SWNT-FETs, however, such a model seems not appropriate at a first glance. This is, because carbon nanotubes are often referred to as “one dimensional” opposed to bulk semiconductors. That means that the diameter of the tubes is very small compared to their length. That may lead to the assumption that measuring the pH response of a back-gated SWNT-FET and an electrolyte-gated SWNT-FET would lead to the same results. However as discussed above and shown in Figure 6.5 and Figure 6.6 it was observed, that the threshold voltage shifts towards more negative gate voltages for lower pH values in back-gated devices opposed to SWNT electrolyte-gated ones.[83] The shift that was extracted from our data was around 70 mV per pH. At this point it is worth noting that the carbon nanotube network does not cover the surface of the chip and the gate oxide completely, accordingly also defects or adhesion promoters like APTES could contribute to the pH response of the devices. Indeed several publications indicate that APTES on the semiconductors surface plays a role in pH sensing as protonation of the amine groups may occur at low pH values.[105,106] Hence, the pH response can be also associated to the presence of APTES molecules on the SiO_2 surface. However the pH sensitivity with APTES modified FETs was studied also in the electrolyte-gated mode and qualitatively the same behavior was observed as for

devices without APTES. As afore mentioned, unwanted buffer effects were excluded by conducting the same experiment with PBS buffers of the same concentration. The experiments with PBS gave the same results as the experiment with the citric acid buffer, which is shown if Figure 6.5 (b). This effect was not reported before and further experiments need to be conducted accompanied with additional theoretical work to fully understand these phenomena. Also a comparison with back-gated field-effect transistors based on one single SWNT can be relevant.

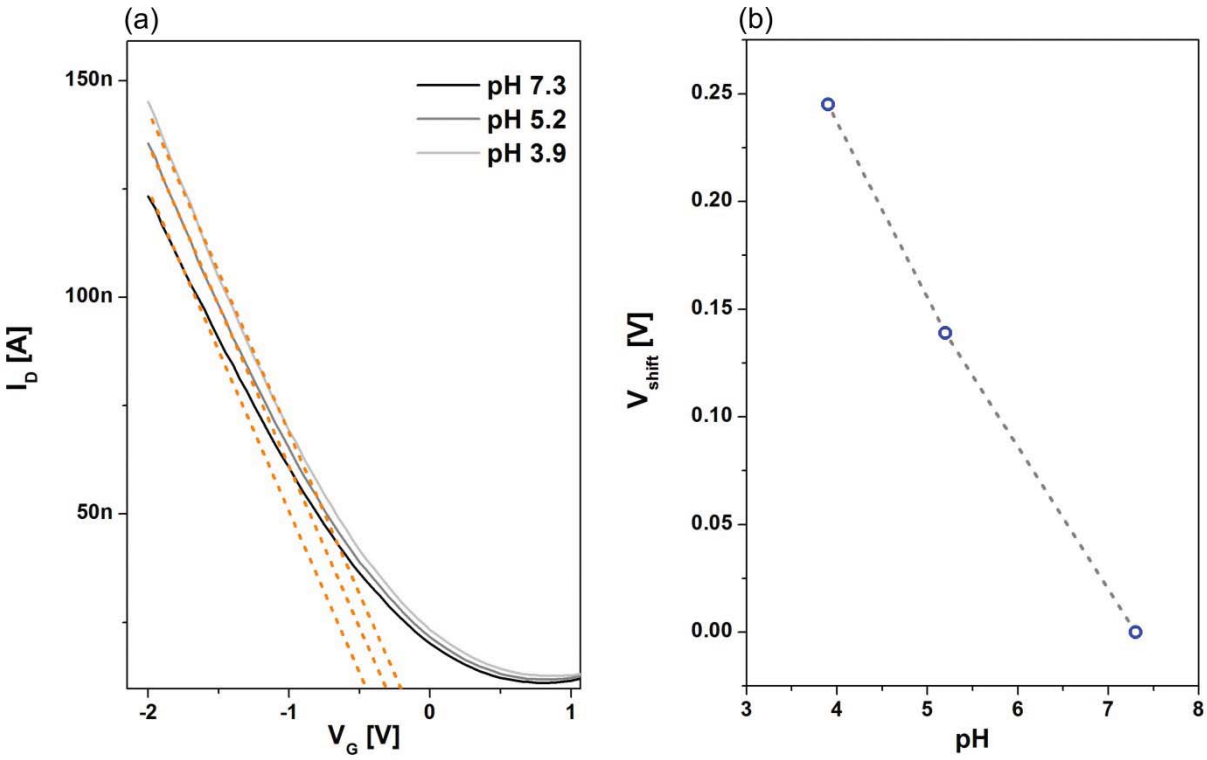

Figure 6.6: In (a) exemplary transfer curves from the measurement in Figure 6.5 (a) are presented to illustrate the threshold voltage shift. The orange dashed lines are linear fits to the transfer curves. V_{shift} is plotted (b) with respect to the threshold voltage at pH 7.3. Herein the dashed black line is a guide to the eye.

6.4 Conclusion

In this chapter back-gated SWNT field-effect transistors and their response on different electrolytic conditions were discussed. Herein the carbon nanotubes were spray-deposited onto silicon pre-patterned silicon dioxide substrates. The field-effect transistors revealed good[22] performance when operated in dry environment (without liquid electrolyte on top of the active layer) and also when operated in an electrolytic environment. Back-gated devices are generally easier to integrate in smart, portable sensors and in microfluidics. This is as no hindering Ag/AgCl electrode needs to be integrated in a fluidic setup. This preliminary work gives an insight in the performance of our SWNT-FET devices under electrolytic conditions and assesses the feasibility of back-gated SWNTFETs as biosensors. The response of the transistors upon exposure to different concentrations of KCl was analyzed and an exponential dependence of the drain current on the KCl concentration was obtained, which is caused by a shift in the threshold voltage. Furthermore our devices have been exposed to buffer solutions with a wide range of pH values leading to a linear shift of the threshold voltage towards more negative values with increasing pH.

7 Protein sensing with Poly(3-hexylthiophene)

This section of the thesis discusses protein sensing with electrolyte gated P3HT-FETs. P3HT is amongst polymeric semiconductors one of the most prominent ones that is used for biological sensing. This is due to the commercial availability, the ease of fabrication of P3HT devices and it offers a good solubility in solvents like DCB, toluene or chloroform.[107] Further the application of P3HT onto substrates resulting in a fairly homogeneous P3HT film is effective in terms of time and costs. That is, that spin-coating of the polymer including an annealing step after coating to remove the excess solvent does not take longer than 15 minutes and does not require expensive evaporation machines nor high-vacuum pumps. It is also possible to remove the P3HT from the substrate after experiments by a short ultrasonication in DCB and to reuse the substrate. This is especially applicable if experiments are performed using the electrolyte-gated device architecture. Herein the silicon dioxide does not serve as the gate-dielectric but rather as a part of the substrate and the thus it is not affected by electrical stress during the experiment. In other words, the fabrication of a working P3HT field-effect transistor is extremely cost-effective and can be conducted in a very short amount of time. In our opinion this fact suggests that approaches for the biofunctionalization of those devices should be inexpensive and uncomplicated.

Here biosensing experiments with P3HT thin-film transistors decorated with biotin molecules in order to specifically detect the biotin-binding protein CaptAvidin are

shown. For this purpose the biotin molecules were attached unspecifically onto the P3HT surface.

7.1 Unspecific binding of proteins onto the P3HT surface

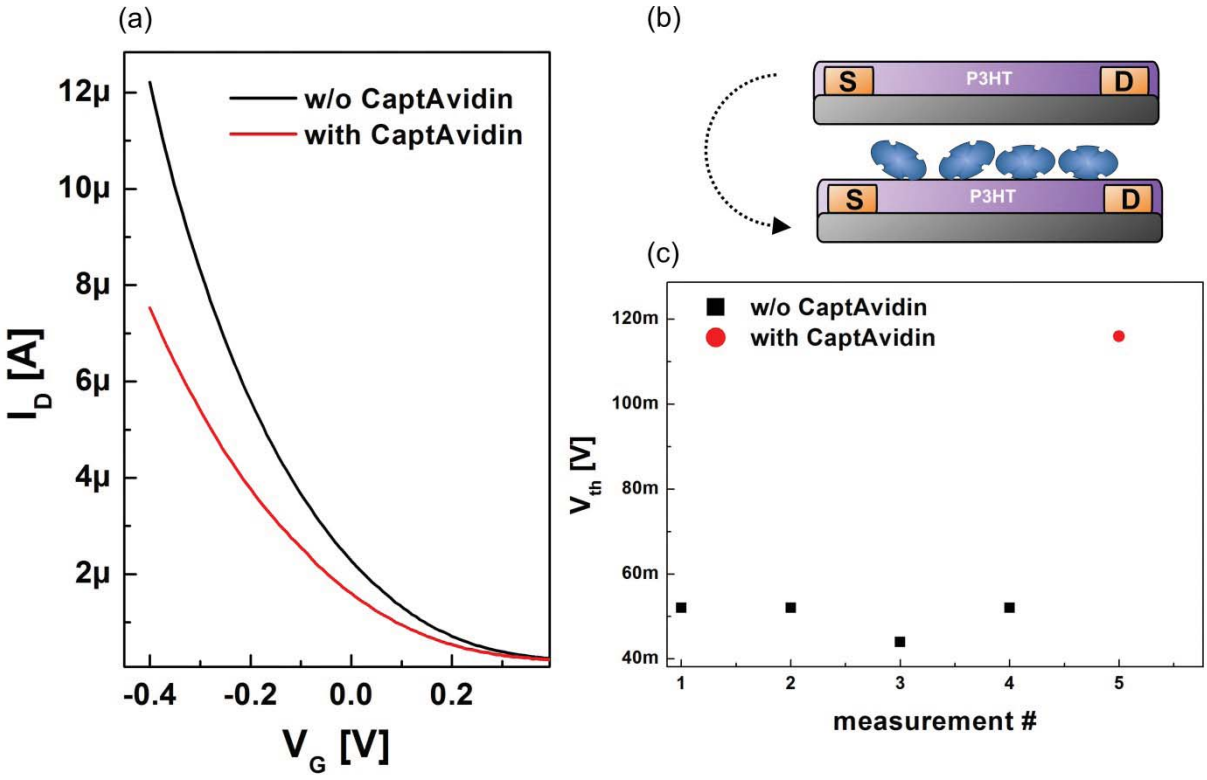

Figure 7.1: (a) transfer curves of a P3HT-FET before (black curve) and after CaptAvidin (5 nM) incubation for 15 minutes (red curve) in pH 7.8. In (b) a sketch of the unspecific adsorption of a protein onto the P3HT surface is shown. (c) The absolute value of the threshold voltage as a function of the number of the measurement. Four transfer curves were recorded before protein incubation (black squares) and another one after protein incubation (red circle).

Unspecific binding of proteins is probably the most perturbing factor when carrying out biological assays and biosensing experiments, as it may cause parasitic sensor signals that superimpose the desired signals.[108,61] To test the response of a P3HT thin-film transistor upon unspecific protein adsorption an experiment was conducted in a 100 mM citric acid buffer at pH 7.8. The protocol was as follows:

First a transfer curve was conducted, after that the buffer in the liquid compartment was exchanged and then another transfer curve was conducted. This procedure was repeated until no significant change upon the treatment was observed, or in other words until a stable response of the transistor was reached. Then the P3HT transistor was exposed to a buffer containing 5 nM CaptAvidin for 15 minutes. After that the device was thoroughly rinsed with the buffer and a transfer curve was taken. The results of this experiment are presented in Figure 7.1. Figure 7.1 (a) shows two transfer curves, one before CaptAvidin incubation (black) and one after (red). A shift of the threshold voltage towards more negative gate voltages along with a decrease of the maximum of the transconductance from about 50 µS to 25 µS was observed. In Figure 7.1 (b) a sketch of the unspecific adsorption of CaptAvidin on the unfunctionalized P3HT surface is shown: Before protein incubation no proteins were in physical contact with the clean P3HT surface. However, after protein incubation it is expected that at least a certain amount of proteins that were injected into the fluidic setup cannot be washed away from the polymer surface and thus sticks unspecifically to it.[108] This may cause alterations in the charge transport between the source and drain electrodes of the transistor, because proteins bear electrically

charged moieties that can act as additional scattering barriers on the P3HT surface. In Figure 7.1 (c) the threshold voltages of this experiment are presented. In this case the threshold voltage was chosen as a parameter to depict the electrical changes upon protein adsorption. Alternatively another parameter like the drain current at a fixed gate voltage could also be presented. A shift of the threshold voltage towards more negative gate voltages was observed along with a change of the transconductance. The latter indicates that the unspecific adsorption of the proteins causes an increase of the amount of scattering barriers at the P3HT surface and thus a change of the carrier mobility.[109]

Generally a significant change of the transistor characteristics upon unspecific CaptAvidin adsorption was observed. It is worth emphasizing at this point that only a very low protein concentration was used, namely solely 5 nM of CaptAvidin and yet the sensor response was relevant and could not be neglected. In order to be able to put the value for the protein concentration in relation with other values used for protein experiment performed by different research groups, some experiments and protein concentrations are presented in Table 7-1.

Semiconductor	Functionalization	Mode	Protein	Concentration	Ref.
SWNTs, CVD	non-covalently functionalized	back gate	streptavidin	2.5 µM	[26]
P3HT (polymeric semiconductor)	non-covalently functionalized	electrolyte-gate	streptavidin	100 µg/ml	[39]
SWNTs, CVD	unfunctionalized	back gate	streptavidin	40 nM	[110]

SWNTs, CVD	non-covalently	back gate	B. burgdorferi flagellar antigen	1 ng/ml	[111]
Pentacene	covalently	back gate	anti-BSA	50 nM	[112]
Graphene	non-covalently	back gate	IgG	2 ng/ml	[113]
Graphene	non-covalently	electrolyte gate	lectins	2 nM	[114]
SWNTs, AC DEP	non-covalently	electrolyte gate	lectins	2 nM	[114]
Si nanowire, wet etching	covalently	back gate	streptavidin	10 nM	[22]
Si nanowire,CVD	covalently	AC trapping	PSA	100 aM	[115]
Si nanowire, wet etching	covalently	electrolyte gate	streptavidin	2 nM (down to 200 fM)	[116]

Table 7-1: : A list of selected publications. The column "protein concentration" gives the value of protein concentrations at which the respective sensor responded significantly upon protein adsorption. The adsorption can be a specific interaction with a protein ligand or an unspecific interaction with the surface of the semiconductor.

The meaning of this finding may be double-edged; on the one hand the P3HT-sensors used within this thesis seem very sensitive towards changes on the surface of the polymer, yet on the other hand, already at very low protein concentrations unspecific protein adsorption seems to play an important role. This fact needs to be considered for the design of all experiments involving proteins and furthermore the potential demand of a passivation towards unspecific protein binding.

In the following section a possible functionalization scheme is presented, which considers not only the provision of protein binding sites onto the surface of P3HT but also of molecular sites that function to repel unspecific protein adsorption.

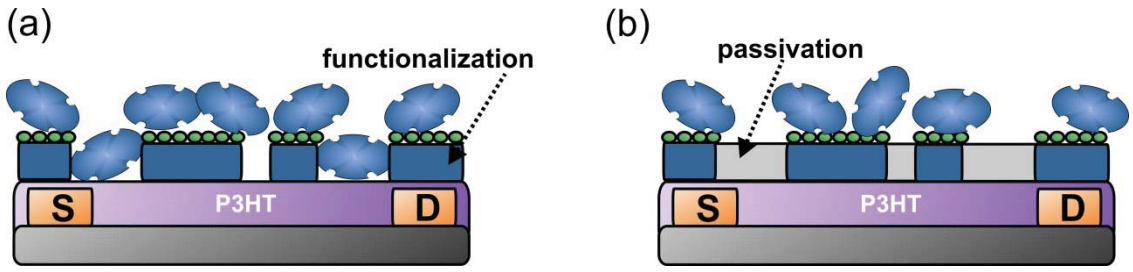

Figure 7.2.: A sketch depicting protein sensing with P3HT-FETs, whereas in (a) a P3HT-FET with a functionalization layer and in (b) a P3HT-FET with a functionalization layer and a passivation layer is shown. The functionalization layer is depicted realistically as a layer with a certain amount of gaps. These gaps expose the surface of the semiconductor and are thus prone to unspecific binding of proteins. A passivation layer which is located in between the functionalized regions may function as a protein repellant and hence to sensor signal would occur from transistor regions that are not functionalized with protein ligands.

7.2 Non-covalent P3HT functionalization with PEG-Biotin molecules

As discussed in the section above, there exist several requirements for the functionalization of a biosensor, namely the functionalization should render the surface of the sensor tethered with protein ligands and, if possible, also with molecules that suppress protein binding at specific locations, preferably in the gaps of the bio-functional layer. Another requirement that arises especially when dealing with sensors that are supposed to be disposable one-way-devices is that the functionalization should be accomplishable in a fast and simple procedure. Regarding these aspects the functionalization of the P3HT-surface was carried out with the molecule that is depicted in Figure 7.3 – mPEG-Biotin, which was purchased from Nanocs Inc.

As the name already suggests, the molecule comprises two functional parts, one end of the molecule is the protein ligand biotin and the other, a polyethylene glycol with a molecular weight of 1000, should serve to prevent from unspecific binding.[117,118] The functionalization protocol was as follows: 7.5 mg of mPEG-Biotin were dissolved in 1 ml DI water. Subsequently a freshly prepared P3HT-FET was exposed to the solution for roughly 24 hours, followed by thoroughly rinsing of the device and drying with nitrogen.

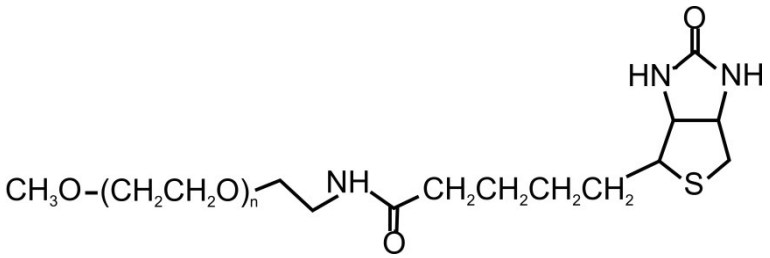

Figure 7.3.: mPEG-Biotin was purchased by NANOCS and used to noncovalently functionalize the P3HT surface with biotin molecules. The PEG-part of this molecule should serve to avoid unspecific binding of protein onto the P3HT surface. Molecules with a molecular weight of 1000 were used for protein binding experiments.

The protein binding experiments were executed according to the subsequent protocol: After the functionalization of the P3HT-FET transfer curves were conducted (three transfer curves were measured each time. For the reason of simplicity only one is shown in the graphs) in a 10 mM pH 4 buffer (citric acid) solution, subsequently the transistor was exposed to 140 nM CaptAvidin for one hour and after that another transfer curve was taken (the reason for the initial incubation for 60 minutes is discussed in more detail below). In order to unbind CaptAvidin from the

biotins on the P3HT surface, the device was exposed to 100 mM pH 10 buffer for 3 minutes. Accordingly the buffer was exchanged to the pH 4 buffer and transfer curve were measured. After this the protein incubation step was performed during a period of 10 minutes, followed by measuring transfer curves and performing a pH 10 recovery step. Except for the initial one-hour-long exposure to the protein this procedure was repeated several times. Also every buffer exchange step that was involved in this procedure was conducted carefully with pipettes and was accompanied by thorough rinsing of the P3HT-FET. Furthermore it should be noted that the discussed experiments were performed by using a platinum wire as the gate electrode. Yet, measurements using platinum can lead to misleading pH-sensitive results (platinum seems to tend to a pH-dependent oxidation or reduction in electrolytes under an applied potential).[53] However, much attention was paid during the experiment that the gate electrode does not get into any contact with pH 10 buffer nor with the protein in order to avoid parasitic signals and all electrical measurements were performed in the same pH 4 buffer solution.

The reason that the first incubation of the protein was executed for a time period of one hour was as follows: it was assumed that the PEG-part of the functionalization molecule provides for at least partially blocking of unspecific binding events and that further blocking may be provided by CaptAvidin molecules that already stick unspecifically to the P3HT surface and thus prevent further proteins to attach onto the surface.

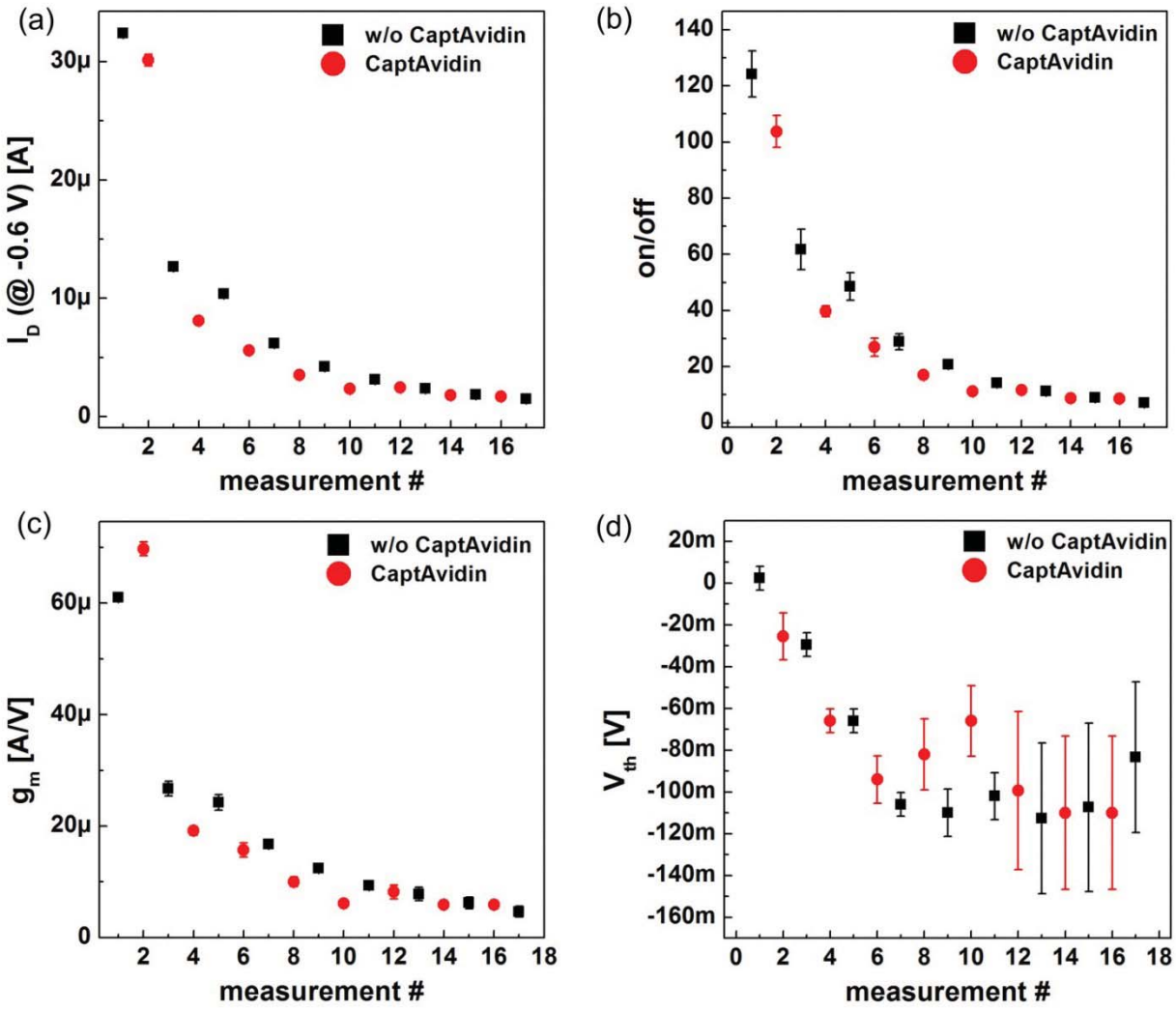

Figure 7.4: in (a) the drain current at the maximum gate bias of -0.6 V is plotted in order of the measurement. (b) shows the corresponding on/off ratio, (c) the maximum transconductance and (d) the threshold voltage. The black squares depict data of measurements were no protein should be present in the fluid chamber as weather no protein was yet injected in the chamber (only first data point) or the protein was washed away using a pH 10 buffer. The red circles depict data points of measurements where the protein should be bound to biotin and thus present on the surface of the transistor. The error bars result from averaging over the three measured transfer curves.

The results of a typical experiment are shown in Figure 7.4. In order to analyze the sensing mechanism several transfer characteristics such as the drain current at the maximum gate bias of -0.6 V (in Figure 7.4 (a)), the on/off ratio (in Figure 7.4 (b)), the maximum transconductance (in Figure 7.4 (c)) and the threshold voltage (in Figure 7.4 (d)) were plotted in the order of the measurement.

To meet the large amount of data the above mentioned values were extracted from the transfer curves via MATLAB, whereat the corresponding MATLAB code is presented in the Appendix. The black squares depict data of measurements were no protein should be present in the fluid chamber since either no protein was yet injected in the chamber (only first data point) or the protein was washed away using a pH 10 buffer solution. The red circles depict data points of measurements where the protein should be bound to the biotin and thus be present on the surface of the transistor. The error bars result from averaging over the three measured transfer curves. From Figure 7.4 (a) it is obvious that the drain current of the transistor is affected by the experiment. It is eye-catching that the drain current follows an exponential decay, starting with a significant current drop within the first three measurements by roughly 30 % from the initial value. This decay may be attributed to the first incubation with the protein and to the instabilities of the polymer under bias stress.[69]

The data in Figure 7.4 show that the drain current I_D at V_G = -0.6 V, the on/off ratio and the transconductance of the transistor is lower after protein incubation than before or after the pH 10 recovery, respectively. This behavior leads to a “zig-zag”

shape of the respective curves. Additionally to the data presented above corresponding transfer curves of the measurements #3 to #5 are shown in Figure 7.5. It can be seen that protein incubation causes a tilt (meaning a change in the transconductance) of the transistor characteristics and that after the pH 10 recovery this tilt is reversed again.

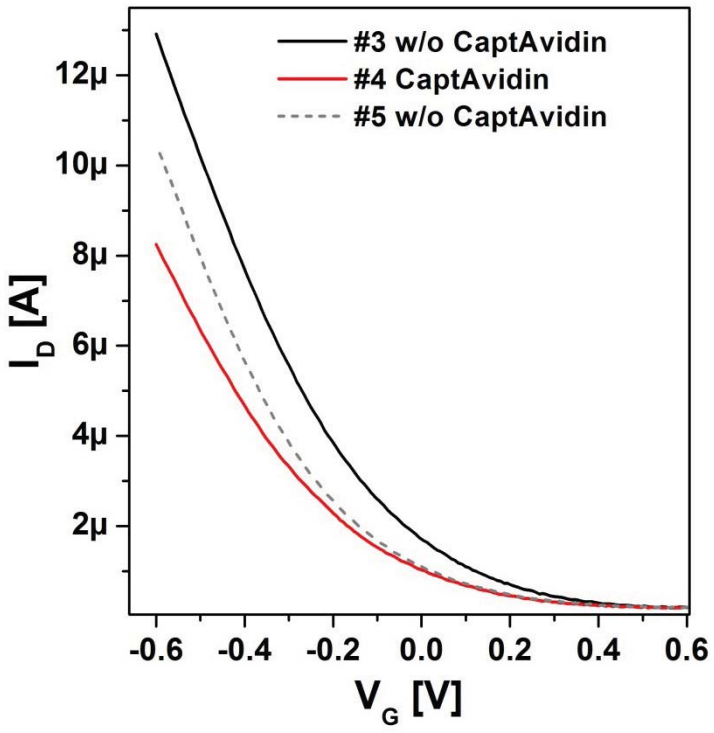

Figure 7.5.: Transfer curves before (black) and after protein incubation (red) for 10 minutes with CaptAvidin and after a pH 10 regeneration for 3 minutes (grey, dashed). Curves were conducted in 10 mM pH 4 buffer.

The threshold voltage of the curves of this experiment decreases similarly to the drain current, starting from an initial value of roughly 0 mV to -120 mV, meaning that a threshold voltage shift towards more negative values was observed during the

whole experiment. The saturation of the threshold voltage at the end of the measurement goes along with an increase of the margin of the error bars (≈ ±40 mV). The increase of the margin of the error bars is attributed to general difficulties to determine the threshold voltage for transistors that do not offer excellent transistor properties. However, it can be seen that also the threshold voltage changes very much during the experiment until a stable mean value is reached towards the end. Yet the dependency regarding protein binding and unbinding does not seem as clear as for the other transistor characteristics like the transconductance or the drain current.

According to equation 3.9 in section 3.2.1 the transconductance is directly proportional to the gate capacitance and to the charge carrier mobility. Assuming that all changes of the transfer curves that are observed within this protein binding experiment are caused by the presence of CaptAvidin on the P3HT surface (or the absence after protein removal after pH 10 washing), the changes of the gate capacitance and/or the changes of the charge carrier mobility may be explained as follows: additional scattering of holes in the channel of the transistor leads to a reduction of the mobility of those holes. In this context extra scattering sights may be provided by proteins on the P3HT surface. Regarding the capacitance, a reduction of the gate capacitance goes along with an increase of the thickness of the gate dielectric, which may be caused by an additional layer of proteins on the P3HT surface, that increase the net thickness of the dielectric.

On the other hand side it could be expected from protein binding experiments that the dependence of the threshold voltage on the presence of the protein is more significant as it was observed and presented in Figure 7.4. The dependence of the threshold voltage is discussed in section 3.2.1 and as explained therein, a protein "layer" at a certain distance to the semiconductor surface is expected to lead to threshold voltage shifts. However, it is worth noting at this point that yet a fairly high buffer concentration was used for those experiments, namely 10 mM citric acid buffer. Knowing the Debye screening length is thus necessary. Equivalently to equation 3.10 the Debye screening length is given by:

$$L_D = \sqrt{\frac{\varepsilon_0 \varepsilon_r k_B T}{2 N_A e^2 I}} \qquad 7.1$$

with

$$I = \frac{1}{2} \sum_i c_i z_i^2 \qquad 7.2$$

Where L_D is the Debye screening length, ε_0 is the permittivity of free space, ε_r is the relative permittivity, k_B the Boltzmann, T is the temperature, I is the ionic strength, c_i is the molar concentration of ion i (mol/l), z_i is the charge number of ion i.

However the calculation of the Debye screening length for a complex buffer would require computational methods as c_i as well as z_i are a function of the buffer pH and of the concentrations of other molecules in solution (see e.g. reference [119]). Yet a first

approximation can be estimating the Debye screening length by using a “monovalent salt model”.

Which means that at least a rough range for the Debye length can be calculated by assuming that all ions presence in the buffer solutions are monovalent ions. Treating the buffer solution for the above mentioned experiment as a monovalent salt the Debye length for the solution would be approximately 3 nm.

If one further assumes that the PEG-part of the functional molecules sticks closely to the P3HT surface, that the biotin-part of the molecule stand free to interact with a protein and that biotin has a length of about 1 nm [120,121] only a fraction of the protein would find itself within the Debye length, which could be one possible explanation for the weak response due to protein incubation with respect to changes of the threshold voltage.

Yet the source of the modifications of the transfer curves after protein injection cannot be elucidated easily and further control experiments need to be performed. Thus the following experiment was developed: the experimental protocol remained the same as before, however, with the significant modification that CaptAvidin was not incubated on the chip in pH 4 buffer but in pH 10 buffer. In theory this means that the protein is not capable of binding to biotin under these conditions und that no change of the transfer characteristics, similar to the changes above, should be observable. In Figure 7.6 the results of this experiment are presented. Overall the data show a response. To what extent this response differs from the response of the

measurement above shall be discussed below. First the changes of the drain current at a fixed potential, I_D at V_G = -0.6 V (shown in Figure 7.6 (a)), shall be discussed: the drain current after the pH 10 washing step (black squares) does not increase compared to the current after protein incubation, which was the case for the measurement at which the CaptAvidin was incubated in pH 4 conditions. This is the case for all measurements except for the measurements numbered #2 and #3, so the data point after the first binding and unbinding. Generally the lower response of I_D compared to the experiment before could be a consequence of the poor efficiency of protein binding at pH 10. However, the fact that there is a significant response for the measurements #2 and #3 may be due to an initial dominance of unspecific binding events compared to specific binding of CaptAvidin to biotin (it is not reported that unspecific binding of CaptAvidin and biotin is also a function of the pH of a solution). In return that indicates that also in the experiment which is presented in Figure 7.4, there is a component of the response of the sensor which may be partially attributed due to unspecific binding that might play a more relevant role during the period of the first protein incubations. This is thinkable under consideration of the following scenario: a certain fraction of the P3HT surface is decorated with PEG-biotin molecules and another fraction might be free from PEG-biotin molecules in a way that CaptAvidin can adsorb unspecifically onto those regions. In addition, it is

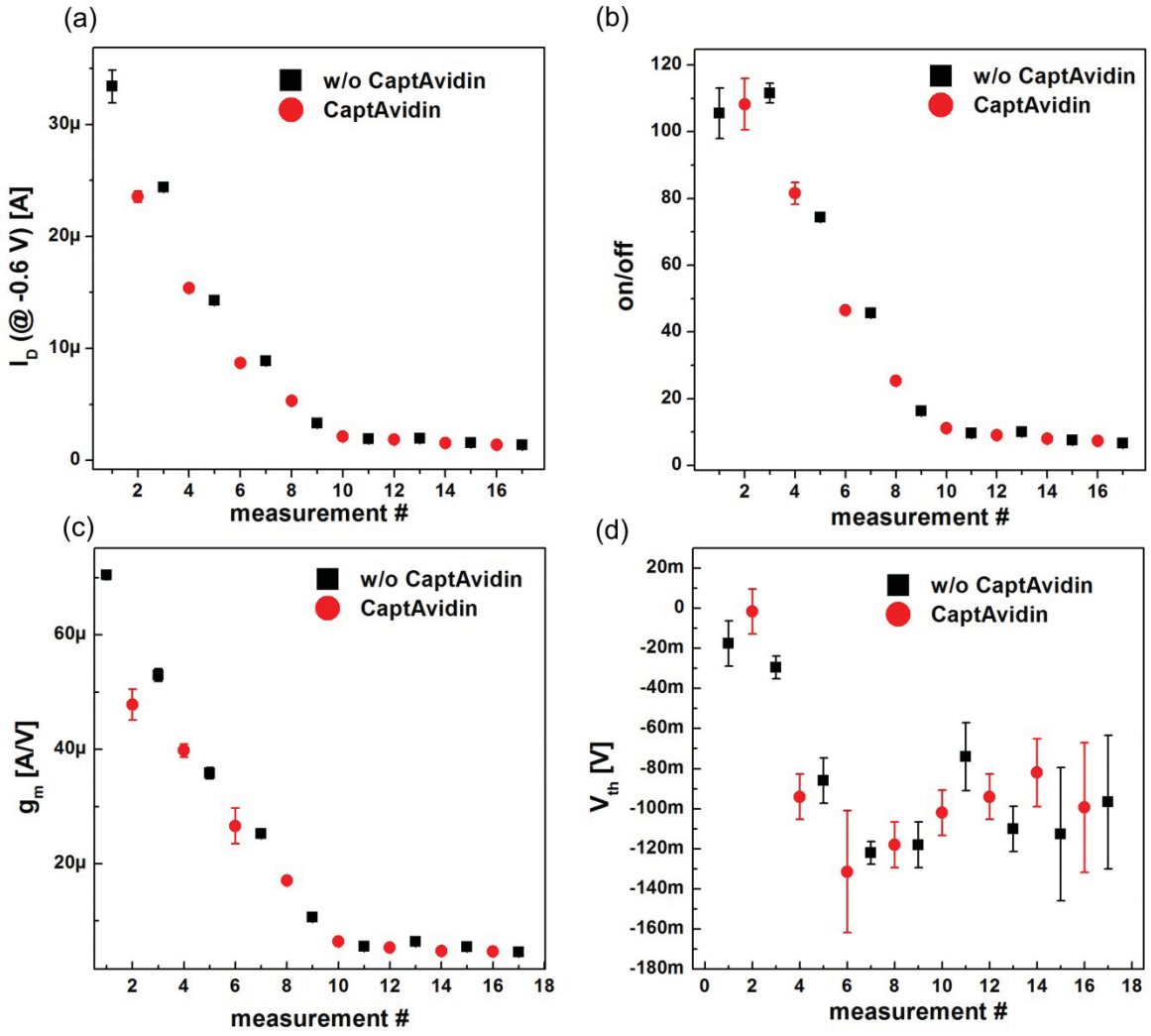

Figure 7.6.: Control experiment in (a) the drain current at the maximum gate bias of -0.6 V is plotted in order of the measurement. (b) shows the corresponding on/off ratio, (c) the maximum transconductance and (d) the threshold voltage. The black squares depict data of measurements were no protein should be present in the fluid chamber as weather no protein was yet injected in the chamber (only first data point) or the protein was washed away using a pH 10 buffer. The red circles depict data points of measurements where the protein should be bound to biotin and thus present on the surface of the transistor. The error bars result from averaging over the three measured transfer curves.

common knowledge that unspecifically bound proteins tend to stick so strong to surfaces that removing the proteins form the surface by washing is barely possible.

Accordingly it is consequential that the places at which CaptAvidin is able to bind are all occupied at one point and that the rate of unspecific binding saturates. This is in correlation with the fact that the protein was incubated for one hour for the first incubation step.

Three transfer curves of the measurements #3 to #5 are shown in Figure 7.7. in analogy to Figure 7.5.

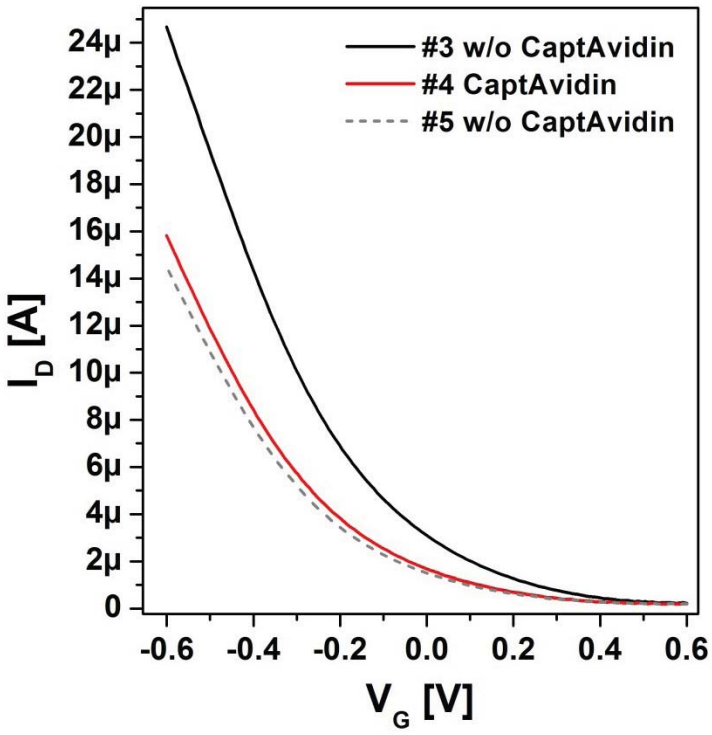

Figure 7.7.: Transfer curves before (black) and after protein incubation (red) in pH 10 buffer for 10 minutes with CaptAvidin and after a pH 10 regeneration for 3 minutes (grey, dashed). Curves were conducted in 10 mM pH 4 buffer.

It can be seen that after pH 10 washing the drain current does not surpass the drain current of the curve that was taken after protein incubation. However, there is a

clear tendency that the curve after protein incubation seems to affect the transistor more than the curve after pH 10 washing. Besides the possible explanation, which was mentioned above, it is moreover possible, that the transistors are additionally affected by the harsh buffer conditions, meaning that there might be sensing artefacts that are caused by the alternating exposure of P3HT to highly acidic and highly basic buffer solutions.

7.3 Discussion

In the case of a rapidly degrading device such as a P3HT transistor bench top experiments using conventional proteins such as avidin and streptavidin that feature exceptionally high binding affinities towards biotin, are not recommendable. This is because the bond between the respective protein and its ligand cannot be broken easily. As a consequence it is very demanding, probably impossible, to tell whether the response of a P3HT transistor is due to a specific protein binding to the ligand in proximity to the surface of the polymer, effects of the protein incubation protocol or unspecific adsorption on the polymer surface directly. On the contrary, protein binding experiments with protein-ligand systems such as CaptAvidin-biotin offer the advantage that a binding experiment can be repeated several times. That is that due to the following reasons:

After repeating an experiment several times the device is reaching equilibrium. For example, most of the experiments reported herein require the use of at least two

different buffers and the pH value of those buffers differs significantly from each other, buffer A and buffer B respectively. At which buffer A reveals an acidic pH and buffer B a basic pH. Thus, a high sensor response after changing the fluid from the flow chamber from buffer A to buffer B and then back to buffer A may be attributed, at least partly, to a protonation and deprotonation of dangling bonds on the P3HT due to the harsh buffer conditions. Additionally, being able to repeat an experiment with the same sensor device is useful as one may perform the same experiment under different experimental conditions as for example using different protein concentrations. This may lead to valuable data such as the binding constant of a protein without the need to prepare a multitude of identical, or at least very similar, transistors, which would be necessary to be able to compare the data of several transistors. Furthermore the repeatability leads to the advantage of a stochastic analysis of an experiment und thus to a “better”, in a sense of “closer to nature” description of protein-ligand binding which is also a stochastic phenomenon.[3,116] As indicated above there is also another advantage due to the repeatability of binding experiments with CaptAvidin, which may be of great interest when sensing with easily degrading, polymeric devices, namely, at least according to our observations, there might be a regime in which the protein sensing signal is not superimposed by the degradation of the device. That leads to further aspects: even if it was not possible to tell if the response of the previous experiments was of specific nature, it could observed that even P3HT transistors, that are degrading extremely fast, seem to reveal a sensitive regime in which the presence of proteins can be observed.

7.4 Non-covalent P3HT functionalization with biotinylated Au-nanoparticles

In this section protein sensing with P3HT-FETs that were decorated gold nanoparticles (AuNPs) is presented. At the beginning AFM images of gold decorated devices along with a sketch of the working principle is shown and then transfer curves of electrical experiments are depicted. Finally a stochastic analysis of the binding events was performed and is presented in this chapter.

Generally it is of great interest that protein sensing can be detected with a second detection method. Preferably this second method should be independent or different from the first detection method. Thus, within this thesis protein sensing was performed with P3HT-FETs that were functionalized with biotinylated Au-NPs. The functionalization with rigid particles offers the advantage of visualizing protein-ligand binding with an atomic force microscope (AFM, a complimentary second method). The particles used for these experiments had a diameter of 20 nm and were purchased from Nanocs Inc. The particles were dispersed in DI water (already by the provider) having a concentration of $9 \cdot 10^{16}$ particles/liter. Additionally 40 nm Au-NPs that were coated with streptavidin proteins were purchased from the same company. The intention of having a protein and its ligand attached to nanoparticles of different sizes was to be able to observe streptavidin binding to a biotinylated P3HT surface, or to be able to check with a second method that the functionalization of the P3HT surface is working at all. The functionalization protocol was as follows: a droplet with a volume of 5 µl was drop-casted onto a certain area of P3HT. It was waited until the

droplet was evaporated. This was performed like that because as much unspecific interactions of the gold particles with the P3HT surface was desired. After that the surface was rinsed with DI water. Subsequently a 1:10 solution of the streptavidin-particles in 10 mM Trizma buffer at pH 7 was put on top of the biotinylated area for 30 minutes. pH 7 and standard salt concentrations were chosen to promote binding of streptavidin to biotin. Good care was taken that the streptavidin solution was not evaporating in those 30 minutes as unspecific adsorption of the streptavidin AuNPs would lead to misleading results. A sketch of the procedure is presented in Figure 7.8 a). In the upper part of the sketch a P3HT device after functionalization with biotinylated 20 nm-AuNPs is shown. The arrow, that points from the upper to the lower part of the sketch in Figure 7.8 represents the step of protein incubation. During the protein incubation step streptavidin that is tethered to the 40 nm-AuNPs should bind to the biotins on the P3HT surface. Intentionally, the device was rinsed extensively after the protein incubation so that the rate of unspecific binding events would be decreased. In Figure 7.8 (b), (c) and (d) AFM images of an exemplary device after protein incubation and with different magnifications are shown. It is possible to identify regions with big (40 nm, protein) particles that are distributed in regions where one can also find are small particles (20 nm, ligand).

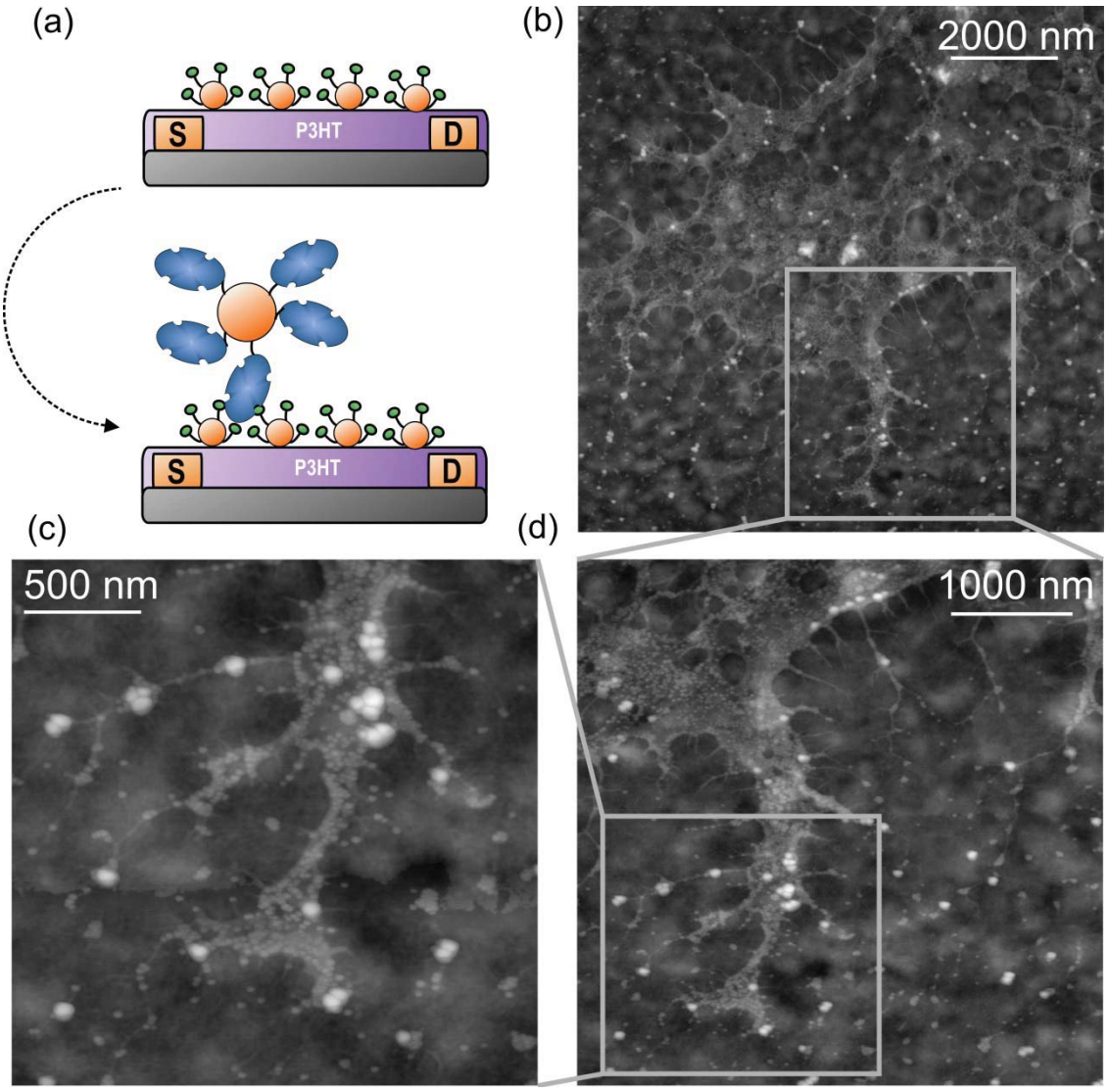

Figure 7.8.: In the upper part of the sketch a P3HT device after functionalization with biotinylated 20nm-AuNPs is shown. The arrow represent the step of protein incubation. (b), (c) and (d) are AFM images of an exemplary device after protein incubation and with different magnifications.

Besides AFM measurements also electrical measurement were performed. However, as in the protein experiments of section 7.2, CaptAvidin was used instead of streptavidin in order to be able to unbind the protein again from the P3HT surface.

7.5 Electrical experiments with AuNP-decorated P3HT-FETs

Electrical experiments with AuNP-decorated P3HT field-effect transistors were performed according the following (functionalization was carried out using the functionalization protocol that was established during AFM pre-characterization): a pre-bias of V_D = -400 mV and V_G = -600 mV was applied to the device for 10 minutes in order to compensate for bias stress effects.[69] After that several reference measurements without CaptAvidin samples were performed (in Figure 7.9 those are the measurements from #12 to #19). That means that a pH 4 sample (without CaptAvidin) was incubated for 15 minutes, subsequently the pH 4 buffer was exchanged with a “fresh” pH 4 buffer in order to take a transfer curve. Further the transistor device was rinsed with a pH 10 buffer, followed by exchanging the pH 10 buffer with a fresh pH 4 buffer in order to take another transfer curve. After these reference measurements CaptAvidin was incubated for the first time (#20) and the standard protein measurement protocol was carried out. Results (I_D at V_G = -0.6 V) of such a measurement are presented in Figure 7.9 (b) and the arrow in the sketch of Figure 7.9 (a) is representing a protein incubation step. The first time CaptAvidin was incubated was between measurement #19 and #20, which is marked by a 1 µA decrease of the drain current, which may be attributed to a significant contribution of unspecific bound proteins onto the P3HT surface. For the rest of the response curve the typical zig-zag behavior can be observed. However, the response that is caused by the CaptAvidin incubation step is decreasing.

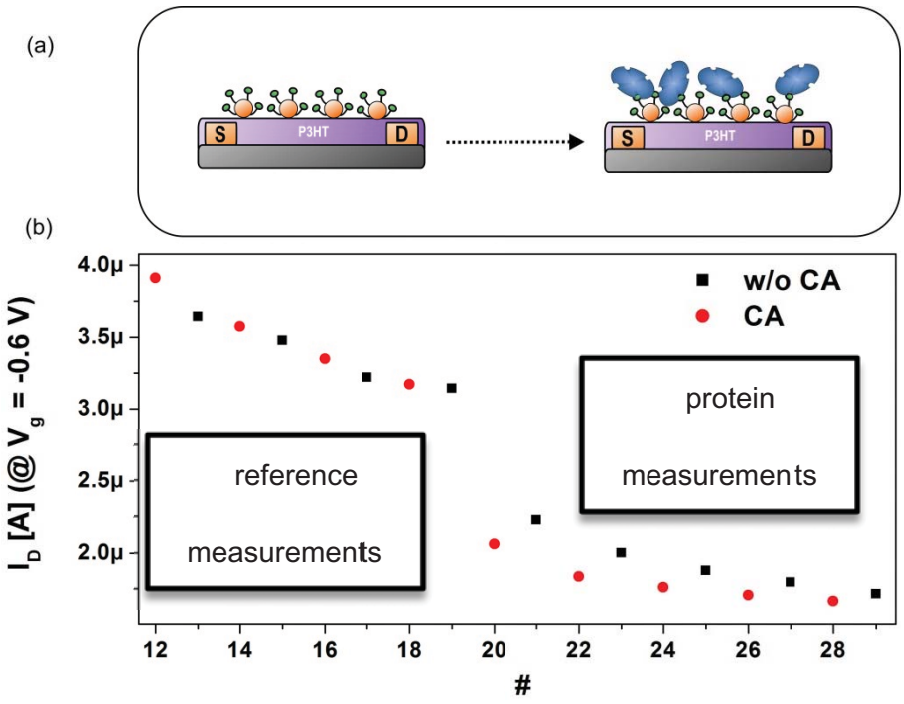

Figure 7.9.: (a) shows a sketch of a P3HT-FET, which is functionalized with biotinylated AuNPs. The arrow indicates a CaptAvidin incubation. (b) shows data of an electrical CaptAvidin binding experiment. Measurements #12 to # 19 are reference measurements (without CaptAvidin sample but else the same measurement protocol). Starting from measurement #20 140 nM CaptAvidin was used

In Figure 7.10 a set of transfer curves that belong to the measurements of Figure 7.9 are presented. (a) shows transfer curves of a reference measurement (#17 – #19) and (b) shows a measurement with CaptAvidin (#21 – #23). The curves that were taken before protein incubation are presented in black solid lines. The ones after adding CaptAvidin are presented in red lines and the dashed black lines correspond to measurements that were taken after rinsing with pH 10. From (a) it can be deduced that the treatment upon buffer exchange does not affect the characteristics of the transistor. However, as soon as CaptAvidin is added to the system a shift of the threshold voltage is observed: the threshold voltage shifts towards more negative

voltages when CaptAvidin is bound to biotin and shifts back towards more positive voltages after the pH 10 recovery.

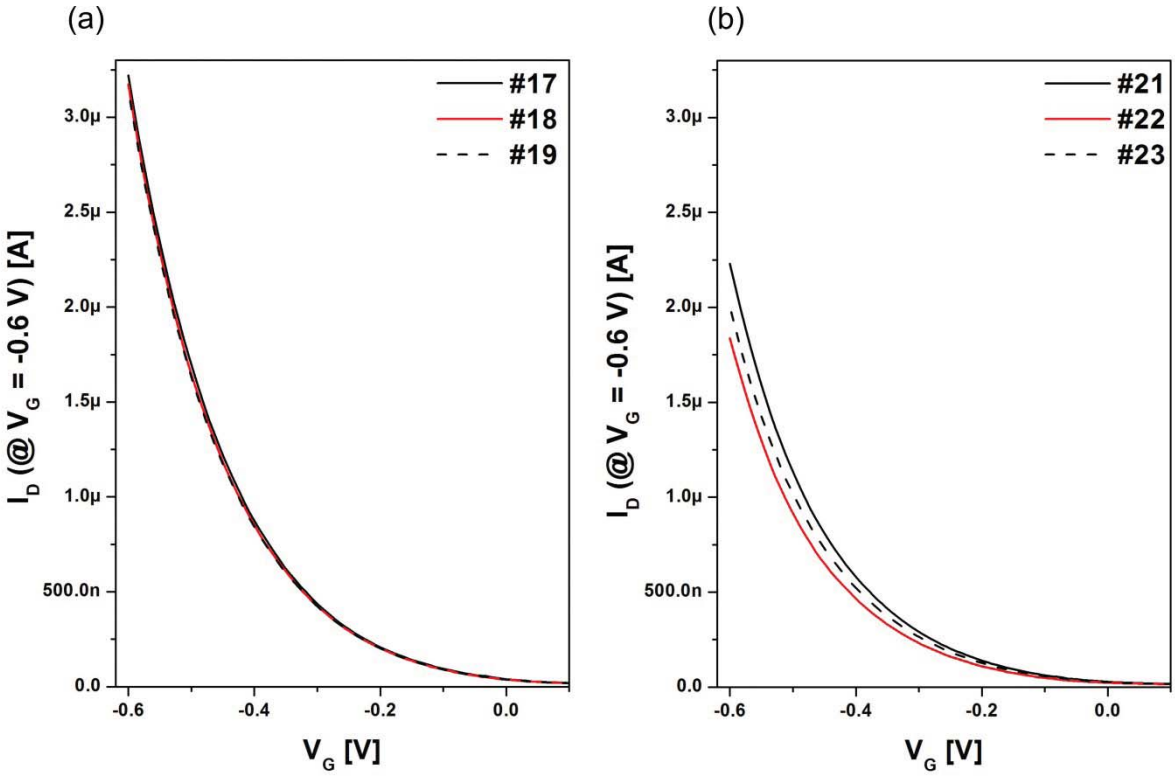

Figure 7.10.: (a) is a reference measurement without CaptAvidin and (b) is a measurement with CaptAvidin. For both measurements the same buffers and the same parameters were used. The solid black lines represent data before and the red lines are data after protein incubations. The black dashed lines are data after, which were taken after the pH 10 recovery step.

Yet the transfer curve that was taken after pH 10 rinsing does not return to its initial value (solid black line), which shall be discussed below with the help of a "gedankenexperiment": According to the findings of other research groups, protein-ligand binding results in a shift of the threshold voltage. If a tilt of the transfer curve occurs other effects cause the change in drain current, such as charge transfer from

adsorbed proteins into the semiconductor layer or generally unspecific binding.[21,61] That is, if the entire P3HT surface was covered with biotinylated nanoparticles, CaptAvidin incubations would cause a shift of the threshold voltage that is ideally in the range of the zeta potential of the protein. Further if the pH 10 recovery would work in a way that 100 % of the protein is rinsed away; the threshold voltage shift is reversed. In our experiment the threshold voltage shifts roughly about 30 mV after protein incubation, which is in the order of magnitude of the zeta potential of avidin[121,], and after the pH 10 incubation step the threshold shifts by about 15 mV in the opposite direction. The fact that it is obviously the shift of the threshold voltage that is the predominant factor that leads to the changes of the transfer curves may indicate that also unspecific binding plays a minor role in sensing here. However the reason why the pH 10 recovery is less efficient as expected remains a question. At this point it is worth noting that for the pH 10 rinsing step several different methods and exposure times have been tried out but no significant differences were observed. The following scenarios as well as a mixture of the following scenarios are thinkable: Also unspecific binding of a protein onto the P3HT surface can result in a threshold voltage shift and thus a certain amount of protein remains on the P3HT surface. Probably this part of the surface is not covered with biotinylated nanoparticles; furthermore, the pH 10 recovery is not efficient due to reasons that are not known; Additionally it is possible, that binding of CaptAvidin to biotin is affected by the presence of the nanoparticles (opposed to biotins that may be equally distributed on the surface of a semiconductor. The distance of the biotins of the gold surface is not

known (technical requests about details of the functional layer on the gold particles remained without result) for example and a very tight packing of biotins may lead to some steric effects; Another reason could be, that repeating the measurement procedure too many times renders the system damaged and unstable.

In Figure 7.11 an equivalent CaptAvidin experiment is shown with the difference that the protein was already injected into the system in an early stage of the experiment, namely already at the third measurement. At the regime where the P3HT degradation reveals a linear behavior the response of the transistor offers a steady zig-zag shape.

The results of this measurement may indicate that the duration of the experiment affects up to a certain point the quality of the experiment.

What can be deduced from the data in this section is, above all, that even though a sensing signal upon protein incubation is measured, it is necessary to properly analyze the cause of this signal and the underlying sensing mechanism, control measurements are needed as well as a large amount of data in order to perform a stochastic analysis.

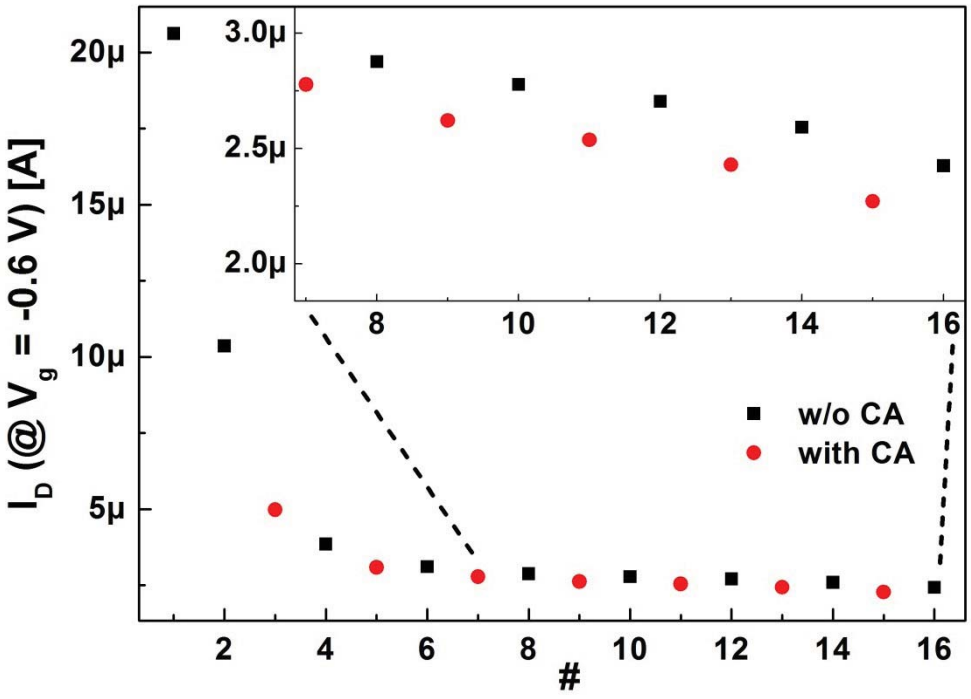

Figure 7.11.: Drain current at a constant gate biase of -0.6 mV. Red circles represent data that were taken after protein incubation and the black square represent data after the pH 10 recovery.

7.6 Stochastic analysis of protein-ligand binding

For a proper analysis a standardized analysis method was necessary, which will be described below and is illustrated in Figure 7.12. An exponential function was fitted into the data points that were taken after protein incubation. This was done in order to be able to subtract a data point between two consecutive protein data points (orange cross) from the black square, illustrating a data point after pH 10 recovery, directly above the orange cross. By using this method it is possible to conveniently analyze the data even in regimes that are not linear but show a rather exponential behavior.

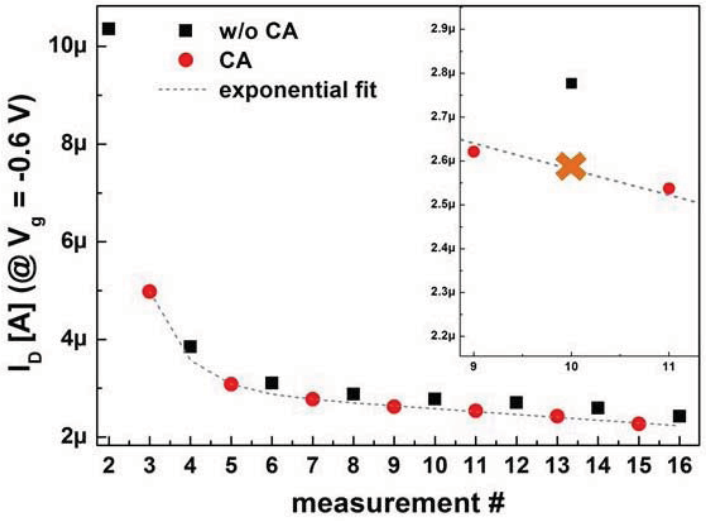

Figure 7.12.: Drain current at a constant gate biase of -0.6 mV. The dashed grey lines is an exponential fit of the data point that were obtained after CaptAvidin incubation. The inset illustrates the standardized analysis method: the difference between the black data point and the orange cross was taken

With the data obtained in this way, numerous protein-ligand binding experiments were analyzed and the results are presented in Figure 7.13. The data herein are plotted as histograms (counts over the difference of the drain currents at -0.6 V). In (a) the data for the reference measurements are presented. As above the reference measurements are measurements where no protein was used but else exactly the same buffer conditions were applied. And in (b) measurements where CaptAvidin was incubated on the surface of the P3HT transistors is shown. Further the solid lines represent Gaussian fits of the histograms.

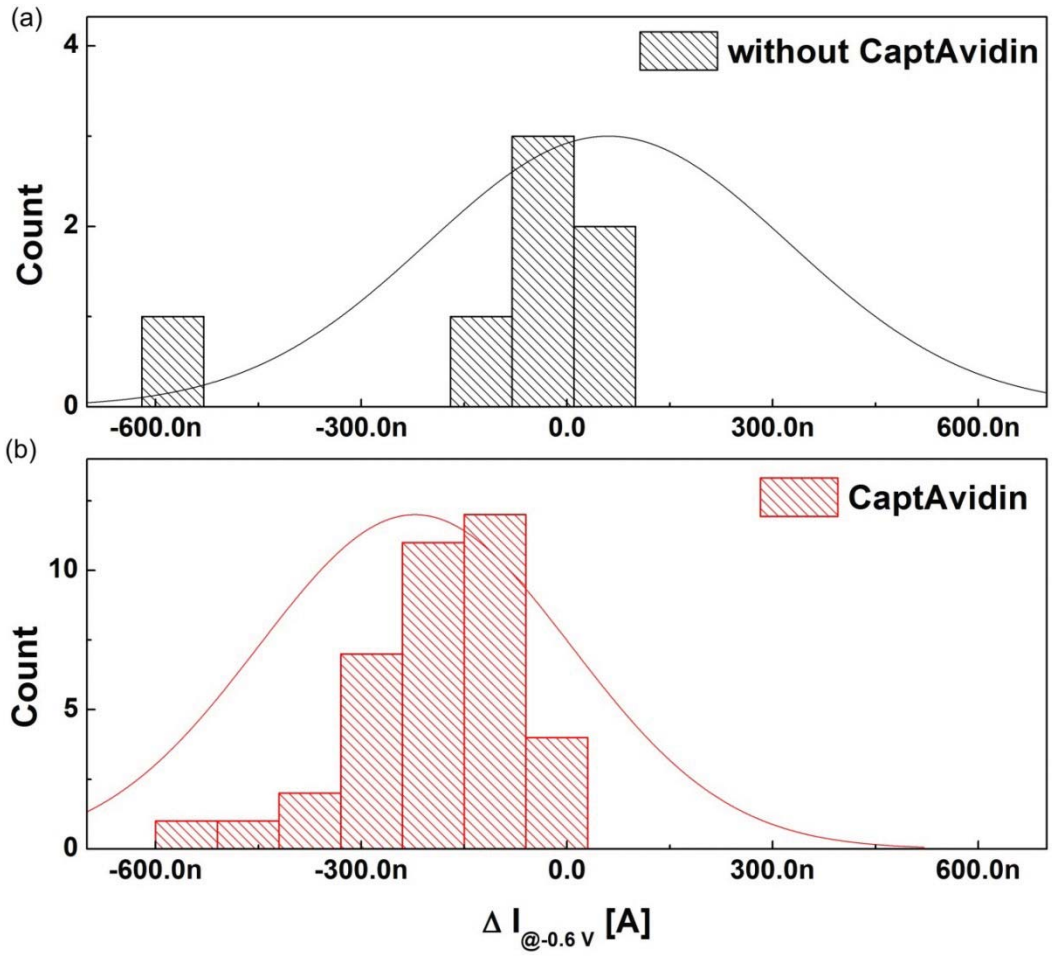

Figure 7.13.: Histograms of measurements without the incubation of CaptAvidin (a) and measurements where CaptAvidin was incubated on the P3HT-FET (b). The solid lines represent Gaussian fits.

The histogram in Figure 7.13 (a) reveals a peak at roughly 0 A, meaning that there is no sensing signal. Additionally it can be seen that upon CaptAvidin incubation there is a significant peak at roughly -200 nA.

For a better presentation of the data in Figure 7.13 another type of plot was established, namely an integrated histogram that is especially useful for a low amount of data. In Figure 7.14 such a histogram is shown. The red circles present data that were extracted from transfer curves after protein incubation and the black

squares result from measurements without sample. Herein it can be seen clearly that the P3HT transistors give a distinct response as soon as CaptAvidin is present on the P3HT surface. Additionally it is easy to see that without protein the peak of the curve is around 0 A and with CaptAvidin a drain current difference of about 200 nA is obtained.

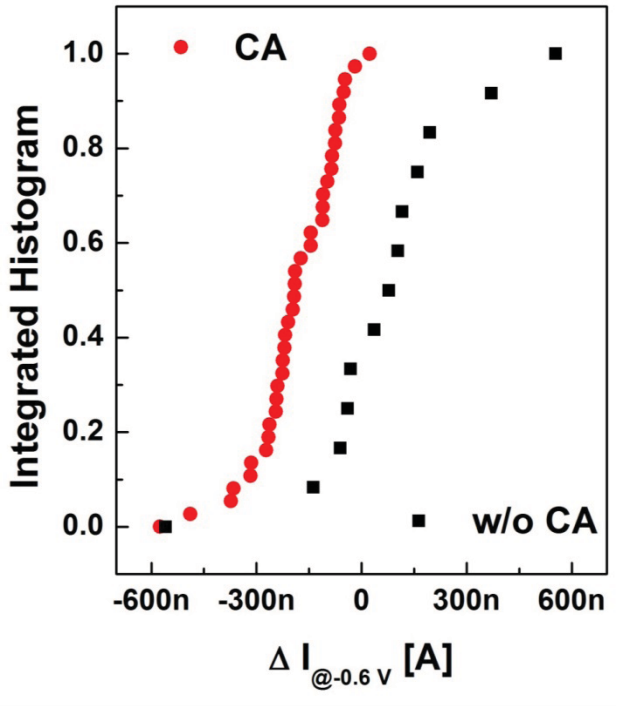

Figure 7.14.: Integrated histogram: the red circles show the difference that were obtained from subtracting drain current values of transfer curves after CaptAvidin incubation. The black squares are references that were obtained from measurements without CaptAvidin samples.

Yet, not only a stochastic analysis of the interactions between CaptAvidin and biotin was performed, but also a control experiment that is discussed in the following: For this purpose standard experiments were performed. Yet, the standard experiments

were modified in a way that the P3HT surface was not functionalized with biotinylated gold nanoparticles. That means that the protein was allowed to solely interact unspecifically with the P3HT surface. Hence the corresponding data may result only from unspecific interaction of the CaptAvidin proteins with the P3HT surface.The results of this experiment are presented in Figure 7.15. The data that are depicted with red circles and black squares are the same data as shown above in Figure 7.14. The green triangles result from measurements where the P3HT-FET was not functionalized with biotinylated gold nanoparticles. One can see that the control measurements gave almost the same results as the measurements with the functionalized FETs, just a slight difference of the histograms is indicating the control signal is a little bit lower than the signal that resulted from protein measurements with a functionalized surface. The cause for the parasitic control signal may be as already mentioned an unspecific adsorption of the proteins onto the P3HT surface. Yet it is also thinkable that the changes of the pH conditions may additionally lead to parasitic effects.

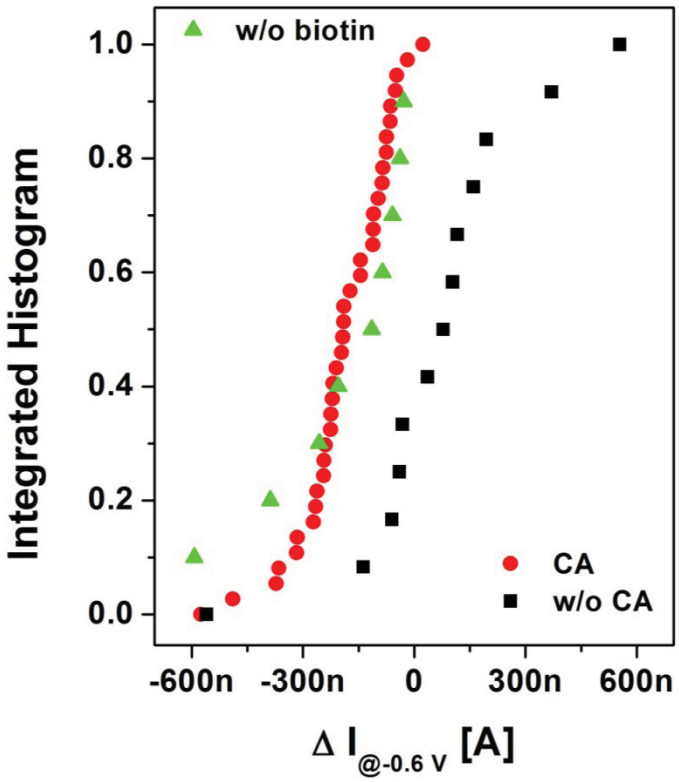

Figure 7.15.: Integrated histogram: the red circles show the difference that were obtained from subtracting drain current values of transfer curves after CaptAvidin incubation. The black squares are references that were obtained from measurements without CaptAvidin samples. The green triangles result from measurements where the P3HT-FET was not functionalized with biotinylated gold nanoparticles. Hence the corresponding data may result from unspecific interaction of CaptAvidin with the P3HT surface.

7.7 Conclusion

In this chapter two different techniques to functionalize the surface of a P3HT field-effect transistor with biotin molecules were presented. Both techniques have in common that they rely on non-covalent ways to incubate the P3HT surface with biotin. This is of interest, especially when it comes to protein sensing with polymeric, disposable one-way sensors where fast methods that are easy to carry out are demanded. The latter approach, featured the advantage that it is generally possible

to conduct experiments using a second experimental method, besides electrical measurements. Unfortunately, it was not achieved to clearly distinguish unspecific protein binding events from binding to biotin. Yet it is believed that conducting further experiments with biotinylated Au-nanoparticles could help to emend the existing protocols.

8 Sensing with SWNT-FETs

In this chapter protein sensing with SWNT-FETs is presented. As in the foregoing chapter the active area of the sensor was functionalized with protein ligands. However, opposed to the previous chapter, the functional molecules were not purchased but designed and synthesized in collaboration with the Star research group of the Chemistry Department of the University of Pittsburgh.[121]

The CaptAvidin-biotin binding system represents an alternative biosystem, a biosystem that is closer to real-life demands of SWNT-FET sensors (opposed to avidin-biotin). Thus this system can be used to optimize SWNT-FET sensors in a way that they can finally be established as sensors in real-life applications, such as point-of-care (POC) testing. The CaptAvidin-biotin system offers a pH-tunable binding affinity with the strongest affinity occurring at pH 4 and a complete dissociation of the protein-ligand complex at pH 10. Hence biotinylated devices can be regenerated by washing with pH 10 buffer, rendering this system interesting for engineering protein sensors.[60,122] Additionally CaptAvidin experiments were also performed with gold nanoparticle (Au-NP) decorated devices, offering the possibility for additional surface enhanced Raman measurements. Furthermore a new area of application for SWNT-FETs is suggested, namely the use as protein fingerprint sensors, which exploit the protein's specific FET response under varying pH values.

8.1 Experimental

8.1.1 Device Fabrication

Single-walled carbon nanotube field-effect transistors were fabricated similar to previous reports from the group of Alexander Star.[28,123] Interdigitated electrodes, with channel length of 10 µm and a width to length ratio of 1150, were patterned via standard photolithography on silicon substrates. Therefore a gold layer with a thickness of 100 nm was deposited on a titanium layer with a thickness of 30 nm adhesion layer using electron beam physical vapor deposition. A picture of a chip and the corresponding lithography mask are presented in Figure 8.1. Four devices are patterned on one chip (the chip exhibits has an edge length of 2 mm), which allows for mounting onto ceramic dual in-line packages. Using a wire bonder, the source and drain electrodes of the devices are bonded to the leads of the package. Subsequently a plastic tube (Eppendorf) with a volume of approximately 1 ml was glued with polydimethylsiloxane (PDMS) onto the package. This fluid chamber allowed for further liquid handling such as deposition of carbon nanotubes from solution, fabrication of gold nanoparticle decorated SWNT-FETs, characterization of the transistors and protein sensing. Figure 8.2 shows photographs of a fully fabricated device including the fluid chamber.

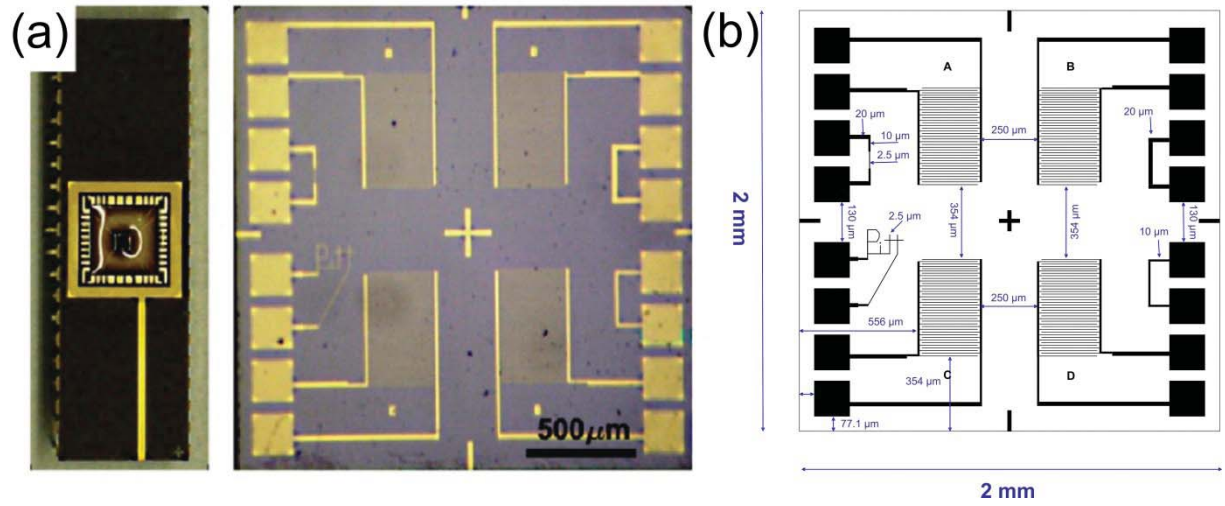

Figure 8.1.: (a) Device package and chip used for protein sensing experiments. Four transistors equivalent transistors were wire-bonded onto the package in order to conveniently perform protein-sensing experiments. (b) Drawing of the photolithography mask. Four transistors are patterned on a SiO_2 chip, which allows for better statistical analysis of the sensing data.[123]

Carbon nanotubes were deposited on the prepatterned electrodes from solution. P2-SWNTs from Carbon Solutions Inc. (purity >90%) were purchased and dispersed in N,N-dimethylformamide (DMF, 0.01 mg/ml). DMF is a common organic solvent and is often used in combination with ultrasonication to disperse carbon nanotubes in solution. The advantage over using surfactants or other dispersants is that there is no need of removing the dispersant for further processing. However the stability of the SWNT solution is an issue.[66] We observed aggregation of the carbon nanotubes within a few days, which required additional ultrasonication for 20 min directly before use. Prolonged sonication, however, is undesirable as it causes physical and chemical modification of the tubes.[65]

SWNTs were deposited by alternating current dielectrophoresis.[124,125] For this purpose source and drain electrodes were connected to a function generator. A peak-to-peak voltage of 10 V was applied at a frequency of 10 MHz. The generator was switched on, and 5 µl droplet of SWNT solution was drop-casted onto the chip. After a deposition time of 60 s, the device was thoroughly rinsed with DMF and ethanol and blown dried under nitrogen. Subsequently the package including the chip was left baking on a hotplate for 3 hours at 120 °C. AC DEP deposition method was chosen because it features good control over the resulting density of the deposited SWNTs, whereas alternative solution-based methods such as drop casting would result in an inhomogeneous SWNT distribution on the chip (coffee stain effect)[126]. Furthermore AC DEP results in an alignment of the SWNTS between the source and the drain electrodes.[127] The combination of homogeneity and alignment of the SWNT-film further pays off in a higher sensitivity towards protein attachment. This is because the current that flows through one nanotube or a bunch of aligned tubes is more easily affected by the presence of a protein than a randomly distributed network of SWNTs. The advantage of the AC DEP deposition is that it is, as other solution based approaches, cost-effective, very simple and can be even applied to flexible plastic substrates. Yet in contrast to other solution-based approaches AC DEP features more benefits such as the possibility to align the SWNTs between the source and drain electrodes, a better control over the SWNT density and the chance of producing several different FETs conveniently on the same chip.

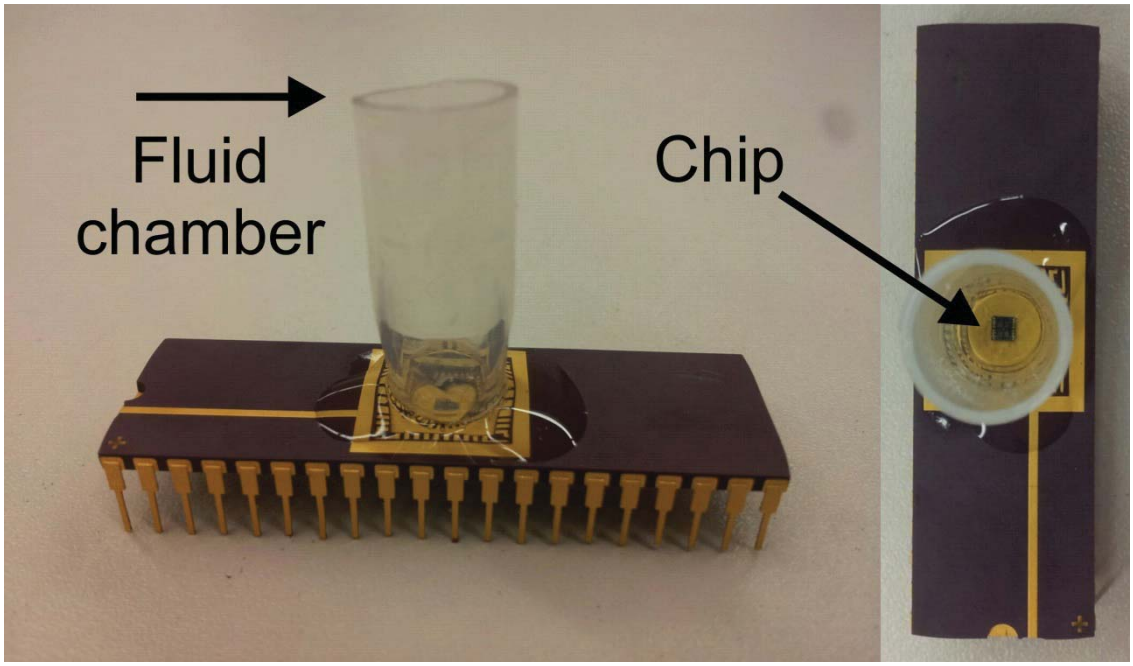

Figure 8.2.: SWNT-FET chip mounted on a dual ceramic inline package. Liquid handling is provided by mounting a plastic tube onto the package and fixing it with PDMS. With this configuration was used for nanotube deposition as well as for functionalization of the tubes and protein experiments.

Before electrical characterization the device was allowed to cool down to room temperature and further to equilibrate in DI water. Subsequently the characterization measurements were also conducted in DI water instead of buffer solution to avoid contamination of the clean SWNT surface with buffer and salt molecules before the biofunctionalization. After the first I_D-V_G measurement the devices have been placed on the hotplate again, so that the remaining water was removed.

8.1.2 Electrical Characterization

Transfer curves were recorded by applying a constant source-drain bias of 50 mV and gate potentials between -0.6 V and 0.6 V, using a Ag/AgCl electrode, which was

immersed in the liquid dielectric. All electrical measurements were conducted using two Keithley 2400 sourcemeters.

8.1.3 Buffer Conditions

For protein experiments with SWNT-FETs we chose a universal buffer system, which offers the advantage that a broad range of pH buffers can be obtained (opposed to experiments of other sections in this thesis where citric acid buffers were used to obtain acidic pH-values and phosphor buffers to obtain basic pH-values). The universal Britton-Robinson buffer consists of a mixture of boric acid (40 mM H_3BO_3, pK_a = 9.2), phosphoric acid (40 mM H_3PO_4, pK_a = 2.2, pK_a = 7.2, pK_a = 12.3) and acetic acid (40 mM $C_2H_4O_2$, pK_a = 4.8).[128,129] Mixing these acids together one obtains a pH 2 buffer, which was titrated with 200 mM KOH to the desired pH value. Undiluted Britton-Robinson buffer (X) was used, when proteins were incubated for 15 minutes on the chip. Albeit this does not result in ideal electrolytic conditions for FET experiments, it provides a better ambiance for protein-ligand interactions.[130] For electrical experiments buffers were diluted, depending on the respective requirements. In all experiments a KCl background of 0.25 mM was used. If not other stated, for all CaptAvidin experiments, the buffers were diluted by a factor of 133 (1/133 X). Leading to a total molarity of approximately 1.3 mM (including KCl) and thus to an approximate Debye length (monovalent salt approximation) of 8.5 nm. For the CaptAvidin experiment, which is shown in Fig 1 (d) a lower buffer concentration (1/794 X) was chosen to allow a concentration variation of KCl to dominate the

Debye length of this experiment. Streptavidin and NeutrAvidin fingerprint experiments require a broader pH range and thus the buffer dilution factor was chosen slightly lower than for standard CaptAvidin experiments (1/100 X, yielding molarities between 1.6 – 2 mM). For other experiments even a more diluted buffer (1/266 X) was tested with total molarities of about 0.8 – 0.9 mM (< 1 mM).

8.2 Noncovalent functionalization

8.2.1 Noncovalent Functionalization of Carbon Nanotubes

Functionalization with biomolecules is inevitable when it comes to the fabrication of specific biosensors. Regarding field-effect transistor sensors, as discussed in this thesis, the functionalization molecules need to be tethered directly onto the most sensitive element of the device, namely the semiconductor itself. Thus noncovalent approaches to functionalize the sidewalls of carbon nanotubes for FET biosensing devices have become widely accepted. This is because electrical properties of carbon nanotubes can be critically changed upon covalent functionalization.[27,131] By now carbon nanotube sidewall functionalization using 1-pyrenebutanoic acid as linker to the nanotubes emerged as one of the most prominent methods to immobilize biomolecules on the carbon nanotubes. Interaction between the nanotubes and the aromatic pyrenyl group is provided by π-π interaction.[132] In SWNT field-effect devices this molecule was implemented successfully to detect a broad range of biomolecules. For example, the group of Philipp Collins used it to immobilize single proteins and enzymes onto a single carbon nanotube FET to detect enzyme dynamics or the

effects of charged moieties of proteins.[25,30] Thrombin was detected via aptamer-pyrene linkers down to 20 pM concentration with a low-density SWNT network fabricated using CVD.[133] Aptamer-pyrene linkers were also used to detect immunoglobuline E.[96] Also the pH sensitivity of a single nanotube FET could be altered by immobilizing glucose oxidase onto the tube with pyrene.[134]

For the detection of biotin-binding proteins in our work the SWNTs were functionalized with pyrene-biotin (P-B) molecules. The pyrene-biotin molecules were synthesized from a member of the star research group.

8.2.2 SWNT-FET Functionalization with Pyrene-Biotin

This subsection shall provide a protocol of how SWNT field-effect devices were functionalized with biomolecules and how electrical characterization attends this process.

Single-walled carbon nanotubes were functionalized with pyrene-biotin directly on the chip. For this purpose P-B was dissolved in anhydrous methanol and 100 µl of the 50 µM solution was allowed to react with the devices. To avoid evaporation of the solvent the Eppendorf tube on the package (Figure 8.2) was sealed with Parafilm. The transistors were characterized electrically, before and after incubation with P-B, using the following protocol: Directly after the device fabrication I_D-V_G curves were taken. After cooling the devices down to room temperature for a couple of minutes the device was exposed to water for 30 minutes to equilibrate. Subsequently the

measurements were conducted in DI water to avoid contamination of the clean SWNT surface with buffer and salt molecules before the biofunctionalization. After the first I_D-V_G measurement the devices have been placed on the hotplate again, so that the remaining water was removed. After P-B incubation overnight, the liquid compartment was filled with methanol. During approximately two hours the molecule containing solution was subsequently replaced with fresh methanol, allowing for a concentration gradient to help releasing loosely bound P-B molecules from the device surface. Finally the methanol was exchanged with DI water and a transfer curve was taken. Desiccation of the functionalized device was clearly avoided during this procedure.

A typical transfer measurement before and after functionalization of a SWNT-FET with pyrene-biotin molecules is shown in Figure 8.3. Generally changes in the conductance, transconductance and threshold voltages of devices before and after functionalization have been observed. However we want to note that those observations are not necessarily due to the attachment of the P-B molecules on the nanotubes. They can also arise because of the differences in the treatment of the devices before and after functionalization. The heat treatment and the exposure of the device to different solvents for unequal amounts of time contribute significantly to the performance of carbon nanotube field-effect transistors. The expected effects that may occur due to attachment of molecules onto the nanotube sidewalls is a decrease in the mobility of the transistors since molecules on the sidewalls may act as additional scattering barriers for the charge carriers. The maximum gate current,

which was observed for those devices, was below 100 nA. That indicated that no additional electrochemical or other parasitic currents effects affected the measurements.

The inset of Figure 8.3 presents a sketch of the device before, after functionalization with pyrene-biotin as well as the chemical structure of the synthesized molecule. One can see the conductance of the FET decreases, which may result from the presence of additional scattering sights (pyrene molecules) on the surface of the carbon nanotubes.

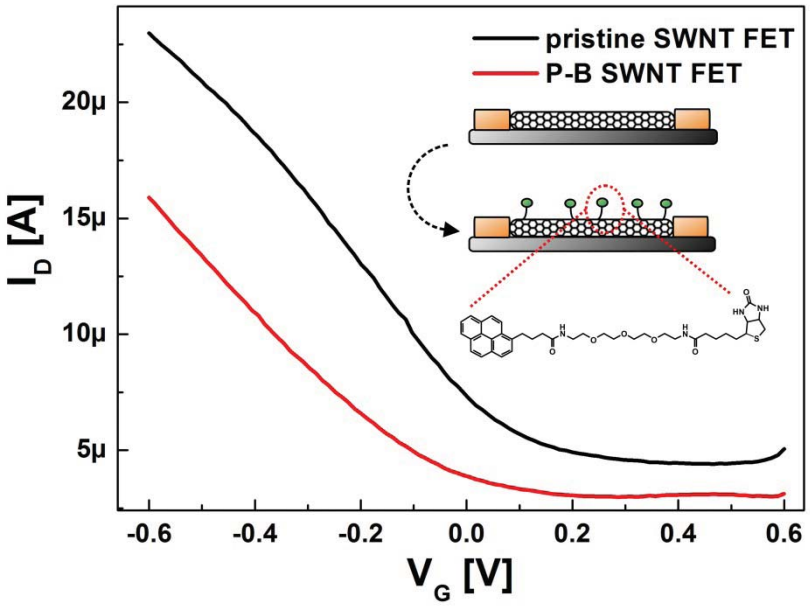

Figure 8.3.: I_D-V_G characteristic of a typical device before (black) and after (red) functionalization with pyrene-biotin molecules.

8.3 CaptAvidin detection with SWNT-FETs

A multitude of experiments using the biotin-binding protein CaptAvidin were performed. Those experiments were carried out by measuring the transfer characteristics of the FETs. The reasons for that was to be able to prevent parasitic signals that could eventually result from protein attachment onto the gate electrode, which were observed by us and other groups.[94] We realized this by avoiding any contact of the electrode with solutions containing the protein by removing the electrode from the fluid chamber during protein incubation. Figure 8.4 shows the experimental configuration and a typical CaptAvidin experiment.

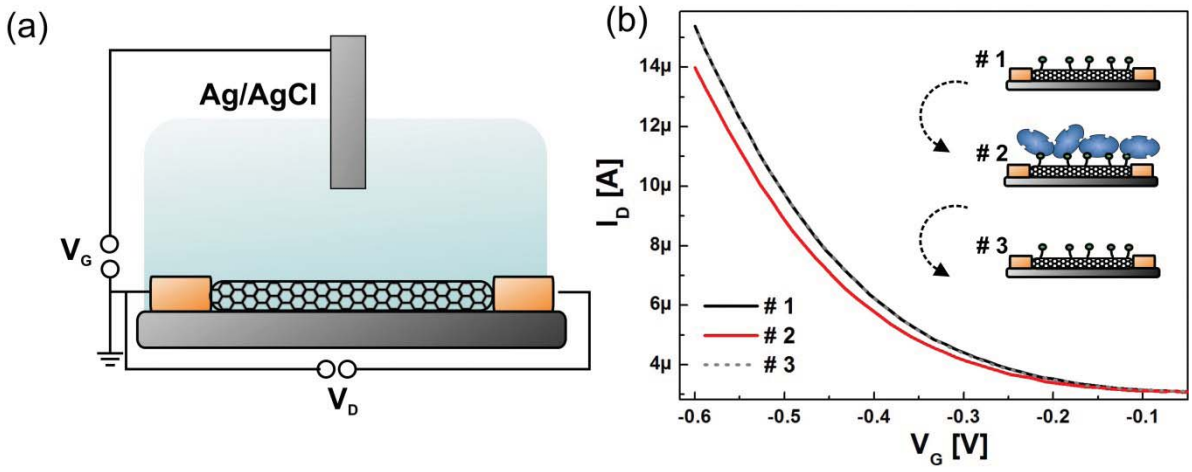

Figure 8.4.: Sketch of the experimental configuration. A Ag/AgCl electrode was immersed in the buffer solution to gate the FET. (b) Typical CaptAvidin experiment. #1 transfer curve before protein incubation. #2 transfer curve after 15 minutes incubation with 140 nM CaptAvidin. #3 Transfer curve after pH 10 washing step

Our measurements met the following protocol: first a transfer curve (I_D vs. V_G) was taken in diluted pH 4 buffer, before the device was exposed to the protein (#1). Subsequently the device was incubated in 140 nM CaptAvidin in pH 4 buffer for 15

minutes. After thoroughly rinsing the device with diluted pH 4 buffer to ensure the removal of all excess protein from the solution, a second I_D vs. V_G characteristic was recorded (#2). Transfer curve #3 was recorded after a 15 minutes pH 10 washing step.

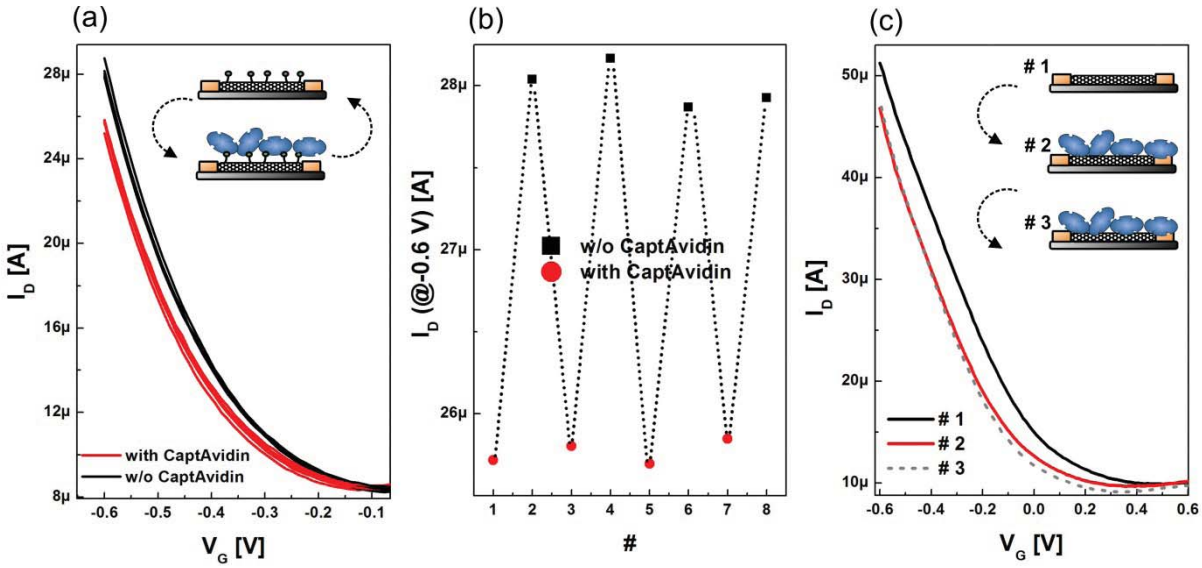

Figure 8.5.: (a) transfer curves of repeated CaptAvidin-biotin binding with the same transistor. 140 nM protein concentration was used. (b) Corresponding drain currents at V_G = -0.6 V in order of measurement. (c) CaptAvidin experiment using an unfunctionalized transistor. (c) shows the irreversibility of that process with the absence of biotin on the surface. After the pH 10 washing step no recovery of the device's transfer characteristic could be observed.

Comparing the I_D-V_G characteristics before and after protein incubation a threshold voltage shift of about 20 mV towards more negative voltages was observed, which is in the order of the zeta potential of avidin at this pH.[135] This shift is reversible, indicating a complete dissociation of the biotin-CaptAvidin complex during the pH 10

washing step. The procedure of reversible CaptAvidin immobilization on P-B functionalized SWNT-FETs is repeatable multiple times, which is shown in Figure 8.5 (a) and (b). A control experiment with an unfunctionalized SWNT-FET is shown in Figure 8.5 (c). It demonstrates that these results can only be obtained with devices that are functionalized with biotin molecules. The pristine device, in fact, shows a response upon unspecific CaptAvidin adsorption, but a recovery by a pH 10 treatment is not possible as a shift towards the initial threshold voltage before protein incubation cannot be observed.

Equivalent experiments were reported by Bradley et al., where the charge transfer from adsorbed streptavidin was analyzed with a back-gated carbon nanotube FET. Similar to our experiment, they detected a threshold voltage shift of 20 mV and attributed it to amine groups of the protein that may donate electrons to the nanotube.[110] The adsorption of proteins onto the sidewalls of carbon nanotubes is well-known and attributed to hydrophobic interactions, however, a reversibility of the adsorption process is not reported.[136] That leads us to the conclusion that the recovery of the initial transfer curve after a pH 10 washing step is due to a dissociation of the biotin-CaptAvidin complex.

8.3.1 Dissociation constant of CaptAvidin

The formation of a protein-ligand complex can be described as a two-state process:

$$P + L \leftrightharpoons C \qquad 8.1$$

with the equilibrium dissociation constant $K_D = [P][L]/[C]$. $[P]$, $[L]$ and $[C]$ are the concentrations of the protein, the ligand and the protein-ligand complex, respectively.

K_D gives the binding strength of a protein to a ligand. The lower K_D the stronger the stronger is the binding affinity. Thus the dissociation constant is an important parameter to characterize a protein-ligand system. How to extract K_D from the sensor response of a field-effect transistor was discussed in literature recently.[116] For this purpose usually responses of multiple devices are analyzed. Thus a method to normalize the response of a transistor is required. This can be obtained by taking the transconductance, as it is a measure for the sensitivity of a field-effect sensing device.[137,138] To obtain K_D it is necessary to measure the sensor signal as a function of the protein concentration.

As the binding affinity of CaptAvidin towards biotin is depending on the buffer pH we measured the responses of several transistors under different pH values as a function of the CaptAvidin concentration. The data obtained from four different transistors are shown in Figure 8.6. In the graph the normalized sensing response is plotted as a function of the CaptAvidin concentration. I_0, I_P and g_m are extracted from transfer curves, herein I_0 is the drain current at V_G = -0.6 V before protein incubation, I_P is the drain current at the same potential after protein incubation and g_m is the

maximum of the transconductance $\partial I_D/\partial V_G$. To obtain the dissociation constant, we adopted the analytical model of Duan et al.:[116]

$$\frac{|I_0 - I_P|}{g_m} = \Delta V_{th} = \frac{q_P}{C_0}[B]_{max} \times \frac{[P]}{[P] + K_D} \qquad 8.2$$

In this equation $[B]_{max}$ is the maximum surface density of binding sites on the surface of the carbon nanotubes, C_0 is the analyte/channel capacitance and q_p is the charge from the protein.

Up till now the investigation of protein binding with nanotube or nanowire field-effect transistors was conducted with irreversible biosystems. Thereby our sensing protocol differs significantly from the work done recently using streptavidin or other proteins with extremely high binding affinities, where sensors need to be disposed after binding as no device regeneration is possible. Here CaptAvidin could be released from the surface of the sensor after incubation with a certain protein concentration by a pH 10 washing step and hence devices could be reused subsequently to obtain data for the next protein concentration. SWNT-FETs are intrinsically sensitive towards changes of the electrolytic environment, such as pH and ionic strength of the buffer as shown in our publications.[69,89] Hence we accurately ensured that all transfer curves were taken at pH 4. This means, that we followed the subsequent protocol: a transfer curve was taken before 15 minutes protein incubation at the buffer pH of interest. Then the device was thoroughly rinsed with pH 4 buffer before another

transfer curve was measured. After a third transfer curve previous the pH 10 washing step, the device was subsequently used for the next CaptAvidin concentration. That I_D-I_V measurements were performed in pH 4 buffer was consciously chosen, as it is the condition at which dissociation of the biotin-CaptAvidin complex should be minimized. In Figure 8.6 the results for pH 4 and pH 5 buffers are presented. At pH 4 a dissociation constant of 43 ± 7 nM and at pH 5 one of 308 ± 170 nM was obtained. As expected, the dissociation constant at pH 5 is almost one order of magnitude higher than the one for pH 4.

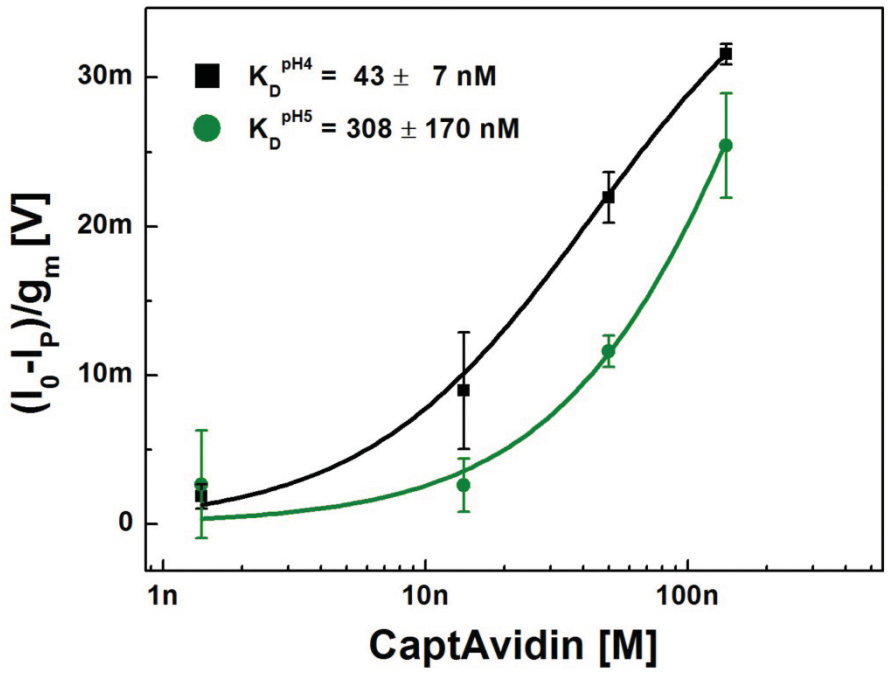

Figure 8.6.: Normalized sensor response $(I_0-I_P)/g_m$ at different buffer pH as a function of CaptAvidin concentration

8.3.2 Effects of the Debye screening length on Protein Sensing

The influence of the Debye screening length is already discussed in previous chapters of this thesis. With the biotin functionalized SWNT-FETs we were also able to conduct experiments at different ionic strengths, which will be discussed here.

We repeatedly sensed the response of the sensor towards of 140 nM CaptAvidin in pH 4 buffers, while the KCl concentration was altered, ranging from 0.25 mM to 50 mM KCl. In total the response of four transistors was analyzed and the results are depicted in Figure 8.7. The graph shows the normalized response as a function of the Debye screening length (L_D), which was calculated by solving equation 8.3 for monovalent ions:

$$L_D = \frac{1}{\sqrt{4\pi L_B \sum \rho_i z_i^2}} \qquad 8.3$$

Here L_B is the Bjerrum length (0.7 nm) and ρ_i and z_i the density and the valence of ion species i. We did not consider the buffer for the calculation of the Debye length. Considering buffers for calculations regarding screening would require computation methods.[139] Yet, we kept the buffer concentration as low as possible. Thus we consider it not to crucially affect the Debye length (see 8.1.3).

Analogue to the report of Sorgenfrei et al. we found that the sensing response depends exponentially on the ionic strength of the electrolyte.[23] Furthermore we find it eminent that the response drops significantly in a L_D regime that is in the order of the hydrodynamic diameter of avidin at a distance from the nanotubes surface that is

given by the length of the functionalization molecule.[135] The P-B molecule length in equilibrium conditions was calculated by using Spartan 10 software, to be around 2.7 nm.

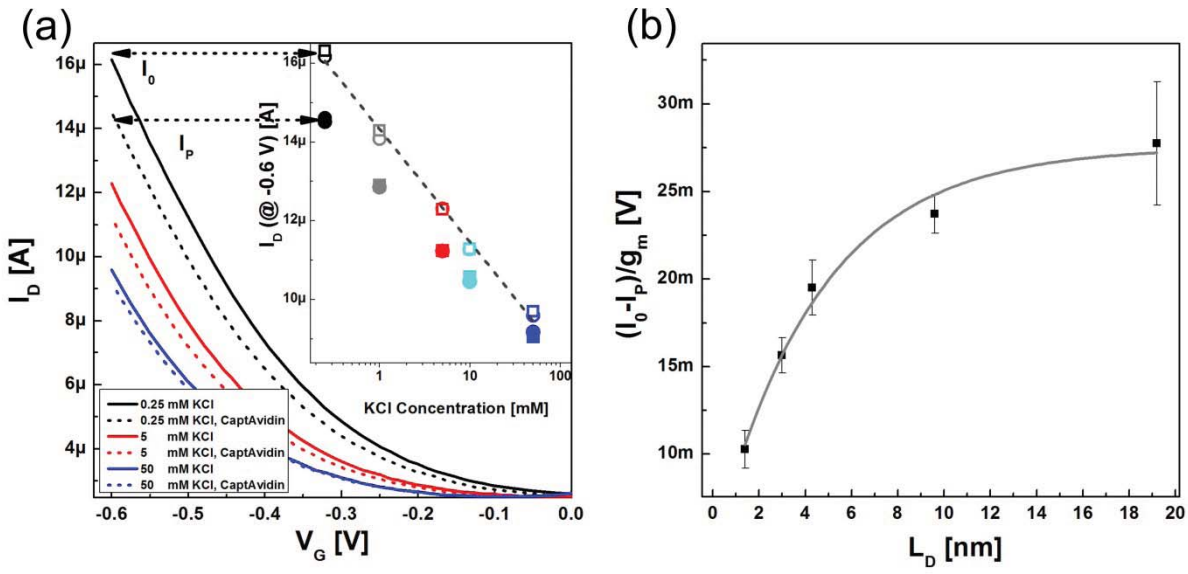

Figure 8.7.: Effect of Debye screening length on CaptAvidin sensing. (a) Transfer curves for 0.25 mM (black), 5 mM (red) and 50 mM (blue) KCl concentration. Solid lines represent the measurements before and dashed lines after 140 nM CaptAvidin incubation. The inset shows the corresponding I_D values at V_G = -0.6 V. For each KCl concentration binding of CaptAvidin was recorded two times, leading to two data points represented in closed circles and squares. (b) shows the corresponding sensor response normalized with the transconductance as a function of the Debye screening length L_D calculated from the KCl concentration

In Figure 8.7 transfer curves for the following KCl concentrations are shown: 0.25 mM (black), 5 mM (red) and 50 mM (blue). Solid lines present measurements before CaptAvidin incubation and dashed lines show transfer characteristics after protein binding to biotin. The measurements were taken consecutively, starting from the

lowest KCl concentration, with the same FET device. In total four transfer curves were taken at every KCl concentration. One before CaptAvidin incubation, one after incubation, one after the pH 10 recovery step and a last one after a second protein incubation. This procedure was repeated for 5 different KCl concentrations as depicted in the inset of Figure 8.7, which shows the drain currents (I_D @ V_G = -0.6 V) of this experiment with one of the measured FETs. Here the black, red and blue data points are corresponding to the transfer curves as depicted with arrows. Open squares and circles represent data taken from curves before protein incubation and filled squares and circles are the ones with attached protein. The dashed-dotted line in the inset is a linear fit showing the linear dependency of the drain current on the ionic strength of the electrolyte. The data clearly show the excellent repeatability of CaptAvidin binding onto biotinylated SWNT-FETs. Furthermore a dependence of the sensor's response on the Debye screening length was observed.

8.3.3 Stability of the pyrene-biotin functionalization

SWNT-FET protein sensors were stored in PBS buffer (pH 7.4). Even after weeks of storage the sensors could be reused and gave stable protein signals while no degradation of the sensor was observed. In Figure 8.8 the FET response upon incubation of 140 nM is shown at "day 0" (squares) and 16 days later (spheres). The device gave almost identical response which demonstrates the stability of the sensor.

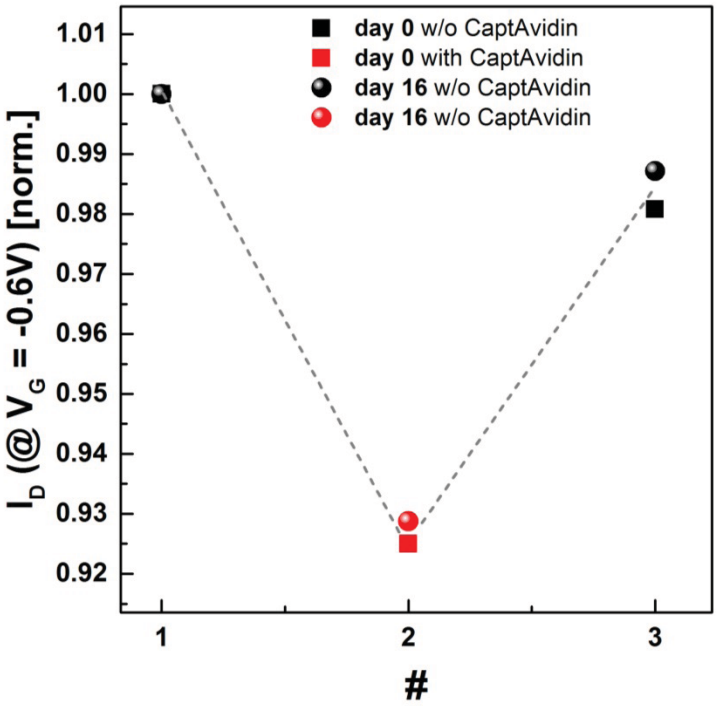

Figure 8.8: Normalized FET response upon incubation of 140 nM CaptAvidin incubation on a pyrene-biotin functionalized SWNT-FET (squares). After 16 days the CaptAvidin response was measured after 16 days of storage in PBS buffer (pH 7.4) with nearly the same result as on "day 0".

8.4 NeutrAvidin and Streptavidin Fingerprints

The formation of an electrical double layer occurs at every solid-liquid interface and is driven by the development of net charges at the surface of a particle or a plane, respectively. It consists of the immobile Stern layer and the loosely associated diffusive layer that holds the opposite charge. The potential at the hydrodynamic shear boundary is referred to as zeta potential. In particular, for proteins those surface charges are arising due to pH-dependent ionization reactions of the acidic or basic side groups of the amino acids that are located at the surface. In this regard the zeta potential gives information of a protein's electric landscape in solution. [140] The zeta potential can be positive or negative depending on the buffer's pH value. At

the transition point from positive to negative charge there is a point of net neutral charge which is called the isoelectric point (IEP). The zeta potential and the IEP are usually determined by measuring the particle motion under an applied electric field in solution for various buffer pH.

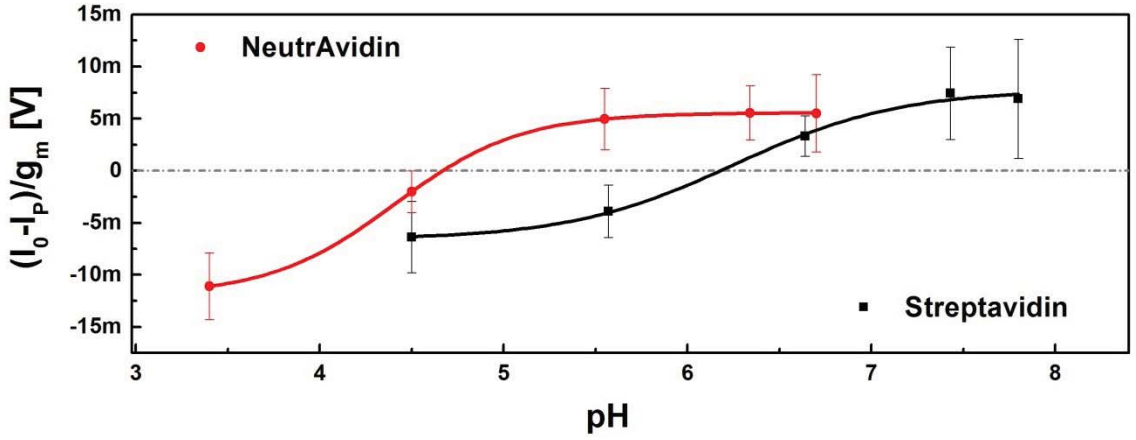

Figure 8.9.: Normalized sensor response $(I_0-I_P)/g_m$ of biotin-functionalized SWNT-FET towards NeutrAvidin (red) and Streptavidin (black) as a function of buffer pH. Error bars are resulting from averaging responses of several devices. The solid lines represent sigmoidal Boltzmann fits.

Equivalently to measurements of the zeta potential and the isoelectric point, a pH dependent transition from a positive to a negative transistor response including a point of zero response (PZR) should be detectable. If a positively charged particle comes close to a SWNTs surface, it will cause a threshold voltage shift towards the positive x-axis, which results in $I_0 - I_P < 0$ and vice versa for negatively charged particles. The PZR does not necessarily have to be identical with the IEP as proteins are immobilized onto the carbon nanotubes rather than freely floating in a solution.

Additionally other effects can lead to a shift of the PZR relative to the IEP, such as pH-dependent surface charges of the carbon nanotubes. [104,69]

We were able to differentiate between two different biotin-binding molecules, namely streptavidin and NeutrAvidin, by their pH-dependent sensor response. In contrast to measurements with CaptAvidin, the sensor cannot be regenerated after binding to biotin. Thus each measurement requires a new transistor. In Figure 8.9 we present the normalized sensor response of streptavidin and NeutrAvidin as a function of the buffer pH. The error bars result from the average response of at least two transistors. For each pH value a transfer curve was recorded before and after incubation of the protein. The protein itself, however, was allowed to bind to biotin in a pH 7 PBS buffer for 15 minutes.

The solid curves represent sigmoidal Boltzmann fits and the dashed grey line depicts zero device response. We observed a PZR of 4.7 for NeutrAvidin and 6.2 for streptavidin. The IEPs of NeutrAvidin (6.3) and streptavidin (5 - 7.5) are reported in literature.[22,20] The PZR shift relatively to the IEP towards more acidic pH values probably occurred as a result of multiple factors, as already discussed before, such as the low ionic strength of the buffer (around 2 mM), the sum of electric field that influences the net charge sensed by the nanotubes and additional influences of the diffusive counter ion layer. Also the protonation equilibrium of acids and bases on the surface of a protein may be altered due to changes of the surface potential at low ionic strengths with respect to standard conditions. The IEP is determined by the

composition of the protein surface by basic and acidic amino acids and is influenced by external electrical potentials. The electrostatic interactions are getting modified by the ionic strength of the solution. That means, a change of the salt concentration can lead to alterations of the isoelectric points. However, the prediction of the IEP at certain ionic strengths requires the exact knowledge of the surrounding potential and the charge distribution of the protein, which is not available for NeutrAvidin in that case.

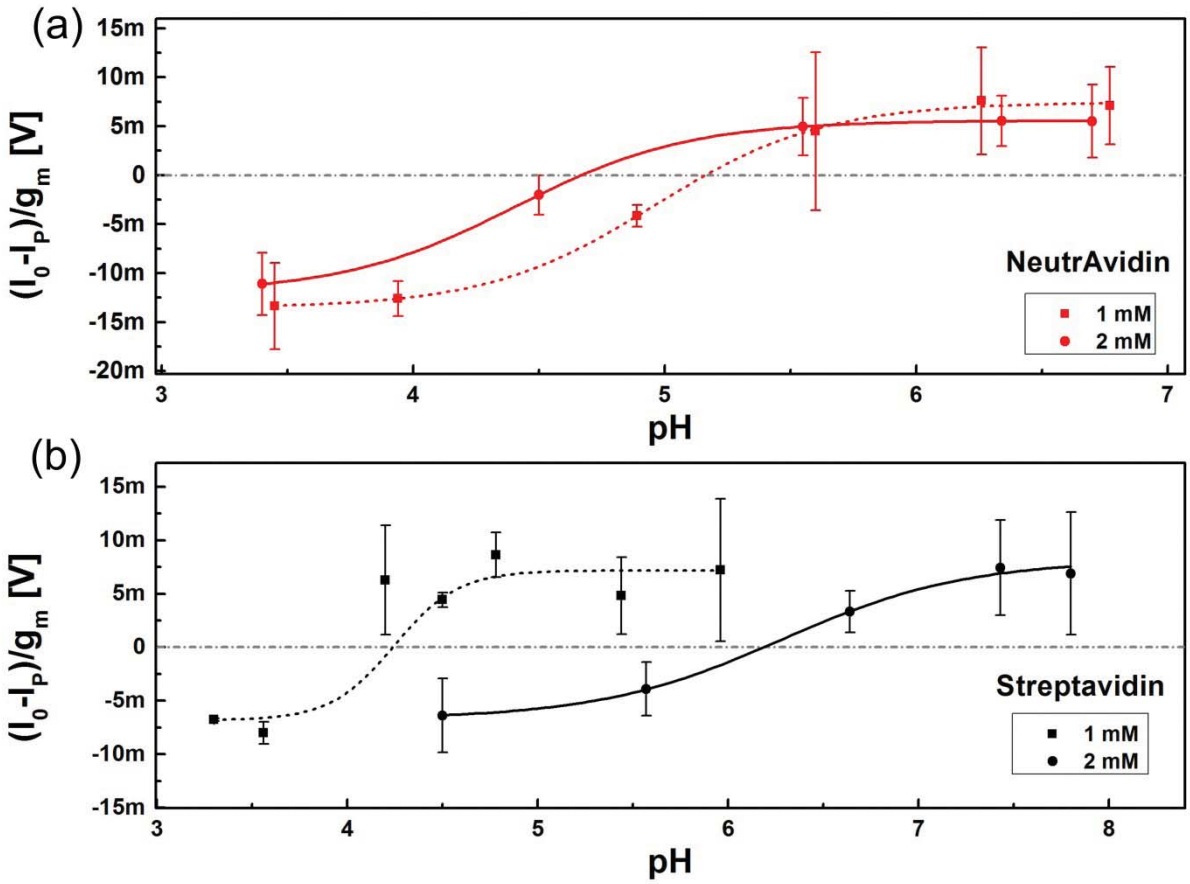

Figure 8.10.: Normalized sensor response $(I_0-I_P)/gm$ of pyrene-biotin-functionalized SWNT-FET. (a) NeutrAvidin response measured in 2 mM (1.6 – 2 mM) buffer (red) and 1 mM (0.8 – 0.9 mM) buffer (black) buffer concentration. (b) Streptavidin response for in 2 mM buffer (red) and 1 mM buffer (black) buffers. Error bars are resulting from averaging responses of several devices. The solid lines represent sigmoidal Boltzmann fits

NeutrAvidin and streptavidin fingerprints were also measured at different ionic strength and the results are presented in Figure 8.10. As explained in 8.1.3 different buffer dilution factors were used, resulting in molarities between 1.6 – 2 mM and 0.8 – 0.9 mM. To simplify these expressions they were named “2 mM” and “1 mM” in the graph. The circles (with fits in solid lines) represent the data that were already shown in Figure 8.9. The dashed lines are sigmoidal fits to the data recorded in lower buffer concentrations. In (a) the measurements for NeutrAvidin are shown and in (b) the ones of streptavidin. Interestingly such measurements with NeutrAvidin and streptavidin do not only reveal a difference of the PZR but also different behavior when measured at different ionic strengths. While the PZR of NeutrAvidin is shifting towards more basic pH for lower buffer concentrations, streptavidin acts vice versa. We do not want to argue that the behavior observed for our two model proteins is universal as batch to batch variations are well-known and a broad spectrum of isoelectric points is reported for streptavidin (probably arising from those variations).

As mentioned above NeutrAvidin is an engineered protein with an almost neutral IEP of 6.3 as stated by the provider (Invitrogen). Various IEPs for streptavidin are reported throughout literature and range from roughly 5 to 7.5.[20] However, those values were not obtained by performing experiments in such low ionic strength as used for the experiments in our report. Hence, to compare our data with data obtained by using a different experimental method, experiments with NeutrAvidin and streptavidin under different pH values were conducted additionally using a zeta

potential analyzer. Zeta potential measurements were performed using a Brookhaven ZetaPals at 25 ˚C under the specified pH. Further the experiment was conducted using PBS buffer (tablets purchased from Sigma Aldrich) adjusted with 0.02 M HCl to the desired pH. The results are presented in Figure 8.11.

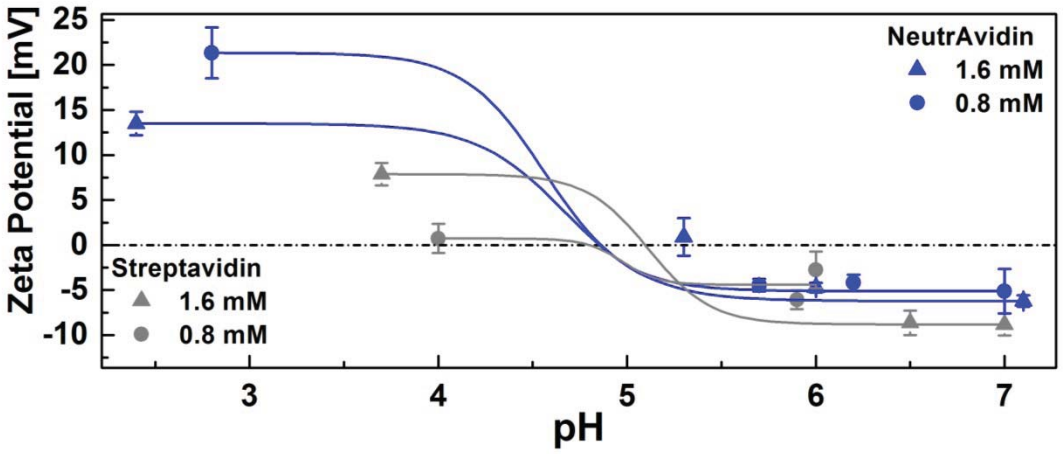

Figure 8.11.: Zeta potential measurements of streptavidin (grey symbols) and NeutrAvidin (blue symbols) measured in 0.8 mM (circles) and 1.6 mM (triangles) PBS buffer respectively. For NeutrAvidin an IEP of 4.8 at 1.6 mM and 0.8 mM PBS buffer was measured. For streptavidin an IEP of 5.1 at 1.6 mM PBS buffer and 4.8 at 0.8 mM buffer was measured.

Resulting from those measurements, NeutrAvidin revealed an IEP of 4.8 for both buffer concentrations and streptavidin yielded an IEP of 5.1 at 1.6 mM PBS buffer concentration and of 4.8 at 0.8 mM PBS concentration. Comparing the results from the NeutrAvidin measurements, the values that were obtained from the two independent experiments are in good agreement. Whereas the discrepancy between the zeta analyzer and the FET experiments is more significant for streptavidin.

However, both experiments, FET and zeta analyzer, give evidence that the IEP and the PZR depend on the electrolytic conditions as the IEP and PZR shift towards more acidic pH for lower buffer concentrations. However, the shift is much higher for the FET measurements. This trend may be due to changes in salt concentration having an effect on the equilibrium of charges in basic and acidic amino acids, which can modify the protein's IEP. However, predicting the PZR obtained with a FET for a specific protein and at a certain ionic strength requires the exact knowledge of the surrounding potential and charge distribution of the protein. While the observed behavior for our two model proteins cannot be considered universal – due to well-known batch-to-batch variations (a broad spectrum of isoelectric points is reported for streptavidin, for example), we believe that such zeta-potential-like measurements can provide a new tool to differentiate between proteins and thus give rise to new cost-effective methods applicable in fields such as protein engineering.

8.5 CaptAvidin Detection with Au-NP decorated SWNT-FETs

Biological sensing stands to benefit from the combination of various detection techniques. There is an increasing interest in surface enhanced Raman spectroscopy (SERS) for applications in chemical and biological sensing, due to its unique sensitivity in regards of molecular fingerprinting.[141,142,143] Thus the combination of electrical detection methods with SWNT-FETs and optical methods such as SERS is advantageous and can be realized by the decoration of carbon nanotubes with metal

nanoparticles.[144] Dielectrophoresis permits the deposition of gold nanoparticles from solution directly on the chip.[145]

8.5.1 Fabrication and Functionalization

Gold nanoparticle (AuNP) decorated SWNT-FETs were fabricated via bulk electrolysis using a CH Instruments (Austin, TX, USA) Electrochemical Analyzer potentiostat. In a three-electrode configuration a Ag/AgCl electrode served as reference electrode, a platinum electrode as the counter electrode and the transistor's source and drain electrodes were connected to serve as working electrode.

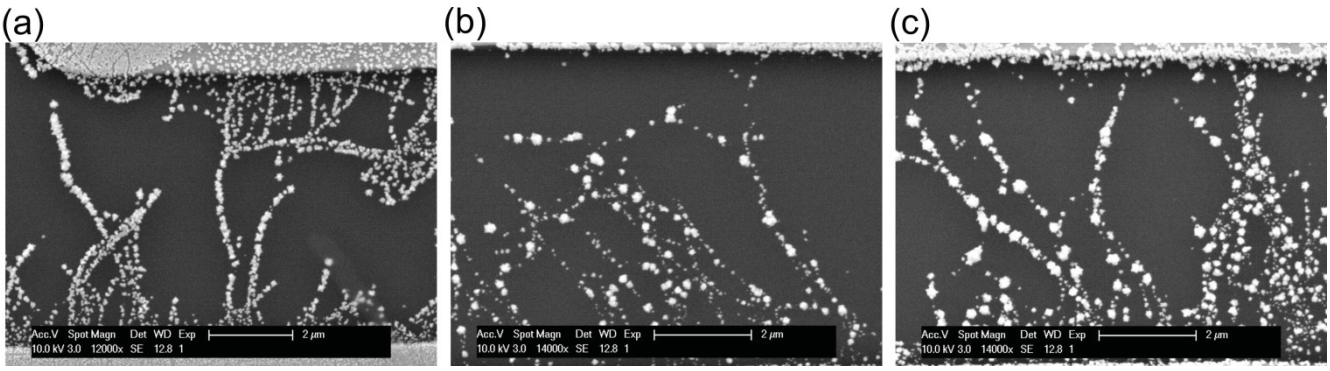

Figure 8.12.: Scanning electron microscope images of Au-decorated SWNT-FETs. The deposition potential was fixed at -0.4 V while the pulse duration was varied. (a) 10 s, (b) 20 s, (c) 40 s.

A predeposition potential of 0.8 V was applied for 30 seconds, subsequently 1 mM $AuCl_3$ in 0.1 M HCl was injected in the fluid chamber. The deposition potential of -0.4 V was applied for varying durations, ranging from 10 to 40 seconds and resulting

in different gold particle sizes. Scanning electron microscope (SEM) images were acquired using a Philips (Andover, MA, USA) XL30 FEG microscope at an accelerating voltage of 10 keV. Figure 8.12 shows SEM images of gold decorated device. A distribution of particle sizes ranging from 53 nm to 210 nm was obtained.

8.5.2 Protein Sensing with Au-decorated SWNT-FETs

The electrical characterization of a SWNT-FET before and after gold deposition is shown in Figure 8.13 (b). We observed a rise in the conductance of the devices after gold deposition, which can be attributed partially to additional metallic paths between the source and drain electrodes.

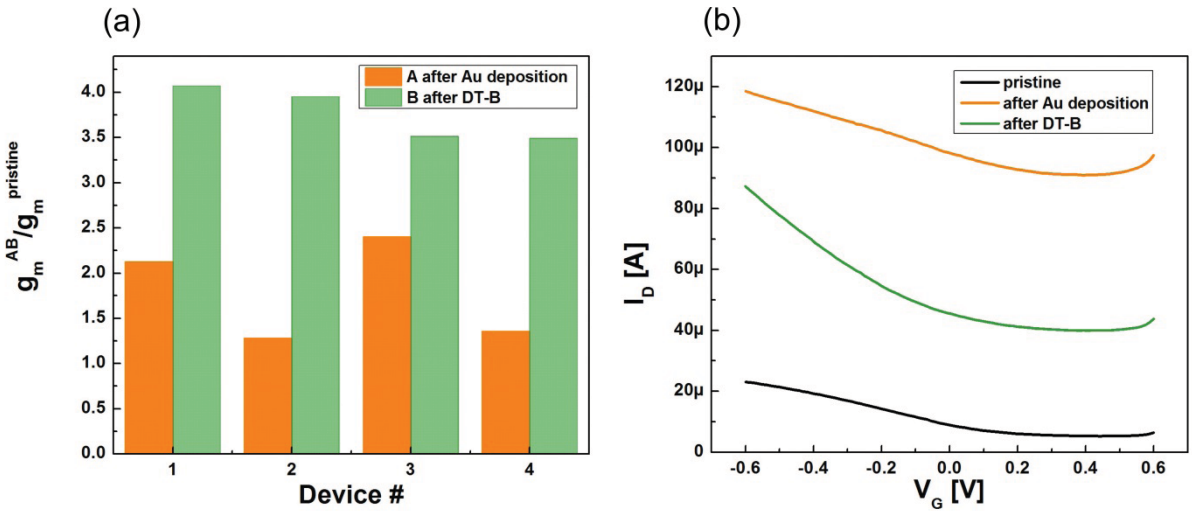

Figure 8.13.: (a) relative change in maximum transconductance after Au-nanoparticle decoration ($g_m^A/g_m^{pristine}$) and after dithiol-biotin functionalization ($g_m^B/g_m^{pristine}$) for four devices with different deposition times 1 (10 s), 2 (20 s), 3 (30 s), and 4 (40 s). (b) Corresponding transfer curves for device 4.

For protein sensing dithiolane-biotin molecules were synthesized to enable covalent biotinylation of the gold particles. Additionally the nanotubes sidewalls were biotinylated with P-B to prevent signals from unspecific protein adsorption onto the pristine nanotubes.[110] In Figure 8.14 (c) transfer curves upon CaptAvidin binding and dissociation are shown. Similar to the experiments without gold nanoparticles we observe a 20 mV shift of the threshold voltage. Confirming the observation of other reports that used gold decorated FETs to detect biomolecules. The additional sensing mechanism herein is based on the modulation of the Au-NP-SWNT Schottky barrier due to the presence of the protein.[146,91]

Figure 8.14 (b) shows the SERS spectra for different gold particle deposition times. The enhancement of the SWNT SERS signal is proportional to the size of the nanoparticles and thus on the duration of the deposition pulse.[147] We do not observe a shift in the frequency of the enhanced modes from which we conclude that electromagnetic enhancement plays the predominant role of SERS here. The Surface-enhanced Raman spectra on SWCNTs functionalized with GNPs at different deposition time were collected on a Renishaw inVia Raman microscope with an excitation laser wavelength of 633 nm at 50% maximum intensity and 10 s exposure time.

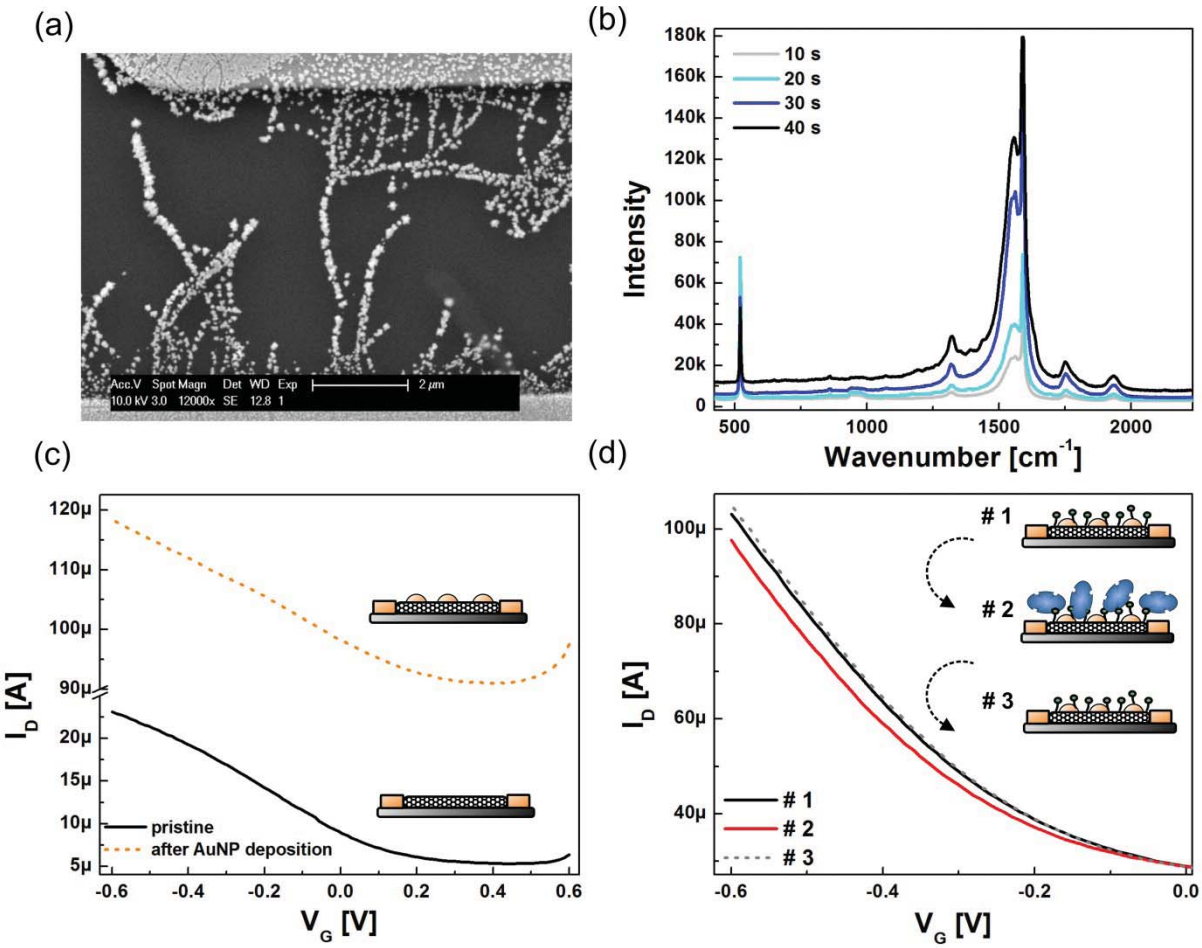

Figure 8.14.: (a) SEM image of gold nanoparticle decorated SWNTs. The particle sizes obtained from the applied parameters for this device are 50 to 200 nm. (b) Raman spectra of gold nanoparticle decorated SWNTs using varying deposition times of AC dielectrophoresis (deposition voltage -0.4 V).(c) Transfer characteristics of a SWNT FET recorded before and after functionalization with gold nanoparticles. (d) Transfer characteristics recorded for CaptAvidin detection with a DT-B functionalized device. #1 Transfer curve was taken before exposure to CaptAvidin, #2 after incubation with 140 nM CaptAvidin, #3 after 15 minutes exposure to pH 10 buffer.

8.6 Conclusion

In conclusion, together with the Star research group of the University of Pittsburgh it was possible to synthesize molecules for the functionalization of carbon nanotube field-effect transistors. Those molecules we successfully detected reversible protein-

ligand binding with pyrene-biotin functionalized SWNT FETs. Hereby, we introduced CaptAvidin, a tyrosine modified avidin, as a useful protein to engineer and optimize FET biosensors due to its reversible binding to biotin. Using this biosystem, we were able to probe the dissociation constant of CaptAvidin at two different pH values and to demonstrate that the sensor signal depends on the Debye screening length. Furthermore, we were able to differentiate between two different biotin-binding molecules, streptavidin and NeutrAvidin, by their pH-dependent sensor response. Additionally, SWNT FETs were decorated with gold nanoparticles to provide a supplemental, optical method for the detection of proteins, namely with surface enhanced Raman spectroscopy.

9 Conclusion and Outlook

9.1 Conclusion

In the frame of this thesis SWNT based field-effect transistors and field-effect transistors based on P3HT were fabricated and used as protein sensors in aqueous environment.

Prior to protein sensing and as a first part of this thesis, the sensors were extensively tested under aqueous conditions. In this context it was found that P3HT-FETs stand out due to the very fast fabrication process, i.e. no passivation of the gold contacts is required nor purification of the polymer itself and, as we did, also the substrates can be cleaned after measurements and be reused, SWNT-FETs show excellent stability and the transistors can be reused even after months and years. Even though the electrical stability of P3HT-devices lacks behind that of SWNT transistors, they perform well as pH sensors and after normalizing the obtained data, the results are comparable to those of carbon nanotube based devices. For P3HT a threshold shift of roughly 28 mV/pH and for SWNTs a shift of ca. 27 mV/pH was extracted from transfer curves. For these measurements both devices were operated in the electrolyte gate mode.

Furthermore back-gated and spray deposited SWNT field-effect transistors were fabricated and their response on different electrolytic conditions was discussed. Back-gated devices are generally easier to integrate in smart, portable sensors and

in microfluidics. This is as no hindering Ag/AgCl electrode needs to be integrated in a fluidic setup. The response of the transistors upon exposure to different concentrations of KCl was analyzed and an exponential dependence of the drain current on the KCl concentration was obtained, which is caused by a shift in the threshold voltage. Furthermore our devices have been exposed to buffer solutions with a wide range of pH values leading to a linear shift of the threshold voltage towards more negative values with increasing pH.

In the second part of this thesis protein binding experiments were performed. In this context two different techniques to functionalize the surface of a P3HT field-effect transistor with biotin molecules were presented. Both techniques have in common that they rely on non-covalent ways to incubate the P3HT surface with biotin. This is of interest, especially when it comes to protein sensing with polymeric, disposable one-way sensors where fast methods that are easy to carry out are demanded. The latter approach featured the advantage that it is generally possible to conduct experiments using a second experimental method, besides electrical measurements. Unfortunately, it was not achieved to clearly distinguish unspecific protein binding events from binding to biotin. Yet it is believed that conducting further experiments with biotinylated Au-nanoparticles could help to emend the existing protocols.

Additionally protein binding experiments were performed with SWNT-FETs. For this purpose´ functional molecules comprising a biotin end-group and a pyrene anchor-group were synthesized in collaboration with the Star research group of the University of Pittsburgh. Those functional molecules were successfully used to detect

reversible protein-ligand binding. Using the CaptAvidin/biotin-system, the dissociation constant of CaptAvidin at two different pH values was probed. Additionally it was demonstrated that the SWNT-sensor signal depends on the Debye screening length. Furthermore, we were able to differentiate between two different biotin-binding molecules, streptavidin and NeutrAvidin, by their pH-dependent sensor response. Further, SWNT FETs were decorated with gold nanoparticles to provide a supplemental, optical method for the detection of proteins, namely with surface enhanced Raman spectroscopy.

9.2 Outlook

Within this work it was demonstrated that organic transistors, and particularly SWNT-FETs, are on their way to being established as a components in commercial biomedical assays.

However, attention still must be paid to several issues: Field-effect transistor based sensors are highly susceptible to Debye screening, and therefore the surrounding media and size of functionalization molecules is vitally important. However, Debye screening could also be used to an advantage in this work: it was found that different proteins leave different “fingerprints” when measured at varying pH and under varying ionic strength. Meaning, that maybe it is possible to convert the bad to good and to use Debye screening in order to differentiate between different proteins. After

all, the observed phenomena deserve further investigation as the results of this work could open a new field of application for FET based biosensors.

Further work must be done to adapt these sensors for applications in complex media. That means, it would be beneficial if future biosensor are able to function in crude blood samples and saliva.

Furthermore protein detection with SWNT-FETs, as shown in this work, was solely performed by measuring the transfer characteristics of the FETs. Thereby it could be ensured that a possible parasitic influence of the Ag/AgCl gate electrode is excluded. However, this renders online monitoring of protein interactions impossible. Yet, it would be beneficial to be able to perform online measurements with proteins and thus more work in this field is required.

Another aspect is the integration of electrolyte gated FET biosensors. Due to the gate electrode they are not easy to integrate in small, microfluidic systems. This could be overcome by integrating a Ag/AgCl reference electrode directly on the chip. In this context, more work needs to be done when it comes to the chip design.

When it comes to sensing with polymeric semiconductors, it can be seen from the results above that still effort needs to be put in functionalizing the surface of the polymer with biofunctional groups. Since the CaptAvidin/biotin binding system turned out to be beneficial to probe the stability of the functionalization, it is recommended to adapt the experiments, which were performed with SWNT-FETS, also to polymeric

semiconductors. In this way both semiconductors could be compared with regards to their sensitivity to proteins.

Publications

Results from this work have been published in these journals:

- Münzer, A. M.; Seo, W.; Morgan, G. J.; Michael, Z. P.; Zhao, Y.; Melzer, K.; Scarpa, G.; Star, A., Sensing Reversible Protein–Ligand Interactions with Single-Walled Carbon Nanotube Field-Effect Transistors. *J. Phys. Chem. C* **2014,** *118* (31), 17193-17199

- Münzer, A. M.; Michael, Z. P.; Star, A., Carbon Nanotubes for the Label-Free Detection of Biomarkers. *ACS Nano* **2013,** *7* (9), 7448-7453

- Münzer, A. M.; Melzer, K.; Heimgreiter, M.; Scarpa, G., Random CNT network and regioregular poly(3-hexylthiophen) FETs for pH sensing applications: A comparison. *Biochimica et Biophysica Acta (BBA) - General Subjects* **2013,** *1830* (9), 4353-4358

- Münzer, A. M.; Heimgreiter, M.; Melzer, K.; Weise, A.; Fabel, B.; Abdellah, A.; Lugli, P.; Scarpa, G., Back-gated spray-deposited carbon nanotube thin film transistors operated in electrolytic solutions: an assessment towards future biosensing applications. *J. Mater. Chem. B* **2013,** *1* (31), 3797-3802

Results from this work have been published in conference proceedings:

- Scarpa, G.; Idzko, A. L.; Münzer, A.; Thalhammer, S. In *Low-cost solution-processable organic thin-film transistors for (bio)sensing applications*, Sensors, 2011 IEEE, 28-31 Oct. **2011**; pp 1581-1583

Results from this work have been presented at conferences and workshops:

- Münzer, A. M. Protein Sensing with Carbon Nanotube Field-Effect Transistors. 3rd International Symposium on Advances in Nanoelectronics, Badwiessee, Germany, July 30th, 2013

- Münzer, A. M.; Haeberle, T.; Scarpa, G. Biosensors Based on Semiconducting Polymers and Random Carbon Nanotube Networks, E-MRS 2012 Spring Meeting, Strasbourg, France, May 15th, 2012

- Münzer, A. M.; Melzer, K.; Scarpa, G. Specific protein detection with gold-nanoparticle decorated poly(3-hexylthiophene) thin-film transistors. ICOE, Grenoble, France, June 19th, 2013

Acknowledgement

This work would not have been possible without the effort and support of the following people:

- Prof. Dr. Paolo Lugli and Dr. Giuseppe Scarpa, thank you for giving me the opportunity to work on that extremely interesting research topic and also for the scientific support and guidance.
- Prof. Dr. Alexander Star, thank you so much for the time I could spend in your lab in Pittsburgh! I learned a lot from you!
- Katharina Melzer, thank you for the fruitful discussions and your scientific contributions.
- Wanji Seo, thanks for synthesizing all those molecules! It finally really worked because of your effort!
- Dr. Bernhard Fabel, thank you for teaching me all important things about transistors.
- Rosi Heilmann, thank you for your help in the lab!
- Rosi Mittermeier, thanks for all your support in the lab!
- Tobias Haeberle, thank you Tobi for the fruitful discussions!
- Morten Schmidt, thanks for our help and our little projects.
- Florin Loghin, thanks for your help in the lab.

References

1. Turner, A., Biosensors: then and now. *Trends Biotechnol.* **2013,** *31* (3), 119-120.
2. Pedone, D.; Langecker, M.; Abstreiter, G.; Rant, U., A Pore−Cavity−Pore Device to Trap and Investigate Single Nanoparticles and DNA Molecules in a Femtoliter Compartment: Confined Diffusion and Narrow Escape. *Nano Lett.* **2011,** *11* (4), 1561-1567.
3. Wei, R.; Gatterdam, V.; Wieneke, R.; Tampe, R.; Rant, U., Stochastic sensing of proteins with receptor-modified solid-state nanopores. *Nat Nano* **2012,** *7* (4), 257-263.
4. Langer, A.; Hampel, P. A.; Kaiser, W.; Knezevic, J.; Welte, T.; Villa, V.; Maruyama, M.; Svejda, M.; Jähner, S.; Fischer, F.; Strasser, R.; Rant, U., Protein analysis by time-resolved measurements with an electro-switchable DNA chip. *Nat Commun* **2013,** *4*.
5. Münzer, A. M.; Michael, Z. P.; Star, A., Carbon Nanotubes for the Label-Free Detection of Biomarkers. *ACS Nano* **2013,** *7* (9), 7448-7453.
6. Poghossian, A.; Schöning, M. J., Label-Free Sensing of Biomolecules with Field-Effect Devices for Clinical Applications. *Electroanalysis* **2014**, 1521-4109.
7. Fan, R.; Vermesh, O.; Srivastava, A.; Yen, B. K. H.; Qin, L.; Ahmad, H.; Kwong, G. A.; Liu, C.-C.; Gould, J.; Hood, L.; Heath, J. R., Integrated barcode chips for rapid, multiplexed analysis of proteins in microliter quantities of blood. *Nat Biotech* **2008,** *26* (12), 1373-1378.
8. Kim, J.; Valdes-Ramirez, G.; Bandodkar, A. J.; Jia, W.; Martinez, A. G.; Ramirez, J.; Mercier, P.; Wang, J., Non-invasive mouthguard biosensor for continuous salivary monitoring of metabolites. *Analyst* **2014,** *139* (7), 1632-1636.
9. Bănică, F.-G., *Chemical sensors and biosensors: Fundamentals and Applications*. John Wiley & Sons, Ltd: 2012.
10. Biosensing Instrument. http://www.biosensingusa.com/Application102.html (accessed February 25, 2015).
11. Liedberg, B.; Nylander, C.; Lundström, I., Biosensing with surface plasmon resonance — how it all started. *Biosensors and Bioelectronics* **1995,** *10* (8), i-ix.
12. Campbell, C. T.; Kim, G., SPR microscopy and its applications to high-throughput analyses of biomolecular binding events and their kinetics. *Biomaterials* **2007,** *28* (15), 2380-2392.
13. Feigel, I. M.; Vedala, H.; Star, A., Biosensors based on one-dimensional nanostructures. *J. Mater. Chem.* **2011,** *21* (25), 8940-8954.
14. Reuel, N. F.; Grassbaugh, B.; Kruss, S.; Mundy, J. Z.; Opel, C.; Ogunniyi, A. O.; Egodage, K.; Wahl, R.; Helk, B.; Zhang, J.; Kalcioglu, Z. I.; Tvrdy, K.; Bellisario, D. O.; Mu, B.; Blake, S. S.; Van Vliet, K. J.; Love, J. C.; Wittrup, K. D.; Strano, M. S., Emergent Properties of Nanosensor Arrays: Applications for Monitoring IgG Affinity Distributions, Weakly Affined Hypermannosylation, and Colony Selection for Biomanufacturing. *ACS Nano* **2013**.
15. Kauffman, D. R.; Star, A., Electronically monitoring biological interactions with carbon nanotube field-effect transistors. *Chem. Soc. Rev.* **2008,** *37* (6), 1197-1206.
16. Bettinger, C. J.; Bao, Z., Organic Thin-Film Transistors Fabricated on Resorbable Biomaterial Substrates. *Adv. Mater.* **2010,** *22* (5), 651-655.
17. Scarpa, G.; Idzko, A. L.; Münzer, A.; Thalhammer, S. In *Low-cost solution-processable organic thin-film transistors for (bio)sensing applications*, Sensors, 2011 IEEE, 28-31 Oct. 2011; 2011; pp 1581-1583.
18. Watson, J. D.; Crick, F. H. C., Molecular Structure of Nucleic Acids: A Structure for Deoxyribose Nucleic Acid. *Nature* **1953,** *171* (4356), 737-738.
19. Hsieh, C.-C.; Balducci, A.; Doyle, P. S., Ionic Effects on the Equilibrium Dynamics of DNA Confined in Nanoslits. *Nano Lett.* **2008,** *8* (6), 1683-1688.
20. Michael Green, N., [5] Avidin and streptavidin. In *Methods Enzymol.*, Meir, W.; Edward, A. B., Eds. Academic Press: 1990; Vol. 184, pp 51-67.
21. Heller, I.; Janssens, A. M.; Mannik, J.; Minot, E. D.; Lemay, S. G.; Dekker, C., Identifying the Mechanism of Biosensing with Carbon Nanotube Transistors. *Nano Lett.* **2007,** *8* (2), 591-595.

22. Stern, E.; Wagner, R.; Sigworth, F. J.; Breaker, R.; Fahmy, T. M.; Reed, M. A., Importance of the Debye Screening Length on Nanowire Field Effect Transistor Sensors. *Nano Lett.* **2007,** *7* (11), 3405-3409.
23. Sorgenfrei, S.; Chiu, C.-y.; Johnston, M.; Nuckolls, C.; Shepard, K. L., Debye Screening in Single-Molecule Carbon Nanotube Field-Effect Sensors. *Nano Lett.* **2011**, null-null.
24. Kulkarni, G. S.; Zhong, Z., Detection beyond the Debye Screening Length in a High-Frequency Nanoelectronic Biosensor. *Nano Lett.* **2012,** *12* (2), 719-723.
25. Choi, Y.; Moody, I. S.; Sims, P. C.; Hunt, S. R.; Corso, B. L.; Perez, I.; Weiss, G. A.; Collins, P. G., Single-Molecule Lysozyme Dynamics Monitored by an Electronic Circuit. *Science* **2012,** *335* (6066), 319-324.
26. Star, A.; Gabriel, J.-C. P.; Bradley, K.; Grüner, G., Electronic Detection of Specific Protein Binding Using Nanotube FET Devices. *Nano Lett.* **2003,** *3* (4), 459-463.
27. Chen, R. J.; Bangsaruntip, S.; Drouvalakis, K. A.; Wong Shi Kam, N.; Shim, M.; Li, Y.; Kim, W.; Utz, P. J.; Dai, H., Noncovalent functionalization of carbon nanotubes for highly specific electronic biosensors. *Proc. Natl. Acad. Sci. U. S. A.* **2003,** *100* (9), 4984-4989.
28. Vedala, H.; Chen, Y.; Cecioni, S.; Imberty, A.; Vidal, S.; Star, A., Nanoelectronic Detection of Lectin-Carbohydrate Interactions Using Carbon Nanotubes. *Nano Lett.* **2010,** *11* (1), 170-175.
29. Hammes, G. G., Multiple Conformational Changes in Enzyme Catalysis†. *Biochemistry* **2002,** *41* (26), 8221-8228.
30. Choi, Y.; Olsen, T. J.; Sims, P. C.; Moody, I. S.; Corso, B. L.; Dang, M. N.; Weiss, G. A.; Collins, P. G., Dissecting Single-Molecule Signal Transduction in Carbon Nanotube Circuits with Protein Engineering. *Nano Lett.* **2013,** *13* (2), 625-631.
31. Reuel, N. F.; Ahn, J.-H.; Kim, J.-H.; Zhang, J.; Boghossian, A. A.; Mahal, L. K.; Strano, M. S., Transduction of Glycan–Lectin Binding Using Near-Infrared Fluorescent Single-Walled Carbon Nanotubes for Glycan Profiling. *J. Am. Chem. Soc.* **2011,** *133* (44), 17923-17933.
32. Scarpa, G.; Idzko, A.; Yadav, A.; Martin, E.; Thalhammer, S., Toward Cheap Disposable Sensing Devices for Biological Assays. *Nanotechnology, IEEE Transactions on* **2010,** *9* (5), 527-532.
33. Melzer, K.; Münzer, A. M.; Jaworska, E.; Maksymiuk, K.; Michalska, A.; Scarpa, G., Polymeric ion-selective membrane functionalized gate-electrodes: Ion-selective response of electrolyte-gated poly (3-hexylthiophene) field-effect transistors. *Organic Electronics* **2014,** *15* (2), 595-601.
34. Scarpa, G.; Idzko, A. L.; Gotz, S.; Thalhammer, S., Biocompatibility Studies of Functionalized Regioregular Poly(3-hexylthiophene) Layers for Sensing Applications. *Macromol. Biosci.* **2010,** *10* (4), 378-383.
35. Khan, H. U.; Roberts, M. E.; Johnson, O.; Förch, R.; Knoll, W.; Bao, Z., In Situ, Label-Free DNA Detection Using Organic Transistor Sensors. *Adv. Mater.* **2010,** *22* (40), 4452-4456.
36. Park, S. K.; Jackson, T. N.; Anthony, J. E.; Mourey, D. A., High mobility solution processed 6,13-bis(triisopropyl-silylethynyl) pentacene organic thin film transistors. *Appl. Phys. Lett.* **2007,** *91* (6), -.
37. Lai, S.; Demelas, M.; Casula, G.; Cosseddu, P.; Barbaro, M.; Bonfiglio, A., Ultra-Low Voltage, OTFT-Based Sensor for Label-Free DNA Detection. *Adv. Mater.* **2012**, 1521-4095.
38. Angione, M. D.; Cotrone, S.; Magliulo, M.; Mallardi, A.; Altamura, D.; Giannini, C.; Cioffi, N.; Sabbatini, L.; Fratini, E.; Baglioni, P.; Scamarcio, G.; Palazzo, G.; Torsi, L., Interfacial electronic effects in functional biolayers integrated into organic field-effect transistors. *Proceedings of the National Academy of Sciences* **2012**.
39. Magliulo, M.; Mallardi, A.; Mulla, M. Y.; Cotrone, S.; Pistillo, B. R.; Favia, P.; Vikholm-Lundin, I.; Palazzo, G.; Torsi, L., Electrolyte-Gated Organic Field-Effect Transistor Sensors Based on Supported Biotinylated Phospholipid Bilayer. *Adv. Mater.* **2013,** *25* (14), 2090-2094.
40. Ahn, J.-H.; Kim, J.-H.; Reuel, N. F.; Barone, P. W.; Boghossian, A. A.; Zhang, J.; Yoon, H.; Chang, A. C.; Hilmer, A. J.; Strano, M. S., Label-Free, Single Protein Detection on a Near-Infrared Fluorescent Single-Walled Carbon Nanotube/Protein Microarray Fabricated by Cell-Free Synthesis. *Nano Lett.* **2011,** *11* (7), 2743-2752.

41. Hammock, M. L.; Sokolov, A. N.; Stoltenberg, R. M.; Naab, B. D.; Bao, Z., Organic Transistors with Ordered Nanoparticle Arrays as a Tailorable Platform for Selective, In Situ Detection. *ACS Nano* **2012,** *6* (4), 3100-3108.
42. Cramer, T.; Campana, A.; Leonardi, F.; Casalini, S.; Kyndiah, A.; Murgia, M.; Biscarini, F., Water-gated organic field effect transistors - opportunities for biochemical sensing and extracellular signal transduction. *J. Mater. Chem. B* **2013,** *1* (31), 3728-3741.
43. Zhang, R.; Zhang, Y.; Zhang, Q.; Xie, H.; Qian, W.; Wei, F., Growth of Half-Meter Long Carbon Nanotubes Based on Schulz–Flory Distribution. *ACS Nano* **2013,** *7* (7), 6156-6161.
44. Saito, R.; Fujita, M.; Dresselhaus, G.; Dresselhaus, M. S., Electronic structure of chiral graphene tubules. *Appl. Phys. Lett.* **1992,** *60* (18), 2204-2206.
45. Charlier, J.-C.; Blase, X.; Roche, S., Electronic and transport properties of nanotubes. *Reviews of Modern Physics* **2007,** *79* (2), 677-732.
46. Correa, J. D.; Silva, A. J. R. d.; Pacheco, M., Tight-binding model for carbon nanotubes from ab initio calculations. *J. Phys.: Condens. Matter* **2010,** *22* (27), 275503.
47. Zhang, Y.; Tang, T.-T.; Girit, C.; Hao, Z.; Martin, M. C.; Zettl, A.; Crommie, M. F.; Shen, Y. R.; Wang, F., Direct observation of a widely tunable bandgap in bilayer graphene. *Nature* **2009,** *459* (7248), 820-823.
48. Kitamura, M.; Arakawa, Y., Pentacene-based organic field-effect transistors. *J. Phys.: Condens. Matter* **2008,** *20* (18), 184011.
49. Wolfgang, B., *Physics of Organic Semiconductors*. Wiley-VCH: Weinheim, 2005.
50. Bao, Z.; Dodabalapur, A.; Lovinger, A. J., Soluble and processable regioregular poly(3-hexylthiophene) for thin film field-effect transistor applications with high mobility. *Appl. Phys. Lett.* **1996,** *69* (26), 4108-4110.
51. Sirringhaus, H.; Tessler, N.; Friend, R. H., Integrated Optoelectronic Devices Based on Conjugated Polymers. *Science* **1998,** *280* (5370), 1741-1744.
52. Devine, R. A. B., Time dependent evolution of the carrier mobility in poly(3-hexylthiophene) based field effect transistors. *J. Appl. Phys.* **2006,** *100* (3), -.
53. Melzer, K. Fabrication and Characterization of Organic Devices for Biosensing Applications. Diplomarbeit, Technische Universität München, München, 2013.
54. Salzner, U.; Lagowski, J. B.; Pickup, P. G.; Poirier, R. A., Comparison of geometries and electronic structures of polyacetylene, polyborole, polycyclopentadiene, polypyrrole, polyfuran, polysilole, polyphosphole, polythiophene, polyselenophene and polytellurophene. *Synth. Met.* **1998,** *96* (3), 177-189.
55. Salleo, A., Charge transport in polymeric transistors. *Materials Today* **2007,** *10* (3), 38-45.
56. Zaumseil, J.; Sirringhaus, H., Electron and Ambipolar Transport in Organic Field-Effect Transistors. *Chemical Reviews* **2007,** *107* (4), 1296-1323.
57. Sze, S. M.; Ng, K. K., MOSFETs. In *Physics of Semiconductor Devices*, John Wiley & Sons, Inc.: 2006; pp 293-373.
58. Bruesch, P.; Christen, T., The electric double layer at a metal electrode in pure water. *J. Appl. Phys.* **2004,** *95* (5), 2846-2856.
59. Morag, E.; Bayer, E. A.; Wilchek, M., Reversibility of biotin-binding by selective modification of tyrosine in avidin. *Biochem. J.* **1996,** *316* (1), 193-199.
60. Garcia-Aljaro, C.; Munoz, F. X.; Baldrich, E., Captavidin: a new regenerable biocomponent for biosensing? *Analyst* **2009,** *134* (11), 2338-2343.
61. Calvaresi, M.; Zerbetto, F., The Devil and Holy Water: Protein and Carbon Nanotube Hybrids. *Acc. Chem. Res.* **2013**.
62. Takahashi, T.; Tsunoda, K.; Yajima, H.; Ishii, T., Dispersion and Purification of Single-Wall Carbon Nanotubes Using Carboxymethylcellulose. *Japanese Journal of Applied Physics* **2004,** *43*, 363-3639.
63. Abdellah, A.; Yaqub, A.; Ferrari, C.; Fabel, B.; Lugli, P.; Scarpa, G. In *Spray deposition of highly uniform CNT films and their application in gas sensing*, Nanotechnology (IEEE-NANO), 2011 11th IEEE Conference on, 15-18 Aug. 2011; 2011; pp 1118-1123.

64. Abdellah, A.; Abdelhalim, A.; Horn, M.; Scarpa, G.; Lugli, P., Scalable Spray Deposition Process for High-Performance Carbon Nanotube Gas Sensors. *Nanotechnology, IEEE Transactions on* **2013,** *12* (2), 174-181.
65. Cheng, Q.; Debnath, S.; O'Neill, L.; Hedderman, T. G.; Gregan, E.; Byrne, H. J., Systematic Study of the Dispersion of SWNTs in Organic Solvents. *J. Phys. Chem. C* **2010,** *114* (11), 4857-4863.
66. Ausman, K. D.; Piner, R.; Lourie, O.; Ruoff, R. S.; Korobov, M., Organic Solvent Dispersions of Single-Walled Carbon Nanotubes: Toward Solutions of Pristine Nanotubes. *The Journal of Physical Chemistry B* **2000,** *104* (38), 8911-8915.
67. Idzko, A.-L. Organic Field-Effect Transistors for Application in Radiation Biophysics. 2011.
68. New Era Pump Systems, I. http://www.syringepump.com/NE-1000.php (accessed February, 23, 2015).
69. Münzer, A. M.; Melzer, K.; Heimgreiter, M.; Scarpa, G., Random CNT network and regioregular poly(3-hexylthiophen) FETs for pH sensing applications: A comparison. *Biochimica et Biophysica Acta (BBA) - General Subjects* **2013,** *1830* (9), 4353-4358.
70. Hoshino, S.; Yoshida, M.; Uemura, S.; Kodzasa, T.; Takada, N.; Kamata, T.; Yase, K., Influence of moisture on device characteristics of polythiophene-based field-effect transistors. *J. Appl. Phys.* **2004,** *95* (9), 5088-5093.
71. Hintz, H.; Egelhaaf, H. J.; Lüer, L.; Hauch, J.; Peisert, H.; Chassé, T., Photodegradation of P3HT−A Systematic Study of Environmental Factors. *Chem. Mater.* **2010,** *23* (2), 145-154.
72. Bobbert, P. A.; Sharma, A.; Mathijssen, S. G. J.; Kemerink, M.; de Leeuw, D. M., Operational Stability of Organic Field-Effect Transistors. *Adv. Mater.* **2012**, 1146–1158.
73. Sirringhaus, H., Reliability of Organic Field-Effect Transistors. *Adv. Mater.* **2009,** *21* (38-39), 3859-3873.
74. Yang, R. D.; Park, J.; Colesniuc, C. N.; Schuller, I. K.; Trogler, W. C.; Kummel, A. C., Ultralow drift in organic thin-film transistor chemical sensors by pulsed gating. *J. Appl. Phys.* **2007,** *102* (3), 034515.
75. Lin, H.; Tiwari, S., Localized charge trapping due to adsorption in nanotube field-effect transistor and its field-mediated transport. *Appl. Phys. Lett.* **2006,** *89* (7), 073507.
76. Zschieschang, U.; Weitz, R. T.; Kern, K.; Klauk, H., Bias stress effect in low-voltage organic thin-film transistors. *Applied Physics A* **2009,** *95* (1), 139-145.
77. Qingqing, G.; Albert, E.; Fabel, B.; Abdellah, A.; Lugli, P.; Chan-Park, M. B.; Scarpa, G. In *Solution-processable random carbon nanotube networks for thin-film transistors*, Nanotechnology (IEEE-NANO), 2011 11th IEEE Conference on, 15-18 Aug. 2011; 2011; pp 378-381.
78. Dimitrakopoulos, C. D.; Mascaro, D. J., Organic thin-film transistors: A review of recent advances. *IBM Journal of Research and Development* **2001,** *45* (1), 11-27.
79. Kergoat, L.; Herlogsson, L.; Braga, D.; Piro, B.; Pham, M.-C.; Crispin, X.; Berggren, M.; Horowitz, G., A Water-Gate Organic Field-Effect Transistor. *Adv. Mater.* **2010,** *22* (23), 2565-2569.
80. Laiho, A.; Herlogsson, L.; Forchheimer, R.; Crispin, X.; Berggren, M., Controlling the dimensionality of charge transport in organic thin-film transistors. *Proceedings of the National Academy of Sciences* **2011,** *108* (37), 15069-15073.
81. Street, R. A.; Salleo, A.; Chabinyc, M. L., Bipolaron mechanism for bias-stress effects in polymer transistors. *Physical Review B* **2003,** *68* (8), 085316.
82. Salleo, A.; Street, R. A., Kinetics of bias stress and bipolaron formation in polythiophene. *Physical Review B* **2004,** *70* (23), 235324.
83. Haeberle, T.; Münzer, A. M.; Buth, F.; Garrido, J. A.; Abdellah, A.; Fabel, B.; Lugli, P.; Scarpa, G., Solution processable carbon nanotube network thin-film transistors operated in electrolytic solutions at various pH. *Appl. Phys. Lett.* **2012,** *101* (22), 223101-5.
84. Mzoughi, N.; Abdellah, A.; Gong, Q.; Grothe, H.; Lugli, P.; Wolf, B.; Scarpa, G., Characterization of novel impedimetric pH-sensors based on solution-processable biocompatible thin-film semiconducting organic coatings. *Sensor Actuat B Chem* **2012,** *171–172* (0), 537-543.
85. Scarpa, G.; Idzko, A.-L.; Yadav, A.; Thalhammer, S., Organic ISFET Based on Poly (3-hexylthiophene). *Sensors* **2010,** *10* (3), 2262-2273.

86. Roberts, M. E.; Mannsfeld, S. C. B.; Queraltó, N.; Reese, C.; Locklin, J.; Knoll, W.; Bao, Z., Water-stable organic transistors and their application in chemical and biological sensors. *Proceedings of the National Academy of Sciences* **2008,** *105* (34), 12134-12139.
87. Bartic, C.; Palan, B.; Campitelli, A.; Borghs, G., Monitoring pH with organic-based field-effect transistors. *Sensor Actuat B Chem* **2002,** *83* (1–3), 115-122.
88. Buth, F.; Kumar, D.; Stutzmann, M.; Garrido, J. A., Electrolyte-gated organic field-effect transistors for sensing applications. *Appl. Phys. Lett.* **2011,** *98* (15), 153302.
89. Münzer, A. M.; Heimgreiter, M.; Melzer, K.; Weise, A.; Fabel, B.; Abdellah, A.; Lugli, P.; Scarpa, G., Back-gated spray-deposited carbon nanotube thin film transistors operated in electrolytic solutions: an assessment towards future biosensing applications. *J. Mater. Chem. B* **2013,** *1* (31), 3797-3802.
90. Artyukhin, A. B.; Stadermann, M.; Friddle, R. W.; Stroeve, P.; Bakajin, O.; Noy, A., Controlled Electrostatic Gating of Carbon Nanotube FET Devices. *Nano Lett.* **2006,** *6* (9), 2080-2085.
91. Kim, B.; Lee, J.; Namgung, S.; Kim, J.; Park, J. Y.; Lee, M.-S.; Hong, S., DNA sensors based on CNT-FET with floating electrodes. *Sensor Actuat B Chem* **2012,** *169* (0), 182-187.
92. Chen, R. J.; Choi, H. C.; Bangsaruntip, S.; Yenilmez, E.; Tang, X.; Wang, Q.; Chang, Y.-L.; Dai, H., An Investigation of the Mechanisms of Electronic Sensing of Protein Adsorption on Carbon Nanotube Devices. *J. Am. Chem. Soc.* **2004,** *126* (5), 1563-1568.
93. Banerjee, S.; Hemraj-Benny, T.; Wong, S. S., Covalent Surface Chemistry of Single-Walled Carbon Nanotubes. *Adv. Mater.* **2005,** *17* (1), 17-29.
94. Minot, E. D.; Janssens, A. M.; Heller, I.; Heering, H. A.; Dekker, C.; Lemay, S. G., Carbon nanotube biosensors: The critical role of the reference electrode. *Appl. Phys. Lett.* **2007,** *91* (9), 093507-093507-3.
95. Abdelhalim, A.; Abdellah, A.; Scarpa, G.; Lugli, P., Fabrication of carbon nanotube thin films on flexible substrates by spray deposition and transfer printing. *Carbon* **2013,** *61* (0), 72-79.
96. Maehashi, K.; Katsura, T.; Kerman, K.; Takamura, Y.; Matsumoto, K.; Tamiya, E., Label-Free Protein Biosensor Based on Aptamer-Modified Carbon Nanotube Field-Effect Transistors. *Anal. Chem.* **2006,** *79* (2), 782-787.
97. Thu-Hong, T.; Jae-Hong, K.; Kyong-Soo, L.; Lee, J.-W.; Byeong-Kwon, J. In *pH Sensor Using Carbon Nanotubes as Sensing Material*, Communications and Electronics, 2006. ICCE '06. First International Conference on, 10-11 Oct. 2006; 2006; pp 490-493.
98. Abdellah, A.; Abdelhalim, A.; Horn, M.; Scarpa, G.; Lugli, P., Scalable Spray Deposition Process for High Performance Carbon Nanotube Gas Sensors. *Nanotechnology, IEEE Transactions on* **2013,** *PP* (99), 1-1.
99. Abdellah, A.; Fabel, B.; Lugli, P.; Scarpa, G., Spray deposition of organic semiconducting thin-films: Towards the fabrication of arbitrary shaped organic electronic devices. *Organic Electronics* **2010,** *11* (6), 1031-1038.
100. Sorgenfrei, S.; Chiu, C.-y.; Johnston, M.; Nuckolls, C.; Shepard, K. L., Debye Screening in Single-Molecule Carbon Nanotube Field-Effect Sensors. *Nano Lett.* **2011,** *11* (9), 3739-3743.
101. Kergoat, L.; Piro, B.; Berggren, M.; Pham, M.-C.; Yassar, A.; Horowitz, G., DNA detection with a water-gated organic field-effect transistor. *Organic Electronics* **2012,** *13* (1), 1-6.
102. Gruner, G., Carbon nanotube transistors for biosensing applications. *Anal. Bioanal. Chem.* **2006,** *384* (2), 322-335.
103. Back, J. H.; Shim, M., pH-Dependent Electron-Transport Properties of Carbon Nanotubes. *The Journal of Physical Chemistry B* **2006,** *110* (47), 23736-23741.
104. Heller, I.; Chatoor, S.; Männik, J.; Zevenbergen, M. A. G.; Dekker, C.; Lemay, S. G., Influence of Electrolyte Composition on Liquid-Gated Carbon Nanotube and Graphene Transistors. *J. Am. Chem. Soc.* **2010,** *132* (48), 17149-17156.
105. Opatkiewicz, J. P.; LeMieux, M. C.; Bao, Z., Influence of Electrostatic Interactions on Spin-Assembled Single-Walled Carbon Nanotube Networks on Amine-Functionalized Surfaces. *ACS Nano* **2010,** *4* (2), 1167-1177.
106. Yuqing, M.; Jianrong, C.; Keming, F., New technology for the detection of pH. *J. Biochem. Biophys. Methods* **2005,** *63* (1), 1-9.

107. Idzko, A.-L. Organic Field-Effect Transistors for Application in Radiation Biophysics. Dissertation, Universität Augsburg, Augsburg, 2011.
108. Norde, W.; Buijs, J.; Lyklema, H., 3 Adsorption of globular proteins. In *Fundamentals of Interface and Colloid Science*, Lyklema, J., Ed. Academic Press: 2005; Vol. Volume 5, pp 1-59.
109. Hecht, D. S.; Ramirez, R. J. A.; Briman, M.; Artukovic, E.; Chichak, K. S.; Stoddart, J. F.; Grüner, G., Bioinspired Detection of Light Using a Porphyrin-Sensitized Single-Wall Nanotube Field Effect Transistor. *Nano Lett.* **2006,** *6* (9), 2031-2036.
110. Bradley, K.; Briman, M.; Star, A.; Grüner, G., Charge Transfer from Adsorbed Proteins. *Nano Lett.* **2004,** *4* (2), 253-256.
111. Lerner, M. B.; Dailey, J.; Goldsmith, B. R.; Brisson, D.; Charlie Johnson, A. T., Detecting Lyme disease using antibody-functionalized single-walled carbon nanotube transistors. *Biosens. Bioelectron.* **2013,** *45* (0), 163-167.
112. Khan, H. U.; Jang, J.; Kim, J.-J.; Knoll, W., In Situ Antibody Detection and Charge Discrimination Using Aqueous Stable Pentacene Transistor Biosensors. *J. Am. Chem. Soc.* **2011,** *133* (7), 2170-2176.
113. Bai, S.; Shen, X., Graphene-inorganic nanocomposites. *RSC Advances* **2012,** *2* (1), 64-98.
114. Chen, Y.; Vedala, H.; Kotchey, G. P.; Audfray, A.; Cecioni, S.; Imberty, A.; Vidal, S.; Star, A., Electronic Detection of Lectins Using Carbohydrate-Functionalized Nanostructures: Graphene versus Carbon Nanotubes. *ACS Nano* **2011,** *6* (1), 760-770.
115. Gong, J.-R., Label-Free Attomolar Detection of Proteins Using Integrated Nanoelectronic and Electrokinetic Devices. *Small* **2010,** *6* (8), 967-973.
116. Duan, X.; Li, Y.; Rajan, N. K.; Routenberg, D. A.; Modis, Y.; Reed, M. A., Quantification of the affinities and kinetics of protein interactions using silicon nanowire biosensors. *Nat Nano* **2012,** *7* (6), 401-407.
117. Harbers, G. M.; Emoto, K.; Greef, C.; Metzger, S. W.; Woodward, H. N.; Mascali, J. J.; Grainger, D. W.; Lochhead, M. J., Functionalized Poly(ethylene glycol)-Based Bioassay Surface Chemistry That Facilitates Bio-Immobilization and Inhibits Nonspecific Protein, Bacterial, and Mammalian Cell Adhesion. *Chem. Mater.* **2007,** *19* (18), 4405-4414.
118. Wazawa, T.; Ishizuka-Katsura, Y.; Nishikawa, S.; Iwane, A. H.; Aoyama, S., Grafting of Poly(ethylene glycol) onto Poly(acrylic acid)-Coated Glass for a Protein-Resistant Surface. *Anal. Chem.* **2006,** *78* (8), 2549-2556.
119. Butler, J. N., *Ionic Equilibrium: Solubility and pH Calculations*. John Wiley & Sons: 1998.
120. Livnah, O.; Bayer, E. A.; Wilchek, M.; Sussman, J. L., Three-dimensional structures of avidin and the avidin-biotin complex. *Proceedings of the National Academy of Sciences* **1993,** *90* (11), 5076-5080.
121. Münzer, A. M.; Seo, W.; Morgan, G. J.; Michael, Z. P.; Zhao, Y.; Melzer, K.; Scarpa, G.; Star, A., Sensing Reversible Protein–Ligand Interactions with Single-Walled Carbon Nanotube Field-Effect Transistors. *J. Phys. Chem. C* **2014,** *118* (31), 17193-17199.
122. Campbell, G. A.; Mutharasan, R., Detection and quantification of proteins using self-excited PZT-glass millimeter-sized cantilever. *Biosens. Bioelectron.* **2005,** *21* (4), 597-607.
123. Chen, Y.; Lee, Y. D.; Vedala, H.; Allen, B. L.; Star, A., Exploring the Chemical Sensitivity of a Carbon Nanotube/Green Tea Composite. *ACS Nano* **2010,** *4* (11), 6854-6862.
124. Krupke, R.; Hennrich, F.; Löhneysen, H. v.; Kappes, M. M., Separation of Metallic from Semiconducting Single-Walled Carbon Nanotubes. *Science* **2003,** *301* (5631), 344-347.
125. Zhang, Z.-B.; Liu, X.-J.; Campbell, E. E. B.; Zhang, S.-L., Alternating current dielectrophoresis of carbon nanotubes. *J. Appl. Phys.* **2005,** *98* (5), -.
126. Li, H.; Hain, T. C.; Muzha, A.; Schöppler, F.; Hertel, T., Dynamical Contact Line Pinning and Zipping during Carbon Nanotube Coffee Stain Formation. *ACS Nano* **2014**.
127. Shekhar, S.; Stokes, P.; Khondaker, S. I., Ultrahigh Density Alignment of Carbon Nanotube Arrays by Dielectrophoresis. *ACS Nano* **2011,** *5* (3), 1739-1746.
128. Britton, H. T. S.; Robinson, R. A., CXCVIII.-Universal buffer solutions and the dissociation constant of veronal. *J. Chem. Soc. (Resumed)* **1931,** (0), 1456-1462.

129. Fernández, C. M.; Martin, V. C., Preparation d'un tampon universel de force ionique 0,3 M. *Talanta* **1977,** *24* (12), 747-748.
130. Holmberg, A.; Blomstergren, A.; Nord, O.; Lukacs, M.; Lundeberg, J.; Uhlén, M., The biotin-streptavidin interaction can be reversibly broken using water at elevated temperatures. *Electrophoresis* **2005,** *26* (3), 501-510.
131. Katz, E.; Willner, I., Biomolecule-Functionalized Carbon Nanotubes: Applications in Nanobioelectronics. *ChemPhysChem* **2004,** *5* (8), 1084-1104.
132. Katz, E., Application of bifunctional reagents for immobilization of proteins on a carbon electrode surface: Oriented immobilization of photosynthetic reaction centers. *J. Electroanal. Chem.* **1994,** *365* (1–2), 157-164.
133. Pacios, M.; Martin-Fernandez, I.; Borrise, X.; del Valle, M.; Bartroli, J.; Lora-Tamayo, E.; Godignon, P.; Perez-Murano, F.; Esplandiu, M. J., Real time protein recognition in a liquid-gated carbon nanotube field-effect transistor modified with aptamers. *Nanoscale* **2012,** *4* (19), 5917-5923.
134. Besteman, K.; Lee, J.-O.; Wiertz, F. G. M.; Heering, H. A.; Dekker, C., Enzyme-Coated Carbon Nanotubes as Single-Molecule Biosensors. *Nano Lett.* **2003,** *3* (6), 727-730.
135. Firnkes, M.; Pedone, D.; Knezevic, J.; Döblinger, M.; Rant, U., Electrically Facilitated Translocations of Proteins through Silicon Nitride Nanopores: Conjoint and Competitive Action of Diffusion, Electrophoresis, and Electroosmosis. *Nano Lett.* **2010,** *10* (6), 2162-2167.
136. Balavoine, F.; Schultz, P.; Richard, C.; Mallouh, V.; Ebbesen, T. W.; Mioskowski, C., Helical Crystallization of Proteins on Carbon Nanotubes: A First Step towards the Development of New Biosensors. *Angewandte Chemie International Edition* **1999,** *38* (13-14), 1912-1915.
137. Ishikawa, F. N.; Curreli, M.; Chang, H.-K.; Chen, P.-C.; Zhang, R.; Cote, R. J.; Thompson, M. E.; Zhou, C., A Calibration Method for Nanowire Biosensors to Suppress Device-to-Device Variation. *ACS Nano* **2009,** *3* (12), 3969-3976.
138. Lee, B. Y.; Sung, M. G.; Lee, J.; Baik, K. Y.; Kwon, Y.-K.; Lee, M.-S.; Hong, S., Universal Parameters for Carbon Nanotube Network-Based Sensors: Can Nanotube Sensors Be Reproducible? *ACS Nano* **2011,** *5* (6), 4373-4379.
139. Birner, S.; Uhl, C.; Bayer, M.; Vogl, P., Theoretical model for the detection of charged proteins with a silicon-on-insulator sensor. *Journal of Physics: Conference Series* **2008,** *107* (1), 012002.
140. Bowen, W. R.; Hall, N. J.; Pan, L.-C.; Sharif, A. O.; Williams, P. M., The relevance of particle size and zeta-potential in protein processing. *Nat Biotech* **1998,** *16* (8), 785-787.
141. Vo-Dinh, T.; Yan, F.; Wabuyele, M. B., Surface-enhanced Raman scattering for medical diagnostics and biological imaging. *J. Raman Spectrosc.* **2005,** *36* (6-7), 640-647.
142. Huh, Y.; Chung, A.; Erickson, D., Surface enhanced Raman spectroscopy and its application to molecular and cellular analysis. *Microfluid Nanofluid* **2009,** *6* (3), 285-297.
143. Li, T.; Guo, L.; Wang, Z., Gold Nanoparticle-based Surface Enhanced Raman Scattering Spectroscopic Assay for the Detection of Protein-Protein Interactions. *Anal. Sci.* **2008,** *24* (7), 907-910.
144. Singhal, R.; Orynbayeva, Z.; Kalyana Sundaram, R. V.; Niu, J. J.; Bhattacharyya, S.; Vitol, E. A.; Schrlau, M. G.; Papazoglou, E. S.; Friedman, G.; Gogotsi, Y., Multifunctional carbon-nanotube cellular endoscopes. *Nat Nano* **2011,** *6* (1), 57-64.
145. Quinn, B. M.; Dekker, C.; Lemay, S. G., Electrodeposition of Noble Metal Nanoparticles on Carbon Nanotubes. *J. Am. Chem. Soc.* **2005,** *127* (17), 6146-6147.
146. Pachauri, V.; Kern, K.; Balasubramanian, K., Field-effect-based chemical sensing using nanowire-nanoparticle hybrids: The ion-sensitive metal-semiconductor field-effect transistor. *Appl. Phys. Lett.* **2013,** *102* (2), 023501.
147. Sharma, H.; Agarwal, D. C.; Shukla, A. K.; Avasthi, D. K.; Vankar, V. D., Surface-enhanced Raman scattering and fluorescence emission of gold nanoparticle–multiwalled carbon nanotube hybrids. *J. Raman Spectrosc.* **2013,** *44* (1), 12-20.